Spark Plasma Sintered Nanostructured Ceramics for Bio Ceramic Applications:

Titanium Carbide and Titanium Nitride in an Alumina Matrix

By

Patrick Rokebrand

A dissertation submitted to the Faculty of Engineering and the Built Environment, University of the Witwatersrand, in fulfillment of the requirements for the degree of Master of Science in Engineering.

Johannesburg 2012

Declaration

I declare that this dissertation is my own unaided effort. It is being submitted for the degree of Master of Science in Engineering to the University of the Witwatersrand, Johannesburg. It has not been submitted before for any degree or examination to any other university.

_____

Patrick Pierce Rokebrand (0605506V)

_____ Day of _____ Year 2012

Abstract

Titanium carbide and titanium nitride were used to reinforce an alumina matrix. The composites were prepared from nanopowders in an attempt to produce composites with nanostructured grains and as a result improved hardness and fracture toughness values. The composite powders were sintered using a spark plasma sintering (SPS) furnace which allows for high heating and cooling rates to be implemented.

For the processing of the powders it was imperative that a dispersant that was able to disperse each of the materials being investigated be found. The dispersant would also have to be used in an organic solvent in an effort to prevent oxidation of the non-oxide materials. Due to the high costs associated with the nanopowders, micron sized powders were used in the determination of an effective dispersant. The dispersant that was found to meet all the criteria was Lubrizol 2155 when using hexane as the solvent. An optimum dispersant amount for each of the micron powders was determined through rheology studies. Two samples of each µm particle reinforced composite material (Al_2O_3-50%TiC and Al_2O_3-50%TiN) were prepared, the properties measured and the cross-sections analysed using SEM. From the SEM analysis it was seen that there was homogeneous distribution of the various phases within the sintered micron composites and as a result it was decided that Lubrizol 2155 would be used in the preparation of the nanopowders.

Rheology studies were then carried out on each of the individual nanopowders and on the Al_2O_3-10vol%TiC, Al_2O_3-50vol%TiC, Al_2O_3-10vol%TiN and the Al_2O_3-50vol% TiN nanocomposite systems. These results were used to prepare composites for sintering with additions to alumina of 3%, 10%,30% and 50% (by volume) of TiC and TiN respectively. The samples were then sintered using various conditions in the SPS furnace.

For the Al_2O_3-TiC and Al_2O_3-TiN composites it was evident that the densification of the materials containing 30% and 50% (by volume) of the reinforcing component was below 97%, whereas for the lower additions of the reinforcing components full densification was observed. This gives strong evidence of the hindrance of the sintering by the reinforcing elements. The oxygen content of the starting powders (TiC=3.5wt% and TiN=8.4wt% oxygen) was found to strongly affect the densification behaviour of the nanocomposites and is also assumed to have resulted in deterioration of the mechanical properties. The XRD analysis showed the presence of a solid solution between Ti_3O_5 and $AlTi_2O_5$ in the sintered materials.

The hardness values of the Al_2O_3-TiC nanocomposite materials were higher than those of the Al_2O_3-TiN nanocomposites. For the Al_2O_3-TiC nanocomposites hardness values of up to 23.1 GPa were determined. In the Al_2O_3-TiN nanocomposites, hardness values of up to 20.6 GPa were observed. The hardness values achieved were in line with those achieved in literature however this was particularly for the nanocomposites containing up to 30% of the reinforcing material. The nanocomposites containing 50% of the reinforcing material were typically found to have hardness values lower than expected, and they also had hardness and fracture toughness values that were lower than those of the micro-composites that were investigated.

The fracture toughness values obtained for the materials were relatively similar when comparing the Al_2O_3-TiC and Al_2O_3-TiN nanocomposites which contained similar amounts of the reinforcing components (TiC/TiN). The fracture toughness values determined were in the range of 2.2-3.1 $MPa.m^{0.5}$, however the Al_2O_3-3% TiC and the Al_2O_3-10% TiC nanocomposites sintered at 1800°C at a pressure of 30 MPa were the only samples with a fracture toughness higher than 3.0 $MPa.m^{0.5}$. The fracture toughness values achieved for the nanocomposites were lower than those reported in the literature for nano and micro-composites, as well as those obtained for the microcomposites sintered in this work.

Acknowledgements

- Prof. I. Sigalas for his advice and guidance.
- My friends and family for their love and support.
- DST/NRF Centre of Excellence for their financial assistance.
- My girlfriend Celtia for her understanding, caring and patience, I love you.

Contents

Declaration 1

Abstract 2

Acknowledgements 4

i. List of Tables 9

ii. List of Figures 11

1. Introduction 16

2. Bioceramics 18

2.1. Properties and Applications 21

2.1.1. Calcium Phosphate containing Bioceramics 21

2.1.2. Alumina 22

2.1.3. Zirconia 23

2.1.4. Bioglass® 25

2.1.5. Apatite-Wollastonite 26

2.2. Applications 27

3. Nanoceramics 29

3.1. Suspensions 29

3.2. Sintering 33

3.3. Properties 36

4. Experimental Procedure 41

4.1. Powder Processing 42

4.1.1. Particle Size Analysis 42

4.1.2. SEM Analysis of Powders and Materials 45

4.1.3. XRD analysis of Powders and Materials 45

4.1.4. BET 46

4.1.5. Dispersion 47
4.1.6. Mixing 50
4.1.7. Drying 51
4.1.8. Sieving 52
4.1.9. Dispersant Burn-Off 52
4.2. Sintering 52
4.2.1. Spark Plasma Sintering 52
4.3. Characterization 53
4.3.1. Density 54
4.3.2. Cutting 55
4.3.3. Mounting 55
4.3.4. Polishing 56
4.3.5. Hardness and Fracture Toughness 57
5. Results of the Investigation of the Al_2O_3 Composites with µm-powders 60
5.1. Powder Preparation 60
5.1.1. Particle Size Analysis 60
5.1.2. SEM analysis 61
5.1.3. XRD analysis 62
5.1.4. BET 64
5.1.5. Dispersion 65
5.2. Sintering and Characterization of the composite based µm-powders 69
5.2.1. SEM Analysis 70
5.2.2. Hardness and Fracture Toughness 71
6. Discussion of the Results Concerning the µm-composites 72
6.1. Rheology of the suspensions 72

6.2. Properties 74
7. Results of the investigation of the nanocomposites 75
7.1. Powder Processing 75
7.1.1. SEM Analysis 75
7.1.2. XRD analysis 76
7.1.3. BET 77
7.1.4. Particle Size Analysis 78
7.1.5. Oxygen Content of the Powder 78
7.1.6. Preparation and Properties of the Dispersion 79
7.1.7. Burning off of Dispersant 84
7.2. Sintering and Characterization of the Alumina – Titanium Carbide nanocomposites . 85
7.2.1. XRD Analysis 88
7.2.2. SEM Analysis 89
7.3. Densification and Characterization of the nano Alumina-Titanium Nitride materials . 93
7.3.1. Density, Hardness and Fracture Toughness of the Al_2O_3-TiN Materials 93
7.3.2. XRD Analysis 97
7.3.3. SEM Analysis 99
8. Discussion of preparation and properties of nanocomposites 104
8.1. Rheology of the Suspensions 104
8.2. Discussion of sintering behaviour and properties of the Al_2O_3-TiC nanocomposites. 109
8.2.1. Comparison of Densities 111
8.2.2. Comparison of Hardness and Fracture Toughness Results 119
8.3. Discussion of sintering behaviour and properties of the Al_2O_3-TiN nanocomposites 126
8.3.1. Comparison of Densities 127
8.3.2. Comparison of Hardness and Fracture Toughness Results 133

8.4. Comparison of the Al_2O_3-TiC and the Al_2O_3-TiN nanocomposites 140
9. Conclusion 147
10. Appendix 152
11. References 153

i. List of Tables

Table 1: Compositions and shapes of various bioceramic materials (Kokubo, pp29)[9]. 20
Table 2: Properties of selected Bioceramic materials, adapted from Kokubo[9], Pramanic et al. 2005[18], Park et al. 2008[19] 23
Table 3: The physical and mechanical properties of Biolox® Delta and Biolox® Forteas per the CeramTec datasheet (Zimmer, 2012)[22]. 24
Table 4: Uses of bioceramics in various applications[11][26]. 28
Table 5: Properties of previously sintered alumina, alumina/titanium carbide and alumina/titanium nitride materials 37
Table 6:Suppliers of all materials (excluding powders) used in this project. 41
Table 7:Suppliers of all powders used in this project. 42
Table 8: Grinding/Polishing process information 56
Table 9: Results obtained from the particle size analysis on the µm-powders. 61
Table 10: BET analysis on each of the course powders. 64
Table 11: Sintering conditions used for µm-powdersamples. 69
Table 12: Density results obtained for sintered samples. 70
Table 13: Summary of Hardness and Fracture Toughness Results 71
Table 14: Comparison between the weight percentage of Lubrizol and the surface areas of the powders 73
Table 15: Summary of the properties of the powder obtained compared to those provided by the supplier. 75
Table 16: BET analysis on each of the nanopowders compared to the data received from the supplier. 77
Table 17: Comparison of measured d_{50} particle size to that claimed by the supplier. 78
Table 18: Properties obtained for the Al_2O_3-TiC samples using various sintering conditions 86
Table 19: Theoretical densities of the Al_2O_3-TiC samples not taking into account the oxygen content 87
Table 20: Theoretical densities of the Al_2O_3-TiN samples not taking into account the oxygen content 93
Table 21: Properties obtained for the Al_2O_3-TiN samples using various sintering conditions 94

Table 22: Comparison between the weight percentage of Lubrizol and the surface areas of the powders 105
Table 23: Comparison between the expected and the actual amount of Lubrizol 2155 required and the solid loadings that were used 107
Table 24: Recalculated theoretical density compared to the original theoretical density..... 113
Table 25: Recalculated Relative densities with change in density 114
Table 26: Estimated composition of TiC in order for the following densification values to be obtained. 118
Table 27: Recalculated theoretical density compared to the original theoretical density..... 128
Table 28: Recalculated Relative densities with change in density. 129
Table 29: Best hardness results obtained for each composition of the Al_2O_3-TiN samples that were sintered. 136
Table 30: Best fracture toughness results obtained for each composition of the Al_2O_3-TiN samples that were sintered. 139
Table 31: Best densification results obtained for each composition of both the Al_2O_3-TiCand Al_2O_3-TiN samples that were sintered. 142
Table 32: Best hardness results obtained for each composition of both the Al_2O_3-TiCand Al_2O_3-TiN samples that were sintered. 143
Table 33: Best fracture toughness results obtained for each composition of both the Al_2O_3-TiCand Al_2O_3-TiN samples that were sintered. 145
Table 34: Hardness and fracture toughness results from Table 32 and Table 33 respectively compared to values from literature as shown in Table 5 and those obtained from the sintered µm-composites..... 146
Table 35: Effectiveness of Burn-off Procedure for Removing Lubrizol 2155. 152

ii. List of Figures

Figure 1: Crystal Structure of Calcium hydroxyapatite[14]. 21
Figure 2: SEM image of Biolox® Delta showing alumina matrix grains, zirconia grains (white) and mixed oxide platelets (Kokubo, pp 239)[9]. 25
Figure 3: Compositional diagram for bone-bonding glass. Note regions A, B, C, D. Region S is a region of Class A bioactivity where bioactive glasses bond to both bone and soft tissues and are gene activating (Kokubo, pp 269)[9] 26
Figure 4: Bone in-growth into pores of the Apatite - Wollastoniteglass ceramic (Kokubo, pp 292)[9]. 27
Figure 5: Particle size distribution of alumina ultrafine powder before dispersion (a) and after dispersion by ultrasound in the presence Tiron(b)[33]. 31
Figure 6: Consistency of concentrated suspensions in the presence of (a) PBTCA and (b) Tiron[33]. 32
Figure 7: Effect of inhomogeneous and homogenous green body on densification[35]. 33
Figure 8: Schematic of Spark Plasma Sintering Furnace(Rahaman, pp 828)[6] 35
Figure 9: Schematic of Hot Pressing Furnace(Rahaman, pp 828)[6] 36
Figure 10: Hall–Petch plot of hardness of nanocrystallineZrN coatings against the inverse square-root of grain size.[46] 38
Figure 11: Wear rate with grain size in Y-TZP ceramics. 39
Figure 12: SEM micrographs of Al_2O_3-12%TiO_2 showing wear damage in: (a) Ultra Fine Grained ceramic (1200 min sliding time) and (b) Coarse Grained ceramic (360 min sliding time) [4]. 39
Figure 13: Malvern Mastersizer 2000 particle size analyser 43
Figure 14: Malvern Zetasizer Nano ZS 43
Figure 15: Anton PaarRheolab QC rheometer 47
Figure 16: Fritsch Pulverisette 6 planetary ball mill 50
Figure 17: FCT HP-D5 Spark Plasma Sintering furnace 53
Figure 18: Schematic showing geometry of Vicker's hardness indenter(Callister, pp178)[55] 58

Figure 19:Particle size distribution curve for AKP-50 Alumina after milling in the presence of Dolapix CE64..... 60
Figure 20:SEM micrographs of a) AKP-50 Al_2O_3 powder, b) titanium carbide powder c) titanium nitride powder; the material with the bright appearance was found to be tungsten carbide by EDS analysis..... 62
Figure 21:XRD analysis of pure titanium carbide µm-powder as obtained from supplier..... 63
Figure 22:XRD analysis of titanium nitride powder as obtained from supplier..... 64
Figure 23: Schematic of a succinimide[58]. 65
Figure 24:Relationship between viscosity and a) shear rate for AKP-50 Alumina with various concentrations of Lubrizol 2155 and b)the amount of Lubrizol 2155 added at a shear rate of 100/s for the AKP-50 Alumina powder. 66
Figure 25:Relationship between viscosity and the amount of Lubrizol 2155 added at a shear rate of 100/s for a) the titanium carbide µm-powder and b) the titanium nitride µm-powder 67
Figure 26:Relationship between viscosity and the amount of Lubrizol 2155 added at a shear rate of 100/s for the a) Al_2O_3-50%TiC microcomposite material and b) the Al_2O_3-50%TiN microcomposite material..... 68
Figure 27: SEM images showing dispersion of the various phases for the a) Al_2O_3-50%TiC and the b) Al_2O_3-50%TiN composites..... 71
Figure 28: Comparison of the viscosity of the composites to the pure AKP50 alumina suspension. 72
Figure 29:SEM micrograph of a) TM-DAR Alumina powder, b) ABCR AB255319 TiC nanopowder and c) ABCR AB255327 TiN nanopowder. 76
Figure 30:XRD analysis of the pure titanium carbide and titanium nitride nanopowders as obtained from the supplier. 77
Figure 31: a) Comparison of viscosity at shear rates up to 1000/s for various additions of Lubrizol 2155 for the TM-DAR alumina nanopowder and b) the relationship between viscosity and the amount of Lubrizol 2155 added at a shear rate of 100/s for the TM-DAR alumina powder..... 80
Figure 32:Relationship between viscosity and the amount of Lubrizol 2155 added at a shear rate of 100/s for the a) nanoTiC suspension and b)nanoTiN suspension. 81

Figure 33:Relationship between viscosity and the amount of Lubrizol 2155 added at a shear rate of 100/s for both the Al_2O_3-10%TiC and the Al_2O_3-50%TiC composite suspensions. 83
Figure 34:Relationship between viscosity and the amount of Lubrizol 2155 added at a shear rate of 100/s for both the Al_2O_3-10%TiN and the Al_2O_3-50%TiN composite suspensions. 83
Figure 35:Comparison of effective Lubrizol 2155 burn-off between the Al_2O_3-TiC and Al_2O_3-TiN samples. 85
Figure 36:XRD analysis comparing each composition of Al_2O_3-TiC that was sintered at 1700°C and 50 MPa. 88
Figure 37: Calculation of the TiC lattice parameters in a) the pure TiC powder and b) the Al_2O_3-50%TiC composite sintered at 1700°C and 50 MPa. 89
Figure 38:SEM micrographs of Al_2O_3-3% TiCsintered at 1700°C and 50MPa. 90
Figure 39:SEM micrograph of Al_2O_3-30% TiC sintered at 1700°C and a pressure of 50 MPa. .. 91
Figure 40:EDS spectra of the Al_2O_3-30% TiC composite showing a) the Al_2O_3phase, b) the TiC phase and c) the presence of a titanium oxide containing phase. 91
Figure 41:SEM micrograph of Al_2O_3-50% TiC sintered at a) 1600°C and 50 MPa and b) 1700°C and a pressure of 50 MPa. 92
Figure 42: Comparison of densities of Al_2O_3-10% TiN sintered at various temperatures using different heating rates. 95
Figure 43: Comparison of densification curves for Al_2O_3-10% TiN sintered using a heating rate of 50°C/min and 250°C/min. 95
Figure 44: The effect of the heating rate used on the densification of Al_2O_3-30% TiN sintered at 1500°C and a pressure of 65 MPa. 97
Figure 45:XRD analysis comparing each composition of Al_2O_3-TiN that nano composites that were sintered at 1600°C and 50 MPa. 98
Figure 46: Calculation of the TiC lattice parameters in a) the pure TiN powder and b) the Al_2O_3-50%TiN composite sintered at 1600°C and 50 MPa. 99
Figure 47: SEM micrograph of Al_2O_3-3% TiN sintered at 1600°C and 50 MPa 100
Figure 48: SEM micrograph of Al_2O_3-10%TiNsintered at 1500°C and a pressure of 50 MPa.. 100
Figure 49: SEM micrograph of Al_2O_3-30%TiNsintered at 1500°C at a pressure of 65 MPa, using a heating rate of a) 50°C/min, b) 100°C/min and c) 250°C/min. 101

Figure 50:EDS spectra of the Al_2O_3-30% TiN composite showing a) the Al_2O_3 phase, b) the TiN phase and c) the presence of a titanium oxide containing phase. 102
Figure 51: SEM micrograph of Al_2O_3-50%TiNsintered at a) 1500°C , b) 1600°C and c) 1700°C. 103
Figure 52: Comparison of mixtures containing 10% and 50% (by volume) of the respective reinforcing component (TiC/TiN) to pure alumina. 106
Figure 53:Densification curves for Al_2O_3-TiC sintered at 1700°C and a pressure of 50 MPa... 109
Figure 54:Onset temperatures for start of densification and the main densification and the end of densification with respect to the TiC concentration of the composites sintered at 1700°C and a pressure of 50 MPa. 110
Figure 55:Effect of reinforcing component and sintering pressure on the relative densities obtained for Al_2O_3-TiC composites sintered at 1700°C. 115
Figure 56: Comparison of the densities obtained for the various compositions sintered using a pressure of a) 30 MPa and b) 50 MPa..... 116
Figure 57: Relationship between the relative density and increasing TiC content for composites sintered at 1700°C and 50 MPa. 117
Figure 58:Comparison of hardness of a) Al_2O_3-3% TiC, b)Al_2O_3-10% TiC and c)Al_2O_3-30% TiC sintered at various temperatures and pressures. 120
Figure 59: Comparison of the hardness values obtained for the various compositions sintered using a pressure of 30 MPa. 121
Figure 60: Comparison of the hardness values obtained for the various compositions sintered using a pressure of 50 MPa. 122
Figure 61: Comparison of the fracture toughness values obtained for the various compositions sintered using a pressure of a) 30 MPa and b) 50 MPa. 124
Figure 62: Effect of temperature on the fracture toughness values obtained for the various Al_2O_3-TiC compositions sintered using a pressure of 50 MPa..... 125
Figure 63: Densification curves for Al_2O_3-TiN sintered at 1600°C and a pressure of 50 MPa. 126
Figure 64:Onset temperatures for start of densification and the main densification and the end of densification with respect to the TiN concentration of the composites sintered at 1600°C and a pressure of 50 MPa. 127

Figure 65: Relationship between the relative density and increasing the TiN concentration when using the recalculated theoretical density for the composites densified at 1600°C using a pressure of 50 MPa. 131
Figure 66: Comparison of the hardness of a) Al_2O_3-3% TiN, b) Al_2O_3-10% TiN, c)Al_2O_3-30% TiN and d)Al_2O_3-50% TiN sintered under various conditions. 134
Figure 67: Comparison of fracture toughness a) Al_2O_3-30% TiNand b)Al_2O_3-50% TiN sintered under various conditions. 138
Figure 68: Effect of increasing TiN concentration on the fracture toughness of the Al_2O_3-TiN composites sintered at 1600°C and 50 MPa. 139
Figure 69:Comparison of (a) onset temperatures for start of densification and the main densification and (b) the end of densification with respect to the reinforcing component concentration for both the Al_2O_3-TiC and the Al_2O_3-TiN composites. 141
Figure 70: Comparison of hardness values obtained with respect to their relative density, for the samples as shown in Table 32. 144
Figure 71: Comparison of hardness and fracture toughness values obtained with respect to the reinforcing component concentration for composites sintered under the same conditions at 1600°C and 50 MPa. 145

1. Introduction

Ceramic materials have been used for bio-prostheses for a large number of years already; there is evidence of plaster of Paris being used to fill defects in bone in 1892[1]. Despite the fact that ceramics have been used for this amount of time, it is only in relatively recent years that the level of interest in bioceramics has increased. The properties of ceramic materials such as the high levels of chemical resistance, wear resistance and compressive strength has resulted in a large amount of interest in the study of these materials for biomedical applications[2].

Although these properties of ceramics have made them a popular object of investigation, they are still brittle materials. Ceramics have a low friction coefficient and a low wear rate but they are far more brittle than metallic materials such as stainless steels, titanium and chromium-cobalt alloys which are used for prostheses regularly. The brittleness of the ceramics has resulted in their application being limited to the ball joint for hip prostheses and not for the main shaft[3]. Decreasing the grain size of the ceramics under consideration for body prosthesis down to the nanosized range should improve their hardness and wear resistance[4].

One of the potential problems associated with the use of titanium carbide is that it risks oxidizing in a water based suspension. An organic liquid (hexane, alcohols, ketones, etc.) can be used to form suspensions of materials that are prone to reacting with water (Reed, pp140)[5].

The formation of stable, homogeneous suspensions is another problem that is faced when working with ceramic nanopowders. Agglomeration of the nanopowders readily occurs and as a result, the suspension becomes unstable (Rahaman, pp 211)[6]. In order to overcome this problem, the dispersal mechanisms of the powder used in this work will be studied using a Malvern zeta sizer and arheometer.

When the nanopowders are sintered, grain growth needs to be suppressed in order to obtain a sample with nanosized grains. The use of the spark plasma sintering furnace increases the possibility of this occurring as the samples are heated under pressure very rapidly[7]. The rapid heating results in the time for the grains to grow at higher temperatures being reduced substantially. Obtaining samples that have a density > 99% is imperative in obtaining satisfactory mechanical properties of the sintered ceramics[8].

The aim of this project is to successfully produce sintered ceramic samples with a nanosized grain structure which have a high hardness and good fracture toughness, and are of sufficient density (> 99% of theoretical density).

The main objectives that need to be achieved in this project are:

- Determine the dispersal mechanisms of alumina with titanium carbide and alumina with titanium nitride nanopowders in suspension.
- Determine the densification behavior of titanium carbide and titanium nitride nanopowders in an alumina matrix when forming nanocomposite materials.
- Determine the structure property relationships of alumina-titanium carbide and alumina-titanium nitride nanocomposites.

2. Bioceramics

Ceramic materials that are biocompatible and are used in biomedical or clinical applications are referred to as bioceramic materials (Kokubo, pp 28)[9]. In order for a material to be considered biocompatible, it must have an appropriate response in a specific bio-application. This means that the ceramic must not be toxic or have any long lasting adverse effects to the host[10].

There are four main responses, asreported by Hench et al. 1991, an implant can have when placed inside a surrounding tissue; these arelisted below[11]:

- If the material is toxic, the surrounding tissue dies.
- If the material is nontoxic and biologically inactive (nearly inert), a fibrous tissue of variable thickness forms.
- If the material is non- toxic and biologically active (bioactive), an interfacial bond forms.
- If the material is non-toxic and dissolves in the host's body, the surrounding tissue replaces it with time.

Bioceramics are produced in both crystalline and amorphous forms. The materials are then divided into two groups depending on their chemical composition; those that contain calcium phosphates and those that do not (Kokubo, pp 28)[9].

As a result of their similarities in composition to bone material, hydroxyapatite and tricalcium phosphate are two of the most commonly used calcium phosphate containing materials in bioceramic applications (Kokubo, pp28)[9]. Hydroxyapatite ($Ca_5(PO_4)_3OH$) has a higher stability in aqueous media with a pH of 4.2 - 8 than other calcium phosphate containing materials[2]. Tricalcium phosphate ($Ca_3(PO_4)_2$) is a biodegradable bioceramic which can be dissolved in physiological media and can be replaced by bone material after implantation. The most commonly used forms are α - tricalcium phosphate and β - tricalcium phosphate[2].

There are also a number of ceramic materials that do not contain calcium phosphates which are used as bioceramic materials. These include certain ceramic oxides, bioactive glasses and

bioactive glass-ceramic materials. The ceramic oxide materials that are most commonly used in bioceramic applications are yttria stabilized tetragonal zirconia, alumina and titania (Kokubo, pp 28)[9]. These materials are used as bioceramics as a result of their good mechanical strength and toughness and have also been found to be biocompatible.

Bioactive glasses such as Bioglass® and glass-ceramic materials such as apatite-wollastonite (A-W) are also often used in bioceramic applications[2]. Apatite-wollastonite (A-W) was developed by Kokubo in Japan and was found to have a high bending strength, fracture toughness and Young's modulus[12]. Bioglass® was developed by Hench[11].Bioglass® 45S5 has a composition of 45 wt% SiO_2, 24.5 wt% CaO, 6 wt% P_2O_5, 24.5 wt% Na_2O[13].

Table 1, adapted from Kokubo, shows the compositions and shapes of various ceramic materials that are used as bioceramics.

Table 1: Compositions and shapes of various bioceramic materials (Kokubo, pp29)[9].

Category	Materials and compositions	Shapes
Calcium phosphate (CP) group	Hydroxyapatite (HA) $Ca_5(PO_4)_3OH$	Sintered body (dense and porous)
		Powder
		Coating
		Composite
		Fiber
	β-Tricalcium phosphate (β-TCP) $Ca_3(PO_4)_2$	Sintered body (dense and porous)
		Powder
	Others	
	Dicalcium phosphate anhydrate (monetite, DCP or DCPA) $CaHPO_4$	Powder
	Dicalcium phosphate dihydrate (brushite, DCP2 or DCPD) $CaHPO_{42}H_2O$	Powder
	Calcium pyrophosphate (CPP) $Ca_2P_2O_7$	Powder
	α-Tricalcium phosphate (α-TCP) $Ca_3(PO_4)_2$	Powder
	Tetracalcium phosphate (TeCP) $Ca_4(PO_4)_2O$	Powder
	Octacalcium phosphate (OCP) $Ca_8H_2(PO_4)_{65}H_2O$	Powder
	Amorphous calcium phosphate (ACP) $Ca_3(PO_4)_2nH_2O$	Powder
Others	Yttria-stabilized tetragonal zirconia (Y-TZP) Y_2O_3-ZrO_2	Sintered body (dense)
	Aluminum oxide (alumina) Al_2O_3	Sintered body (dense)
	Titanium oxide (titania) TiO_2	Sintered body (dense)
	Silicon nitride Si_3N_4	Sintered body (dense)
	Silicon carbide SiC	Sintered body (dense)
	Carbon C	Fiber
	Bioactive glasses system	
	SiO_2-P_2O_5-Na_2O-CaO	Bulk
	SiO_2-P_2O_5-Na_2O-K_2O-CaO-MgO	Bulk
	SiO_2-P_2O_5-CaO-Al_2O_3	Bulk
	Bioactive glass-ceramics system	
	SiO_2-P_2O_5-CaO-MgO (A-W)	Bulk
	SiO_2-P_2O_5-Na_2O-K_2O-CaO-MgO (Ceravital)	Fiber

2.1. Properties and Applications

Bioceramics are generally separated according to their bioactivity into two groups; these are bioinert and bioactive materials. Since all materials that are used in a physiological environment will cause a response, bioinert materials here are defined as those that will cause a low level response from the host tissue, whereby the implant is covered in a thin fibrous, non-adherent layer[(2)].

2.1.1. Calcium Phosphate containing Bioceramics

Hydroxyapatite ($Ca_5(PO_2)_3OH$) is a bioactive material and is one of the most widely used synthetic calcium phosphate bioceramic materials[(2)]. As discussed previously, this is due to the similarities in composition of hydroxyapatite to bone. Hydroxyapatite has the following theoretical composition; 39.68 wt% Ca and 18.45wt% P. The crystal structure of hydroxyapatite allows for the Ca^{2+}, PO_4^{3-} and OH^-groups to be substituted by various other ions. These substitutions can affect the lattice parameters, crystal morphology, crystallinity, solubility and thermal stability of hydroxyapatite[(2)]. Hydroxyapatite has a hexagonal, layered structure as shown in Figure 1.Because of its layered nature, hydroxyapatiteis able to accommodate a large number of other ionswithin its structure.

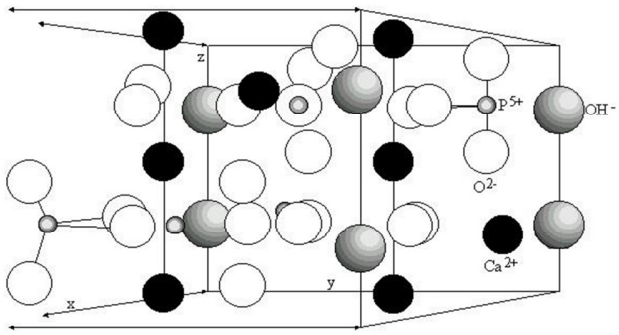


Figure 1: Crystal Structure of Calcium hydroxyapatite[(14)].

As mentioned previously, α - tricalcium phosphate and β - tricalcium phosphate are the main forms of tricalcium phosphate ($Ca_3(PO_4)_2$) that are used in bio prostheses applications. These are bioactive materials which are eventually replaced by bone. The most common way of obtaining α - tricalcium phosphate is by heating β - tricalcium phosphate above 1125°C, followed by rapid quenching. It is also possible to produce α - tricalcium phosphate from amorphous tricalcium phosphate by heating the amorphous tricalcium phosphate between 630°C and 850°C. However, the use of this method does result in small amounts of β – tricalcium phosphate being present as well[15][16]. Typical properties of hydroxyapatite are shown in Table 2.

2.1.2. Alumina

Corundum (α-Al_2O_3) is the stable phase of alumina, and it is used for bioceramic materials. This material needs to be of high purity (> 99.9%) and free of impurities such as alkaline oxides and silicates. The high purity of ceramic materials that are used for biomedical applications is required in order to prevent any unwanted chemical reactions within the body (Kokubo, pp 237)[9]. This Alumina is a bioinert ceramic material and as a result it must have a high corrosion resistance in a physiological environment[17]. These high purity alumina bioceramics have been developed as an alternative to metal alloys that have previously been used for orthopaedic implants. The alumina bioceramic materials have a low friction coefficient, high hardness and have a high corrosion resistance which allows for the rate of wear on these materials in bioceramic application to be very low (Kokubo, pp 231)[9]. Typical properties of the alumina materials are shown in Table 2.

Table 2: Properties of selected Bioceramic materials, adapted from Kokubo[9], Pramanic et al. 2005[18], Park et al. 2008[19]

Bioceramic Material	Hardness (GPa)	Fracture Toughness ($MPa.m^{0.5}$)	Young's Modulus (GPa)	Bending Strength (MPa)
Hydroxyapatite[18][9]	5.3	3.05-3.15	7-13	115
Alumina[9]	>19.6	3-6	420	400-600
Zirconia[9][20]	13.2	6.4-10.9	210	1000
Apatite - Wollastonite[19][9]	6.4	2	118	220

2.1.3. Zirconia

Yttria-stabilised tetragonal zirconia containing 3 mol% yttria (3Y-TZP) is used as a bioceramic material. Tetragonal zirconia is not stable at low temperatures and as a result yttria is added as a stabilizer of the tetragonal phase (Kokubo, pp 243)[9]. The reason for the large interest in zirconia materials for bioceramics is due to the transformation toughening mechanism that exists in the material. A stress induced transformation of the tetragonal to the monoclinic phase occurs in zirconia. This transformation acts as a toughening mechanism due to the change in volume associated with the tetragonal to monoclinic phase change. As a crack propagating through the material encounters a tetragonal zirconia particle, it induces a stress in it. This results in a phase change from tetragonal to monoclinic; the monoclinic phase occupies a larger volume thanthe tetragonal phase (Kokubo, pp 244)[9]. As a result of this volume expansion, compressive stresses are induced around the monoclinic particle and hence around the tip of the crack. In order for the crack to propagate further, it requires a larger amount of energy to overcome the compressive forces generated. Thus the crack is retarded and eventually stopped; thiscauses the high fracture toughness associated with the zirconia materials.Typical properties of zirconia are shown in Table 2.

The alumina and zirconia materials are also combined to produce zirconia toughened alumina ceramics. This is due to the beneficial relationship that is obtained due to the hardness of the

alumina and the fracture toughness of partially stabilized zirconia. CeramTec currently uses these materials in order to produce bioceramics for various applications. CeramTecmakes use of two different materials in the manufacture of their products. These are Biolox® Forte, which is a pure alumina material and the second one is the Biolox® Delta, which is an alumina matrix composite material. The Biolox® Delta material is a zirconia toughened alumina ceramic. It containsapproximately 81% Alumina and 17% yttria-stabilised tetragonal zirconia and 1.4% of other oxide materials, which results in the Biolox® Delta having a hardness similar to that of Biolox® Forte, but a fracture toughness that is significantly higher[21]. This is due to the material having two toughening mechanisms; the first is due to the phase transformation of the zirconia material and the second is due to the oxide platelets that are added which allow for energy to be dissipated by crack deflection[21]. Biolox® Delta has been developed with improved mechanical properties so that new applications, such as spine and knee components, as well as larger and thinner versions of existing components, such as the femoral heads and inserts, can be developed and reliably used clinically (Kokubo, pp. 235)[9]. The table below compares the properties of the two Biolox® products.

Table 3: The physical and mechanical properties of Biolox® Delta and Biolox® Forteas per the CeramTec datasheet (Zimmer, 2012)[22].

Property	Biolox® Delta	Biolox® Forte
Density (g/cm^3)	4.37	3.98
Young's modulus (GPa)	350	380
Bending strength (MPa)	1380	630
Fracture toughness ($MPa.m^{1/2}$)	6.5	3.2
Hardness (HV)	1925	2000
Grain size (μm)	< 1	< 1.8

From this it is seen that the composite material (Biolox® Delta) has a superior flexural strength and fracture toughness when compared to Biolox® Forte. Figure 2shows the microstructure of the Biolox® Delta material.

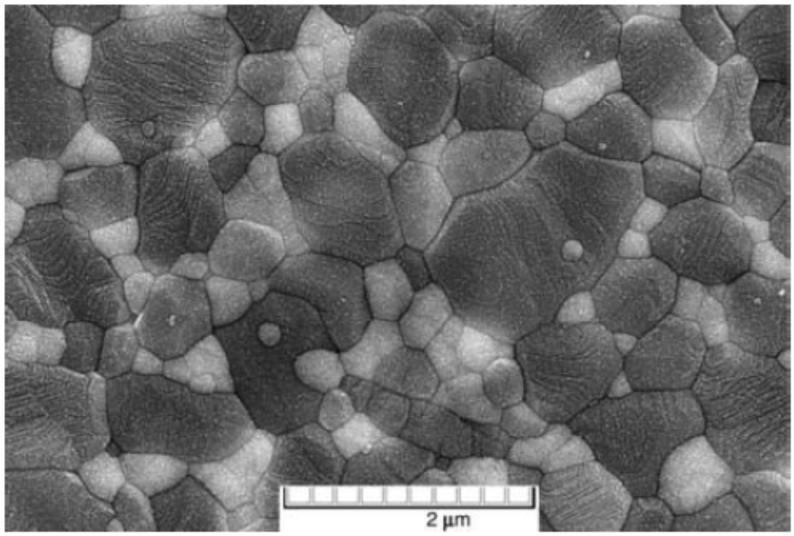


Figure 2: SEM image of Biolox® Delta showing alumina matrix grains, zirconia grains (white) and mixed oxide platelets (Kokubo, pp 239)[9].

2.1.4. Bioglass®

Bioglass® is a bioactive glass material which undergoes a rapid surface reaction which allows the material to bond to bone[11]. It was developed in 1969 by L. Hench and was the first synthetic material to form an interfacial bond with bone[23]. It has also been shown that Bioglass 45S5 is able to bond with soft tissue if the interface is kept stationary[24]. Bioglass® is produced using high purity oxides (SiO_2, Na_2CO_3, $CaCO_3$ and P_2O_5) which are placed in a platinum crucible, in order to avoid contamination, and heated to 1370°C [23].

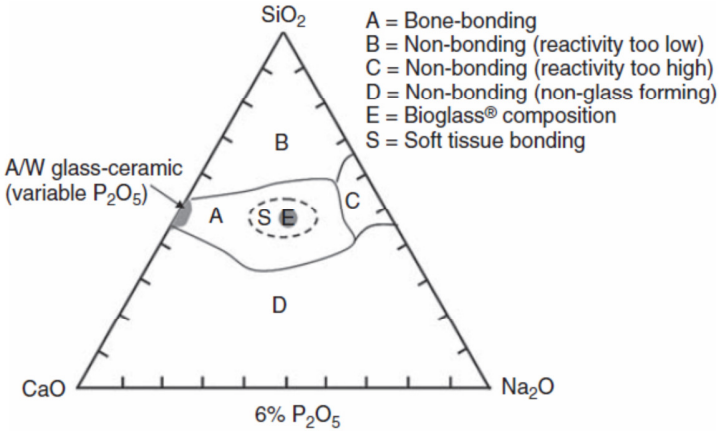


Figure 3: Compositional diagram for bone-bonding glass. Note regions A, B, C, D. Region S is a region of Class A bioactivity where bioactive glasses bond to both bone and soft tissues and are gene activating (Kokubo, pp 269)[9].

From this it is clear that the exact composition of Bioglass® can vary slightly, but the composition can also be varied to produce other bioactive glasses that are still capable of forming an interfacial bond with bone. The materials with compositions in region S above require rapid reaction rates in order to bond with the soft tissue[25].

2.1.5. Apatite-Wollastonite

Apatite-Wollastonite (A-W) glass ceramics have a high bending strength, fracture toughness and Young's modulus; this allows these materials to be used in certain load bearing applications[2]. A-W glass ceramics are made up of 28 wt% wollastonite ($CaO{\cdot}SiO_2$), 34 wt% oxyfluoroapatite ($Ca_{10}(PO_4)_6(O,F_2)$) and 28 wt% glass (MgO 17 wt%, CaO 24 wt%, SiO_2 59 wt%)[2]. A-W glass ceramics are bioactive and bond to the bone material of the host. The bone is then able to grow into the pores of the A-W glass ceramic, as can be seen in Figure 4 (Kokubo, pp 292)[9]. Typical properties of apatite-wollastonite are shown in Table 2.

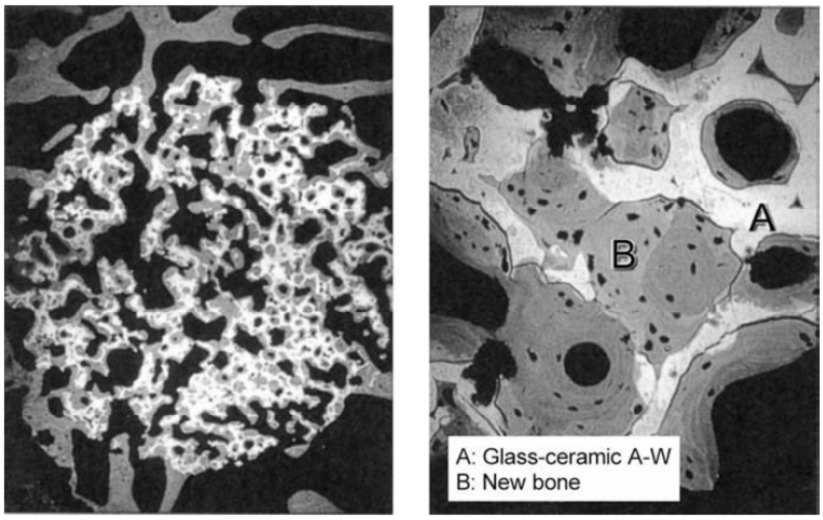


Figure 4: Bone in-growth into pores of the Apatite - Wollastoniteglass ceramic (Kokubo, pp 292)[9].

2.2. Applications

Bioceramics have a number of applications in the human body. Table 4, modified from Hench[11], shows the uses of various bioceramic materials in various applications.

Table 4: Uses of bioceramics in various applications[11][26].

Application	Material
Orthopedic load-bearing applications	Al_2O_3
	Stabilized zirconia
	PE-HA composite
Coatings for chemical bonding (orthopedic, dental, and maxillofacial prosthetics)	HA
	Bioactive glasses
	Bioactive glass-ceramics
Dental implants	Zirconia
	Al_2O_3
	HA
	Bioactive glasses
Alveolar ridge augmentations	Al_2O_3
	HA
	HA-autogenous bone composite
	HA-PLA composite
	Bioactive glasses
Otolaryngological	HA
	Bioactive glasses
	Bioactive glass-ceramics
Artificial tendon and ligament	PLA-carbon-f iber composite
Artificial heart valves	Pyrolytic carbon coatings
Coatings for tissue ingrowth (cardiovascular, orthopedic, dental, and maxillofacial prosthetics)	Al_2O_3
Temporary bone space fillers	TCP
	Calcium and phosphate salts
Periodontal pocket obliteration	HA
	HA-PLA composite
	TCP
	Calcium and phosphate salts
	Bioactive glasses
Maxillofacial reconstruction	Zirconia
	Al_2O_3
	HA
	HA-PLA composite
	Bioactive glasses
Percutaneous access devices	Bioactive glass-ceramics
	Bioactive glasses
	HA
Orthopedic fixation devices	PLA-carbon fibers
	PLA-calcium phosphate-based glass fibers
Spinal surgery	Bioactive glass-ceramic
	HA

3. Nanoceramics

Nanoceramics have been defined as bulk materials in which at least one of the ceramic phases present has a length between 1 and 100 nm. The increase of interest in nanoceramicsover the past few years is a result of the perceived potential to produce materials with properties superior to micron-structured, more conventional ones[27]. It has also been found that in most cases, the temperatures required for the sintering of nano-sized powders is lower than those used for conventional powders[28].

Although the potential of nanoceramics is large, there are difficulties associated with the processing of ceramic nanopowders. This is a result of the significantly increased surface area of the powders; this can result in high contamination of the powders through reaction with their environment (e.g.if the material has an affinity to any of the species in the air) during handling and storage[28]. Another major problem associated with nanopowders is agglomeration. This can result in the material being porous upon densification (Rahaman, pp31)[6].

3.1. Suspensions

The dispersion of the nanopowders is important in order to obtain fully dense sintered samples. When using colloidal shaping methods, a good stability, low viscosity and a high solids loading are needed in order to obtain good quality sintered samples at economic rates[29]. However, when working with pressing systems a good stability is the most importantsuspension property.When working with nanosized powders, agglomeration of the particles occurs as a result of van der Waals forces between the particles (Reed, pp 26)[5]. Therefore, it is necessary to investigate the relative dispersal mechanisms that will allow for the formation of stable suspensions.

Electrostatic, steric and electrosteric stabilization are the main dispersal mechanisms that are employed in order to form stable suspensions. In electrostatic dispersion, the stability of the suspension can be controlled by ensuring that the particles in suspension have like electrical charges on their surfaces. When the charge is high enough, a repulsive force is created between the particles resulting in their dispersion[30]. This is typically done by varying the pH of the suspension. In steric stabilization, macromolecules are added to the suspension. The added molecules attach themselves to the particles in suspension, forming a layer on their surface which separates them from one another[31]. Electrosteric stabilization is a combination of electrostatic and steric stabilization. This makes use of various polyelectrolyte molecules[30] which attach themselves to the particle (as in steric stabilization) with the one end, while the other acquires an electric charge which helps repel adjacent and similarly charged particles. (as in electrostatic stabilization). It must be noted however, that organic solvents typically have a low dielectric constant which results in electrostatic stabilization not being possible[32].

The zeta potential represents the potential at the surface of the shear layer surrounding a particle moving through a solution.By varying the pH of the solution, it is possible to alter the zeta potential of the particles so that they will have a zeta potential that is either negative, positive or zero (Rahaman, pp 211)[6]. Thus it is clear that the more positive or negative the zeta potential of the particles in suspension, the greater the stability of the particles in suspension as they repel each other to a greater extent. In order to obtain stable suspensions, dispersing agents can also be used. These work by changing the surface chemistry of the particles so that they are similarly charged causing them to repel one another (Rahaman, pp. 347)[6].

The effects of dispersing the starting powders can be seen in Figure 5 below. This shows the dispersion of three grades of ultrafine alumina powders using a dispersant (Tiron) and ultrasound[33]. It must be noted that these powders are still not completely dispersed and further dispersal methods such as milling should be employed in order to obtain a well dispersed powder.

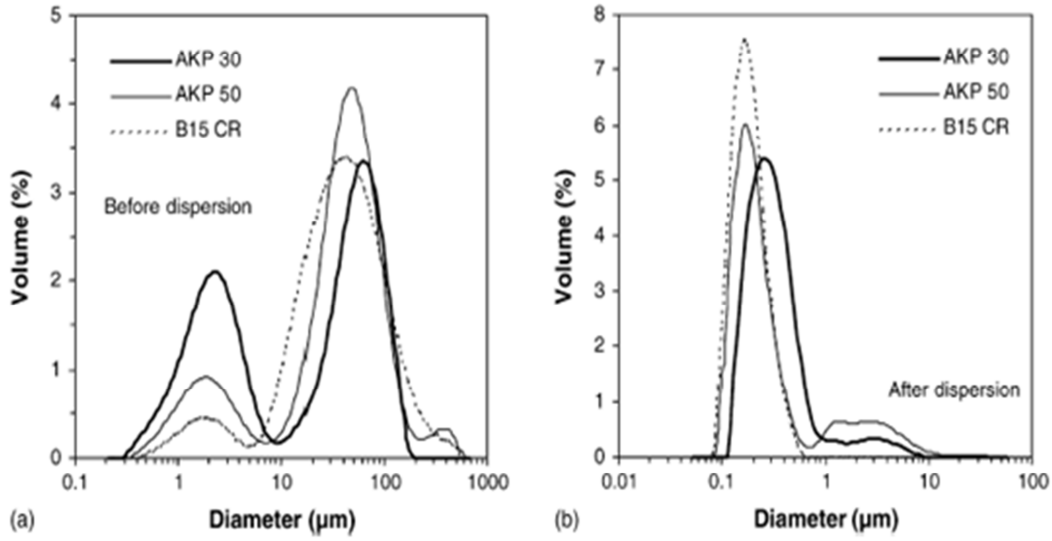


Figure 5: Particle size distribution of alumina ultrafine powder before dispersion (a) and after dispersion by ultrasound in the presence Tiron(b)[33].

Once a suitable dispersant for the material has been chosen, it is important to determine the optimum amount of dispersant that should be added. In order to do this, rheology studies can be carried out.

Rheology is the science of deformation and flow (Reed, pp277)[5] and as a result, these studies are an integral part in the production of ceramic slurries. These studies allow for the viscosity of the slurries to be determined at various shear rates. By performing the studies using various concentrations of dispersant and comparing the viscosity of these slurries at a given shear rate, it is possible to determine which dispersant concentration results in the lowest viscosity of the slurry. It has been found that the rheological behaviour of colloidal dispersions is among their most important properties[34]. The concentration which results in the lowest viscosity corresponds to the dispersant concentration which will produce the most stable suspension. This concentration can then be used during the milling process in order to ensure the best possible dispersion of the powders being processed.

Figure 6 shows the optimum concentration of dispersant for three ultrafine alumina powder slurries made using two dispersants, PBCTA and Tiron[33]. It is this concentration that allows for

the best state of dispersion. When dispersants are added to suspensions, the viscosity initially decreases until a minimum value is reached before it increases again. The decrease in the viscosity is a result of stabilization, where the minimum consistency corresponds to the maximum stability of the suspension and as a result the optimum concentrations of dispersants[33].

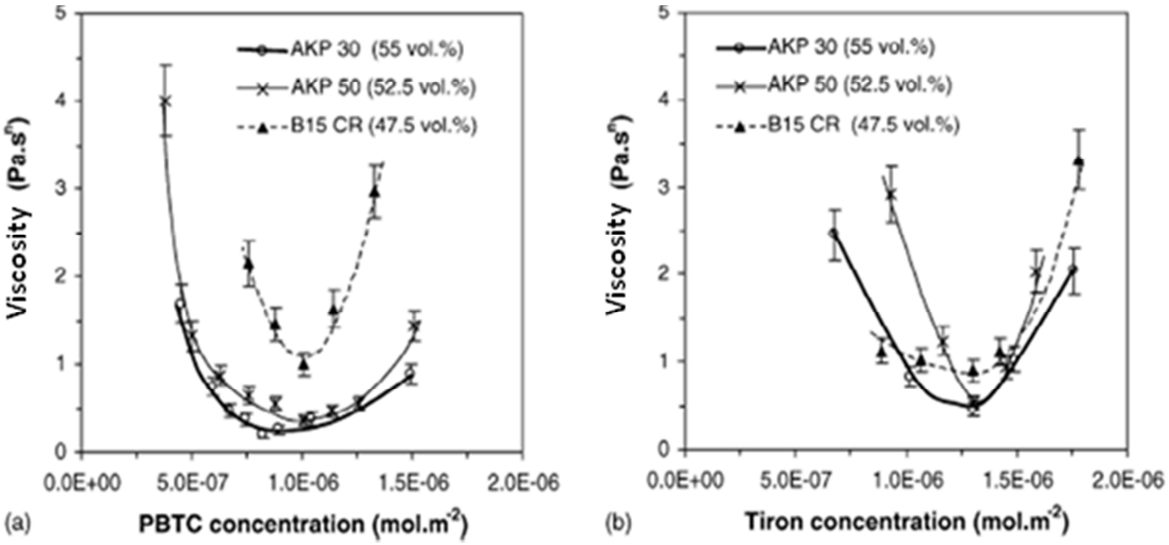


Figure 6: Consistency of concentrated suspensions in the presence of (a) PBTCA and (b) Tiron[33].

It is very important to optimally disperse the ceramic slurries during mixing with the addition of a dispersant in order to produce a homogeneously distributed powder for sintering. The effects of this can be seen in Figure 7, which shows that an inhomogenous distribution of the powders prior to sintering will result in decreased densification and also grain growth.

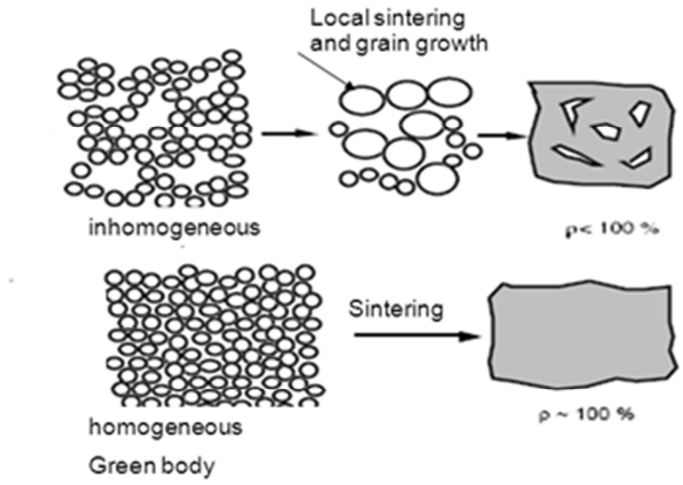


Figure 7: Effect of inhomogeneous and homogenous green body on densification[35].

3.2. Sintering

When the ceramic powders are sintered, the powders are placed in a furnace which can reach the required temperatures for sintering to occur. A furnace is generally fired up in three stages; the heating stage, the soaking period and the cooling stage. The heating rate of the furnace is chosen such that changes of state, stresses that arise due to thermal expansion of the materials and the combustion of binders do not result in the material being sintered to crack or have a high porosity (Carter, pp.148)[36]. The maximum heating rate that can be obtained is dependent on the type of furnace that is used, how it was designed and also on the sample dimensions. The degree of sintering that occurs in the material is a function of temperature and time and as a result, different temperatures and different soaking periods will be required for the complete densification of different materials.

The cooling stage is the final stage in the sintering process. During the cooling stage, phase transformations, crystallization and thermal contraction may occur and must be taken into account. The materials can be cooled fairly rapidly initially since at high temperatures they behave fairly plastically. As a result, the initial cooling does not cause stresses in the material to

increase very much (Carter, pp.148)[36]. However, as the temperature is decreased the material will no longer behave plastically and as a result, if the cooling is carried out rapidly stresses can build up. If any phase transformations that result in a volume change occur with the decrease in temperature, if the cooling rate is too high the resulting stresses can cause cracks to appear in the material (Carter, pp.148)[36].

The two sintering methods that are going to be used in this project are hot pressing and spark plasma sintering. Both the hot pressing furnace and the spark plasma sintering furnace make use of pressure; this increases the driving force for densification by acting against the internal pore pressure (Reed, pp. 617)[5].

The spark plasma sintering furnace makes use of a pulsed direct current (3.3 ms pulses of 0.5 to 10 kA intensity)[7]. This pulsed current allows for the rapid heating and cooling of the sample. The use of the spark plasma sintering furnace is of particular interest in the nanoceramics field as the fast heating rates, reported up to 600°C/min, combined with the application of pressure on the sample allow for high densification rates with minimal grain growth to be obtained (Rahaman, pp 828)[6]. The rapid heating of the compact is further increased due to the efficient heat transfer from the die to the compact because the die itself acts as a heating element, allowing for the thermal energy necessary for densification to be transferred to the sample[7]. However, in samples which are conducting, the sample itself is also heated. A schematic of a spark plasma sintering furnace is shown in Figure 8.

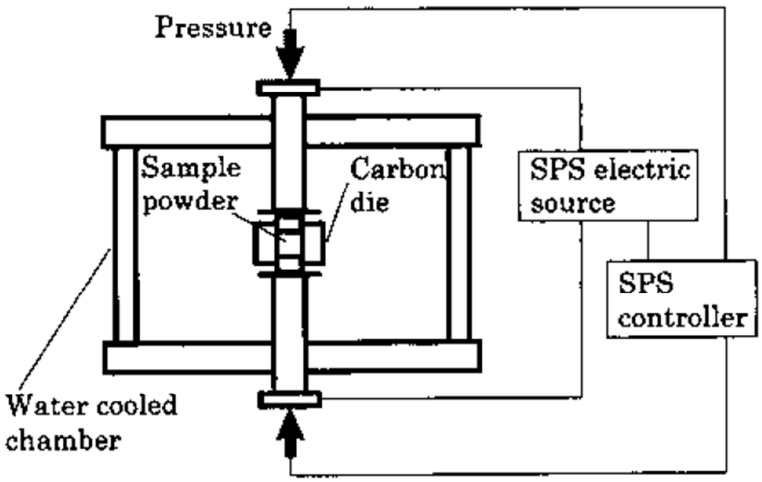


Figure 8: Schematic of Spark Plasma Sintering Furnace(Rahaman, pp 828)[6].

The use of the hot pressing furnace is advantageous over conventional sintering because densification occurs fairly quickly. The faster densification means that the time for grain growth is reduced; thisresults in the materials being produced having a finer grain size and thus better properties (Barsoum, pp 344)[37]. However, there are disadvantages associated with the use of the hot press; there are high costs associated with the tooling and the dies and it is used for batch processing because the sintering is performed in an inert atmosphere or a vacuum (Barsoum, pp 344)[37]. It must be noted however, that these same disadvantages are also apparent with the SPS furnace. When comparing the hot pressing furnace to the spark plasma sintering furnace, it is seen that the hot press uses an external heat source and as a result the rate at which the temperature of the sample can be increased is much slower; this results in the grain growth being limited to a much greater extent with the use of the spark plasma sintering furnace[7]. A schematic of a hot pressing furnace is given in Figure 9.

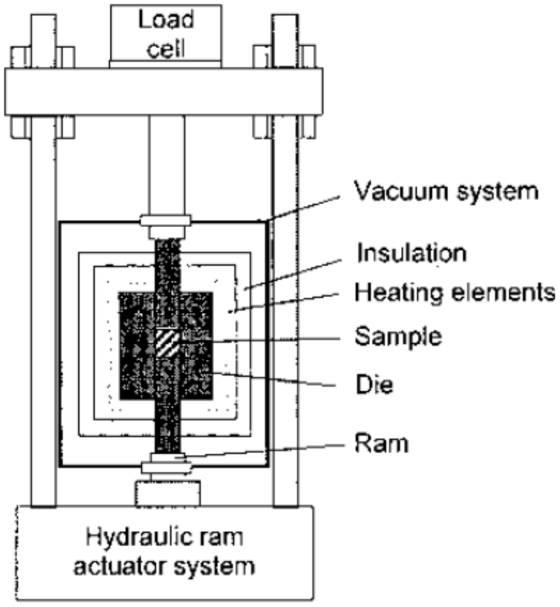


Figure 9: Schematic of Hot Pressing Furnace(Rahaman, pp 828)[6].

3.3. Properties

Typical properties of the materials that will be investigated in this project are shown in Table 5. These properties are for materials produced for different applications using various sintering techniques.

Table 5: Properties of previously sintered alumina, alumina/titanium carbide and alumina/titanium nitride materials

Material	Densification Technique	Relative Density (%)	Hardness (GPa)	Fracture Toughness ($MPa.m^{0.5}$)	Bending Strength (MPa)
Al_2O_3 (bioceramics)[9],[38]	-	> 99	> 19.6	3 - 6	400 - 600
Al_2O_3- 25%TiN[42]	HP, 30 MPa, 1550°C, 1 hr	99.5	17.7 - 19.1	4 - 5.3	600 - 730
Al_2O_3- 60%TiN[41]	SPS, 75 MPa, 1500°C, 3 min	99 – 100	18 - 22	5.7	-
Al_2O_3- 30%TiC[43]	HIP, 120 MPa, 1400°C, 2 hr	> 99	19 -21.6	3.6 - 6	660 - 820
Al_2O_3- 40%TiC[40]	SPS, 50 MPa, 1480°C, 4 min	99.2	21	3.87	940
Al_2O_3- (20%-60%) TiC (Cutting Tools)[39]	HP, 30MPa, 1450-1600°C, 1hr	-	19 - 23	4.5	900 - 1000

* Where HP is Hot Pressed, HIP is Hot Isostatically Pressed and SPS is Spark Plasma Sintered.

It has been found that at larger grain sizes, the hardness of ceramic materials obeys the Hall-Petch relation which shows that as the grain size is decreased, the strength of the material increases and as a result the hardness of the material increases as well.

This however has been found to be true only down to a certain critical grain size. Once the grain size of the material is decreased below the critical grain size, the strength and hardness of the material begins to decrease drastically[44]. It has been shown that the reason for this decrease is due tothe grain boundaries beginning to slide, contributing to plastic deformation more than dislocation slippage[45]. The relationship between the hardness of the material and the grain size can be seen in Figure 10.This effect is shown for ZrN where the critical grain size is approximately 5 nm. Above and below this grain size there is a decrease in the hardness values obtained for the material. However this effect occurs in other materials as well. The difference is that the critical grain size varies for different materials.

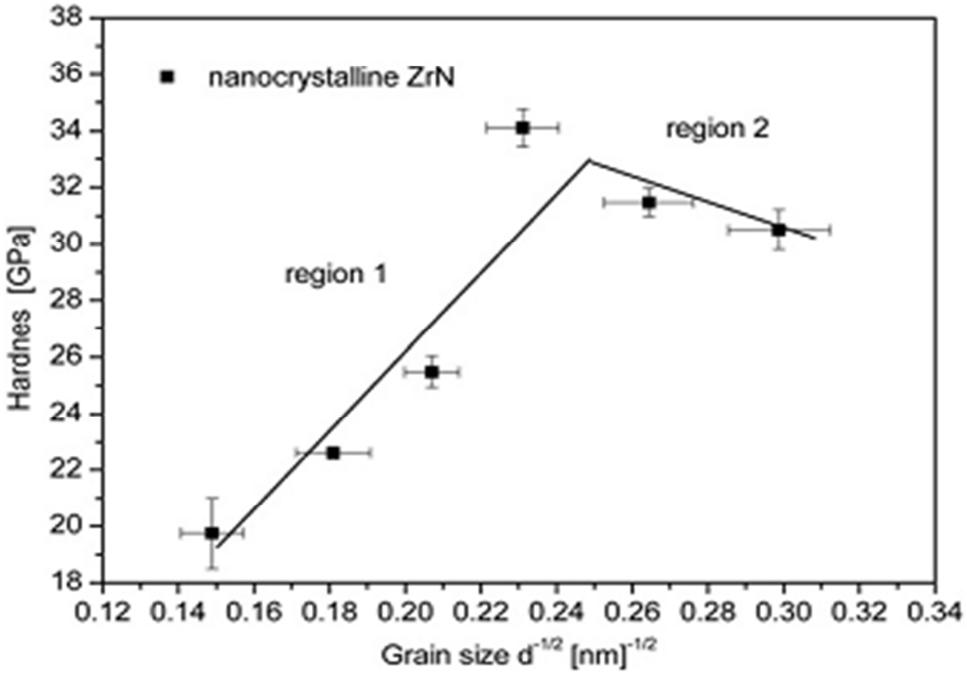


Figure 10: Hall–Petch plot of hardness of nanocrystallineZrN coatings against the inverse square-root of grain size.[46]

The wear resistance of alumina ceramic materials increases as the grain size is decreased[4]. It has also been shown that the rate of wear decreases significantly as the grain size tends towards the nanosize range (≈100 nm) when working with zirconia ceramic materials asseen in Figure 11[47].

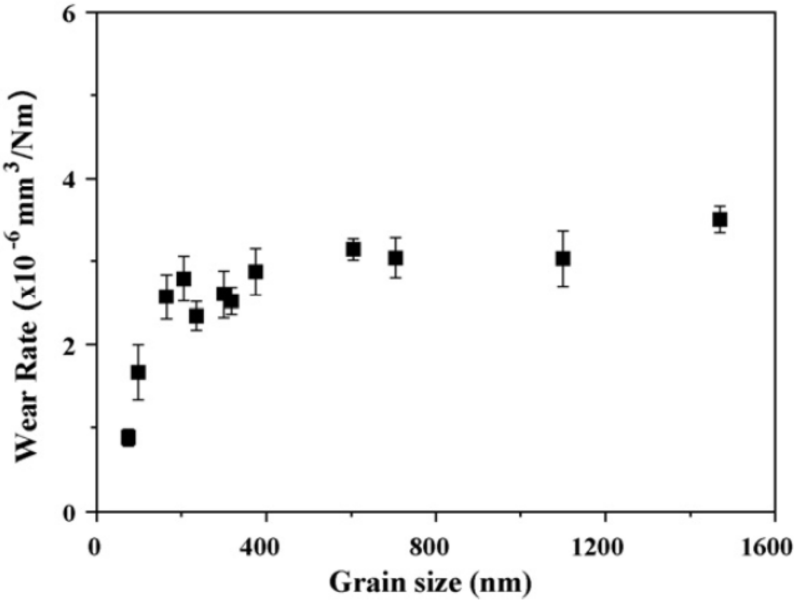


Figure 11: Wear rate with grain size in Y-TZP ceramics.

The effect of the grain size on the material itself can be seen in the diagram below.

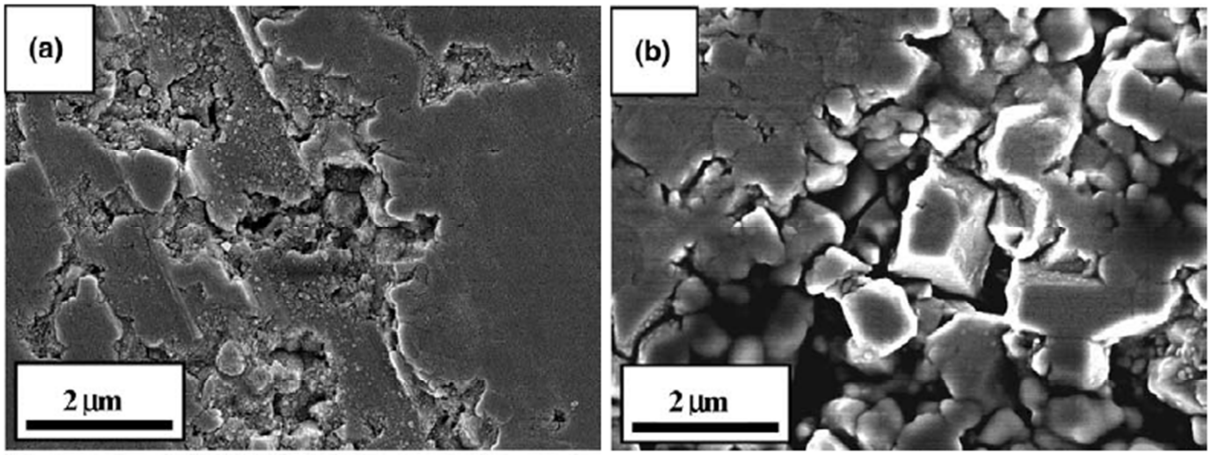


Figure 12: SEM micrographs of Al_2O_3-12%TiO_2 showing wear damage in: (a) Ultra Fine Grained ceramic (1200 min sliding time) and (b) Coarse Grained ceramic (360 min sliding time) [(4)].

From Figure 12 it is clear that the amount of wear, as seen by the amount of grain pullout that has occurred in the coarse grained (2.2 μm grain size) material is significantly greater than that of the ultrafine grained (400 nm grain size) material, even though the sliding time is less[4].

The wear rate of the material can be calculated using the following formula [47].

$$Wear\ \ Rate(mm^3 / Nm) = \frac{Wear\ Volume}{Normal\ \ Load \times Sliding\ \ Dis\tan ce}$$

Since the wear rate is related to the hardness of materials, the decrease in the grain size results in an increase in the hardness of the materials which causes the wear resistance of the materials to also increase. However, as with the hardness of the materials, the wear resistance will reach a maximum at the same critical grain size. At grain sizes less than the critical grain size where the hardness of the material begins to decrease, the wear resistance of the material also decreases [48]

4. Experimental Procedure

This section of the dissertation will discuss the experiments used in order to achieve the objectives of this project. It will discuss the materials, equipment and the methods used in order to perform the relevant experiments. The procedure was broken down into the preparation of the powders, the sintering of these powders and the characterization of the sintered samples.

The materials that were required for the completion of this project are listed inTable 6 and Table 7 below. The tables include the suppliers from which each of the materials were obtained.

Table 6: Suppliers of all materials (excluding powders) used in this project.

Material	Supplier
Iso-Propanol	School of Chemistry, University of the Witwatersrand
Hexane	School of Chemistry, University of the Witwatersrand
Lubrizol 2155	Carst and Walker, Parktown, Johannesburg, South Africa
Dolapix CE64	Zschimmer and Schwarz, GmbH &Co KG, ChemischeFabriken. Lahnstein, Germany
PEG 200	Sigma-Aldrich (Pty) Ltd.
PEG 400	Sigma-Aldrich (Pty) Ltd.
Sodium metahexaphosphate	Sigma-Aldrich (Pty) Ltd.

Table 7: Suppliers of all powders used in this project.

Powder composition	Product Code	Particle size	Supplier
Al_2O_3	AKP-50	0.1-0.3 µm	Sumitomo-Chemical Co., Ltd. Japan
TiC	N/A	Micron Range	Element Six (Pty) Ltd, South Africa
TiN	N/A	Micron Range	Element Six (Pty) Ltd, South Africa
Al_2O_3	Taimicron: TM - DAR	100 nm	KrahnChemie GmbH, Hamburg, Deutschland
TiC	AB 255319	40 nm	ABCR GmbH & Co. KG, Deutschland
TiN	AB 255327	20 nm	ABCR GmbH & Co. KG, Deutschland

4.1. Powder Processing

This section will discuss the various pieces of equipment and the methods that were used in order to characterize the various starting powders received from the suppliers and also those used in preparing these powders and producing the relevant composite powders for sintering.

Exposure to oxygen was limited throughout the process by ensuring all powders that weren't in a suspension were handled in a glove bag with an inert atmosphere. Argon gas was used to create the inert atmosphere.

4.1.1. Particle Size Analysis

Particle size analysis was carried out on the powders that were received. This was done to confirm the size of the particles of the powders required. The Malvern Matersizer 2000 was used in order to determine the particle size of the µm-powders whilst the Malvern Zetasizer Nano ZS was used to determine the size of the various nanopowder materials.

The Mastersizer 2000 (Figure 13) makes use of light scattering patterns, which are produced by passing the material being measured through a laser. The patterns that are produced are then analysed using the Fraunhofer model in order to calculate the size of the particles producing the relative scattering patterns[49].



Figure 13: Malvern Mastersizer 2000 particle size analyser

The ZetasizerNano ZS (Figure 14)makes use of Dynamic Light Scattering (DLS) in order to measure the sizes of the particles. DLS measures Brownian motion, which is the movement of the particles due to collisions with the molecules of the liquid they are in. This is done by using a laser to illuminate the particles and analyzing the resultant fluctuations of intensity in the scattered light. A correlation function is then determined from the intensity fluctuationswhich can then be used to calculate the size distribution using the Zetasizer software[50].



Figure 14: **Malvern Zetasizer Nano ZS**

4.1.1.1. Micron Powders

The powders in the micrometer (µm) range were initially dispersed in the presence of sodium metahexaphosphate using an ultrasonic probe in order to produce a unimodal size distribution. This was found to be sufficient for the titanium carbide and titanium nitride µm-powders but not for the AKP-50 Alumina Powder. The alumina powder was mixed in a planetary ball mill for two hours in the presence of a dispersant, Dolapix CE64, in order to generate a suitable dispersion of the powder. A 250 ml tungsten carbide milling bowl and 2 mm alumina balls were used to disperse the powder. Small amounts of the powder were added to the mastersizer material delivery system until the concentration of the material was in the required range. Three measurements were then performed and the average taken.

4.1.1.2. Nanopowders

The nanopowders were all milled using a planetary ball mill in order to properly disperse them before the particle size analysis was carried out. The milling was performed using a 250 ml zirconia milling bowl with 2 mm zirconia balls. All the powders were mixed using hexane as the solvent and Lubrizol 2155 as the dispersant. During milling the particle size was measured every half hour until a unimodal size distribution was obtained in the region claimed by the supplier. Due to the nature of the agglomeration associated with the nanopowders and a low concentration requirement (attenuation reading between 6 and 9) for the zetasizer measurements, small amounts of each of the powders (1 g of alumina, 0.5 g of TiC and 0.5 g of TiN) were mixed with 150 ml of hexane. Of these suspensions, a small amount was added to the zetasizer cell in order for the measurements to be carried out. The samples were diluted, using hexane, as required in order for an attenuation reading between 6 and 9 to be achieved. Three measurements, consisting of 12 runs each, were performed in each instance and the average was taken.

4.1.2. SEM Analysis of Powders and Materials

Scanning electron microscope (SEM) analysis was carried out at both the University of the Witwatersrand using a FEI Quanta 400 FEG SEM, and also at Element Six (Pty) Ltd using a Philips XL30 FEG ESEM with a Genesis 4000 EDAX detector.

For SEM analysis of the powders, a small amount of the powder was carefully placed onto graphite tape which was attached to a stub. The stub was then blown with compressed air in order to remove any loose powder before being placed in the SEM. Secondary electron images were taken at various magnifications in order to obtain an idea of the extent of agglomeration and more importantly further confirmation of the sizes of the particles present in the powders.

The sintered samples were mounted in polyfast and, after being finely polished (as per section 4.3.4) weretaken for SEM analysis. The samples containing 30% and 50% of the respective reinforcing components (TiC/TiN) were analysed under the SEM without any further treatments. The samples containing 3% and 10% of the respective reinforcing components were sputter coated using carbon in order to minimize charging of the samples as they were not conducting. Two layers of the carbon coating were applied to each of the samples.

4.1.3. XRD analysis of Powders and Materials

A Bruker D2 phaser XRD analysis instrument was used to characterize the initial, as received, powders. This instrument uses Cu Kα radiation to produce X-rays at 30 kV and 10mA. The diffractograms were produced over a 2 Theta range of 10° to 90° using a step size of 0.02(°2θ) and a scan step time of 3.2 seconds. This analysis was carried out in order to identify the phases present in each of the as received powders as well as to determine if there were any impurities present. The phases present were then identified by making use of the Philips Analytical

X'PertHighScore® software which uses the International Centre for Diffraction Data (ICSD) database.

The lattice parameters of the TiC and TiN nanopowders were then determined and compared to those of the Al_2O_3-50%TiC and Al_2O_3-50%TiN composites in order to check if the lattice parameters shifted during the sintering process. Use was made of the d-spacing and the corresponding Miller indices as determined from the XRD analysis of the materials. The following equation was used to calculate the lattice parameters.

$$\frac{1}{d^2} = \frac{\left(h^2 + k^2 + l^2\right)}{a^2}$$

Where;

d = d-spacing

(hkl) = Miller indices

a = Lattice parameter

By plotting (h^2+k^2+l^2) against the ($1/d^2$) values, it is possible to plot a best fit line where the gradient is a^2.By taking the square root of the gradient in each curve, it is possible to obtain the lattice parameters in each case.

4.1.4. BET

In order to determine the specific surface area of the starting powders, BET analysis was carried out.This was done by using a minimum of 0.2 g of sample, which was then degassed in N_2 at 150 °C for four hours prior to analysis using a Micromeritics Flow Prep 060. The specific surface areas and pore size distributions were then obtained at -196 °C. The pore size distribution and

specific surface areas of the samples were determined via nitrogen adsorption/desorption according to the BET method using a MicromeriticsTristarsurface area and porosity analyzer. In order to confirm the accuracy of the results, the tests wereperformedtwicefor each of the samples.

4.1.5. Dispersion

In order to prepare the mixtures of the powders for sintering it was required to disperse the powders during the mixing process. In order to achieve this it was required that a suitable dispersant be found. Once a suitable dispersant had been obtained rheology studies were carried out in order to determine the optimum amount of dispersant required to provide the best dispersion possible. All the rheology studies were carried out using an Anton PaarRheolabQCrheometer (Figure 15). Thisrheometer makes use of the Searle principle. It allows for a test to be done either under a controlled shear rate or a shear stress[51]. As a result of this it is highly suited for determining mixing and stirring behavior of emulsions and dispersions.



Figure 15: **Anton PaarRheolab QC rheometer**

The rheology studies in this project were aimed at determining the viscosity at various shear rates and for various amounts of added dispersant. The objective of the study was to establish which dispersant concentration produces the lowest viscosity in the suspension. This suspension is the most stable and optimally dispersed.

The rheology was performed by adding the relevant volume of powder, hexane and dispersant together in order to produce a total volume of 24 ml of the relevant suspension as per the following equations.

$$V_{Powder} = V_{Total} \times \frac{SL}{100}$$

$$m_{Powder} = V_{Powder} \times \rho_{Powder}$$

$$V_{Lubrizol} = \frac{m_{Powder} \times Wt\%_{Lubrizol}}{\rho_{Lubrizol}}$$

$$V_{Hexane} = V_{Total} - (V_{Powder} + V_{Lubrizol})$$

Where;

V_{Powder} = Volume of the powder to be used (cm^3)

V_{Total} = Total Volume = 24 cm^3

SL = Solids Loading being investigated (Volume %)

m_{Powder} = Mass of the powder to be used (g)

P_{Powder} = Density of the Powder being tested (g/cm^3)

$V_{Lubrizol}$ = Volume of Lubrizol (cm^3)

$Wt\%_{Lubrizol}$ = Weight % Lubrizol being tested

$P_{Lubrizol}$ = Density of Lubrizol (g/cm^3)

V_{Hexane} = Volume of Hexane (cm^3)

In the case of the pure powders the suspension was then placed in an ultrasonic bath and stirred for 10 minutes in order to obtain a suitable suspension for the rheology studies. During this period the sample is weighed every two minutes and any hexane lost due to evaporation replaced. The sample is then carefully poured into the rheology cup up to the 22 ml line mark; the cup is secured to the rheometer and the test started using a CC27/P1 bob. In order to prevent hexane loss during the test, a lid was made to fit the rheometer in order to limit exposure to air as much as possible. Once the test is complete, both the cup and bob are thoroughly cleaned using soapy water.

For the rheology studies on the mixtures, the powders were first mixed in the planetary ball mill for 2 hours, using a 250 ml milling bowl with 2 mm grinding balls. The µm-powder materials made use of a stainless steel milling bowl with a tungsten carbide lining and were mixed using 2 mm alumina balls in order to disperse the materials. The nanopowder materials were mixed using a zirconia milling bowl and 2 mm zirconia balls in order to disperse the materials. The mass ratio of grinding balls to the amount of powder being milled was ≈5 g milling balls to 1 g of powder, and hexane was used as the solvent in order to prevent oxidation and hydrolysis. The amount of hexane used in each case was 150 ml, and the powder was then added in order to give a solids loading of 20 vol% in each case (except for the Al_2O_3-50%TiN composites where a solids loading of 5% was used). The milling balls were then added as discussed above and the powders were mixed at 300 rpm for two hours. They were then dried in a rotary evaporator and sieved down to 250 µm. The same procedure discussed above was then used for the preparation of the mixed powders for the rheology tests to be carried out.

The following parameters were used to perform the rheology studies for this project:

- An initial pre-shear of the suspension was done for 160 seconds using a shear rate of 500/s, followed by a 30 second pause.

- The program then selected on the rheometer was “shear stress”;this allowed for the viscosity to be measured at various shear rates.
- The test was carried out from a shear rate of 1/s to 1000/s over a 300 second period. During this time 50 measurements were taken at 6 second intervals.

4.1.6. Mixing

The mixing of the powders was done using a Fritsch Pulverisette 6 planetary mono mill (Figure 16).This planetary ball mill has a motor-shaft-power of 0.75 kW and is able to operate at speeds of 100 rpm to 650 rpm and perform both wet and dry milling. This mill operates by having a grinding bowl rotate around its own axis while also orbiting around a central axis. This results in forces being exerted on the grinding balls as well as the material which constantly changes direction inside the milling bowl[52]. In the applications for this project, this mill is used to obtain homogeneous mixtures of the materials.



Figure 16: Fritsch Pulverisette 6 planetary ball mill

The samples were mixed in a 250 ml milling bowl with 2 mm grinding balls. The mass ratio of grinding balls to the amount of powder being milled was ≈5 g milling balls to 1 g of powder. The powders were wet milled using hexane as the solvent with the required amount of dispersant as determined in the dispersion studies; the speed used was 300 rpm. The powder and the balls used for the milling were carefully weighed using a mass balance with three decimal places to give 40 g of powder and 200 g of milling balls in each instance. 150 ml of hexane was then added in each instance except for the Al_20_3-50%TiN nanocomposite where 180 ml was used.

There were slight differences between the mixing of the µm-powder and the nanopowdermaterials. In the case of the µm-powders, use was made of a stainless steel milling bowl with a tungsten carbide lining; the mixing was done for two hours using 2 mm alumina balls in order to disperse the materials. The nanopowder materials were mixed using a zirconia milling bowl; the mixing was done for four hours using 2 mm zirconia balls in order to disperse the materials. The reasons for these differences were: to avoid contamination from the tungsten carbide in the nanopowder mixtures, as these powders were milled for a longer period in order to overcome their higher propensity for agglomeration.

4.1.7. Drying

After mixing, the materials were dried in a rotary evaporator. A HeidolphLaborata 4010 digital rotary evaporator was used for this purpose. This equipment dries the mixed sample by heating it up in a round bottom flask which is placed in a warm water bath and is connected to a condenser tube. There is a drawn in the condenser tube which allows for the rapid evaporation of the liquid from the sample. The liquid condenses on the tubes inside the condenser which have cool water running through them. The condensed liquid runs into a second round bottom flask which is also attached to the condenser but is not placed in the warm water bath. The dry powder can then be removed and the liquid from the sample can be discarded.

4.1.8. Sieving

In order to prepare the dried samples for sintering it is required that they are sieved to enable them to flow appropriately during the consolidation process.The powders were sieved consecutively through sieves of 400 μm, 250 μm and 150 μm mesh sizes. The sieves used were 20 cm diameter Retsch®.The sieving operation was carried out in a glove bag under an argon atmosphere. This was done in order to limit the exposure of the materials to air, thus preventing oxidation. The sieved powders were then carefully measured into vials with enough powder to produce sintered samples 20 mm in diameter and 4 mm thick. These samples were then stored under an inert atmosphere whilst waiting to be sintered.

4.1.9. Dispersant Burn-Off

Before the samples can be sintered, it is required that the dispersant present in them be removed.This was done by placing the sieved powders in ceramic boats and inserting them into a tube furnace which was subsequently heated up to 500°C. A heating rate of 5°C/min was used for both the heating and the cooling of the powders and they were held at the burn-off temperature for one hour. The burn-off of the dispersant was done in an inert atmosphere consisting of 5% Hydrogen – Argon gas.

4.2. Sintering

In this section the method and the parameters used to densify the powders will be discussed.

4.2.1. Spark Plasma Sintering

All the powders were sintered using a FCT HP-D5 spark plasma sintering furnace (Figure 17). The samples were sintered using the following set values for the vacuum: a relative gas pressure

of 20 hPa and an absolute gas pressure of 1 hPa. During the heating stages of the process a pulse time of 10 ms with a pause of 5 ms was used.



Figure 17: FCT HP-D5 Spark Plasma Sintering furnace

The heating rate used in the sintering of theμm-powdersand nano Al_2O_3-TiC materials in this project was 250°C/min, slowed down to 100°C/min for the final 100°C before reaching the sintering temperature in order to prevent overshooting.The dwell time used when sintering the materials was 5 minutes. Due to low densifications being obtained in the Al_2O_3-TiN composites, the heating rate for selected samples was lowered in order to observe the effects on densification.

4.3. Characterization

This section aims to discuss the methods used to determine the properties of the sintered samples. It will also discuss the equipment that is required in order for these properties to be determined.

4.3.1. Density

The density of the materials is measured by making use of the Archimedes' principle. The sintered samples were first sand blasted in order to remove any excess graphite foil that was surrounding the sample as a result of the sintering process. The surface of the sample was then wiped down using iso-propanol in order to remove sand and dirt on the surface as a result of the sand blasting process. The density measurements were then performed by first measuring the dry weight of the samples to give W_1. The samples were then boiled in distilled water for 3 hours, and the wet weight (W_2) was determined thereafter. The suspended weight of the samples was then calculated by suspending the samples in distilled water (W_3).

Thus the bulk density and open porosity of the samples was determined using the equations below (as per ASTM C373-88 2006)[53] where ρ_w is the density of water (liquid in which the tests are performed).

$$True\ Volume\ of\ Sample = \frac{W_1 - W_3}{\rho_w}$$

$$True\ Density\ of\ Sample = \frac{W_1 \times \rho_w}{W_1 - W_3}$$

$$Bulk\ Density = \frac{W_1 \times \rho_w}{W_2 - W_3}$$

$$Percent\ Open\ Porosity = \frac{W_2 - W_1}{W_2 - W_3} \times 100$$

By performing three density calculations on two samples over three weeks (once per week), it was seen that the typical error of determination was 0.02 g/cm^3. The bulk densities obtained were

then compared to the theoretical densities of the materials in order to determine the extent of densification. The theoretical densities were calculated using the following equation.

$$\frac{1}{\rho} = \sum_{i=1}^{n} \frac{x_i}{\rho_i}$$

Where;

ρ = Calculated Theoretical Density of the Material (g/cm^3)

x_i = Mass Fraction of Material i

ρ_i = Theoretical Density of the Material i (Al_2O_3=4.0 g/cm^3,TiC=4.9 $g/cm^3$and TiN=5.4 g/cm^3)

4.3.2. Cutting

Once the densities of the samples had been measured they were cut in half in order to examine their cross section. This was done using a Struers Secotom-10 precision cut-off machine. The speed used for the cutting wheel was 3500 rpm and the sample was fed at a rate of 0.015 mm/s. This was the speed recommended by the manufacturer for this particular cutting wheel and the feed rate of the sample was chosen to be 0.015 mm/s as at this speed the load on the cutting wheel is kept to a minimum.

4.3.3. Mounting

One half of the cut sample was then mounted using aStruersCitoPress – 10 sample mounting apparatus. This makes use of a powerful 1000W heating unit which has a heating range of 80°C to 180°C. Its hydraulic system controls the pressure applied with high accuracy. The parameters

that can be individually controlled are the temperature, pressure applied, heating rate and also the cooling rate[54].

PolyFast resin was used to produce the mounted samples which have a 30 mm diameter. Polyfast is made up of a mixture of Bakelite and acarbon filler. This results in the resin being electrically conducting which makes it suitable for samples that require SEM analysis. The PolyFastbuilt-in setting was used when mounting the samples. Each mounting operation lasted for four and a half minutes.

4.3.4. Polishing

The mounted samples were then ground and polished. This was carried out by making use of a Leco Spectrum System 2000. The samples in this project were prepared using a six stage grinding/polishing process. Table 8 summarises the various steps used to grind and polish the samples.

Table 8: Grinding/Polishing process information

Step No.	Disc Used	Grit Size (µm)	Time (min)	Water Used	Suspension used	Diamond Extender Used
1	MD-Piano	220	5	Yes	No	No
2	MD-Piano	1200	30	Yes	No	No
3	MD-Largo	-	20	No	Yes (9 µm diamond)	Yes
4	MD-Dac	-	15	No	Yes (3 µm diamond)	Yes
5	MD-Nap	-	6	No	Yes (1 µm diamond)	Yes
6	MD-Chem	-	2	No	Yes (OPS 0.01 µm silica)	No

All of the grinding/polishing discs were obtained from Struers, as well as the diamond slurry and diamond extender. The process was optimized during the work with the µm-powders and these processing steps were then decided upon. The cross-section of the sintered samples was finely polished down to a grit size of 1 µm using the Struers MD-Nap polishing disc before finally being finished using the 0.01 µm OPS silica suspension. After each step the samples were placed in an ultrasonic bath in order to remove any excess material present on the surface before moving on to the next stage. This resulted in a smooth scratch free surface which was to be used for hardness, fracture toughness and SEM analysis.

4.3.5. Hardness and Fracture Toughness

The hardness and fracture toughness tests were carried out on the polished samples using a Leco V-100-A2 Vickers hardness tester.For the measurement a load of 5 kg was applied over a ten second period.

Hardness

Hardness is a measure of a material's resistance to localized plastic deformation such as a small dent or scratch (Callister, pp.177)[(55)]. The method that was used to determine the hardness values of the various samples was the Vicker's hardness tests. This test makes use of a small diamond indenter, with pyramidal geometry (as shown in Figure 18), which is forced into the material at a chosen load and for a specific indentation time.

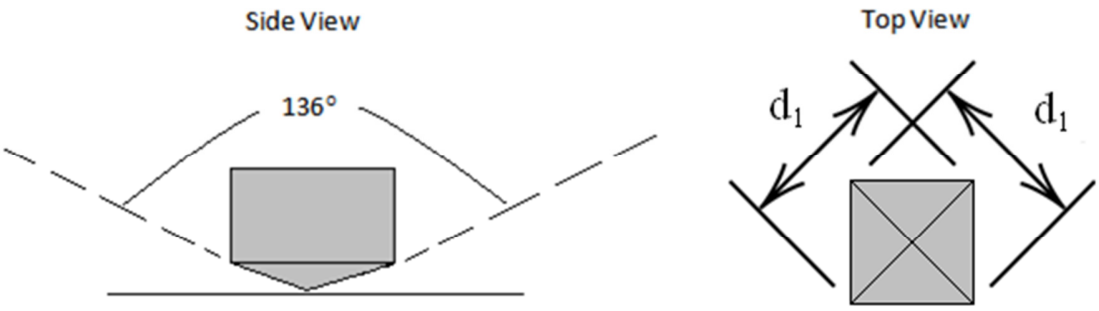


Figure 18: Schematic showing geometry of Vicker's hardness indenter(Callister, pp178)[55]

The hardness test was performed at five different positions on the polished surface of each sample in order for a mean hardness value to be determined. The following formula was used to calculate the hardness values (Callister, pp178)[55].

$$HV = \frac{1.8544 \times P}{d^2}$$

Where;

HV = Vickers Hardness number

P = Load applied (kg)

d = Mean length of diagonals of indentation (mm)

It is then possible to convert the hardness into GPa using the following relationship.

$$H(GPa) = 0.009807\, HV$$

This was done for each of the samples sintered.

Fracture Toughness

The fracture toughness of a brittle material is a measure of its resistance to brittle fracture when a crack is present (Callister, S-46)[55] . The fracture toughness of the samples was then calculated using the half-penny crack method. The cracks initiated from the same indentations used to measure the hardness of the samples were also used for the fracture toughness calculations.The types of crack that were present were investigated by polishing the samples after the indentations were performed. This showed that half-penny cracks were present and thus the Anstis equation was applicable. The fracture toughness was calculated using the following formula[56].

$$K_{IC} = \xi \times \sqrt{\frac{E}{H}} \times \left(\frac{L}{c_{Ave}} \right)^{1.5}$$

Where;

K_{1C} = Fracture Toughness ($MPa.m^{1/2}$)

E = Young's Modulus (GPa)

H = Hardness (GPa)

L = Load (N)

c_{ave} = Average crack length (m)

ξ = 0.016 = 'calibration' constant

5. Results of the Investigation of the Al_2O_3 Composites with µm-powders

The main objective of the µm-powder study is to find a suitable dispersant for use with the materials in this project. Due to the much higher costs involved with the use of nanopowders, the µm-powders were used to determine a suitable dispersant. The powders were then prepared and sintered and the properties analysed. The microstructure of the materials was finally analysed in order to determine the extent of the dispersion of the different phases, ultimately deciding whether this processing technique was suitable for use with the nanopowders.

5.1. Powder Preparation

5.1.1. Particle Size Analysis

The alumina powder was milled with Dolapix CE64 being used as the dispersant and water as the solvent. This produced the following particle size distribution curve where the powder has a d_{10} = 0.142 µm, d_{50} = 0.216 µm and a d_{90} = 0.327 µm.

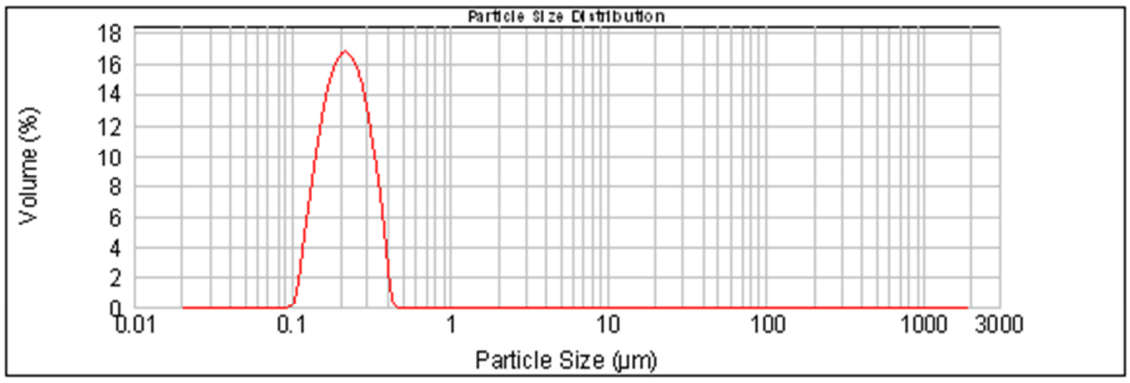


Figure 19: Particle size distribution curve for AKP-50 Alumina after milling in the presence of Dolapix CE64.

The titanium carbide and titanium nitride powders were dispersed using an ultrasonic probe for 5 minutes with iso-propanol as the solvent. The particle size analysis was then performed on each of the powders and the results obtained are shown in Table 9.

Table 9: Results obtained from the particle size analysis on the µm-powders.

Powder	d_{10} (µm)	d_{50} (µm)	d_{90} (µm)
Al_2O_3	0.142	0.216	0.327
TiC	1.365	2.498	5.043
TiN	1.019	2.581	5.653

5.1.2. SEM analysis

SEM analysis was performed on each of the powders being used in the µm-powder study prior to any processing had taken place, in order to confirm the respective particle size of the powders; the resulting micrographs are shown in Figure 20. These micrographs are to be used in conjunction with the particle size analysis reported above, in order to see if the results were in agreement with each other.

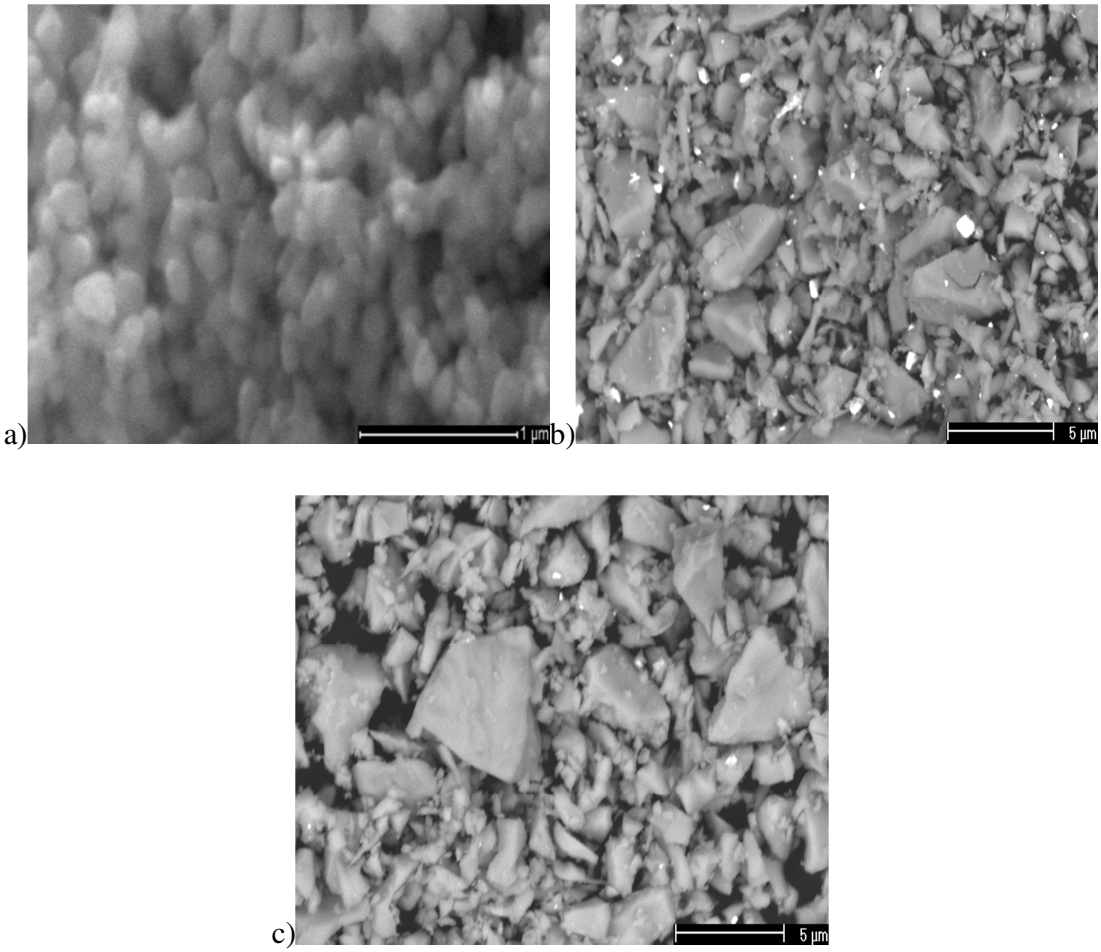


Figure 20:SEM micrographs of a) AKP-50 Al_2O_3 powder, b) titanium carbide powder c) titanium nitride powder; the material with the bright appearance was found to be tungsten carbide by EDS analysis.

5.1.3. XRD analysis

XRD analysis was performed on each of the powders being used in the µm-powder study. From the analysis of the AKP-50 alumina powder, it was seen that the powder contained no impurities and only α-Al_2O_3 was observed.

The XRD pattern shown in Figure 21 was found for the titanium carbide µm-powder.

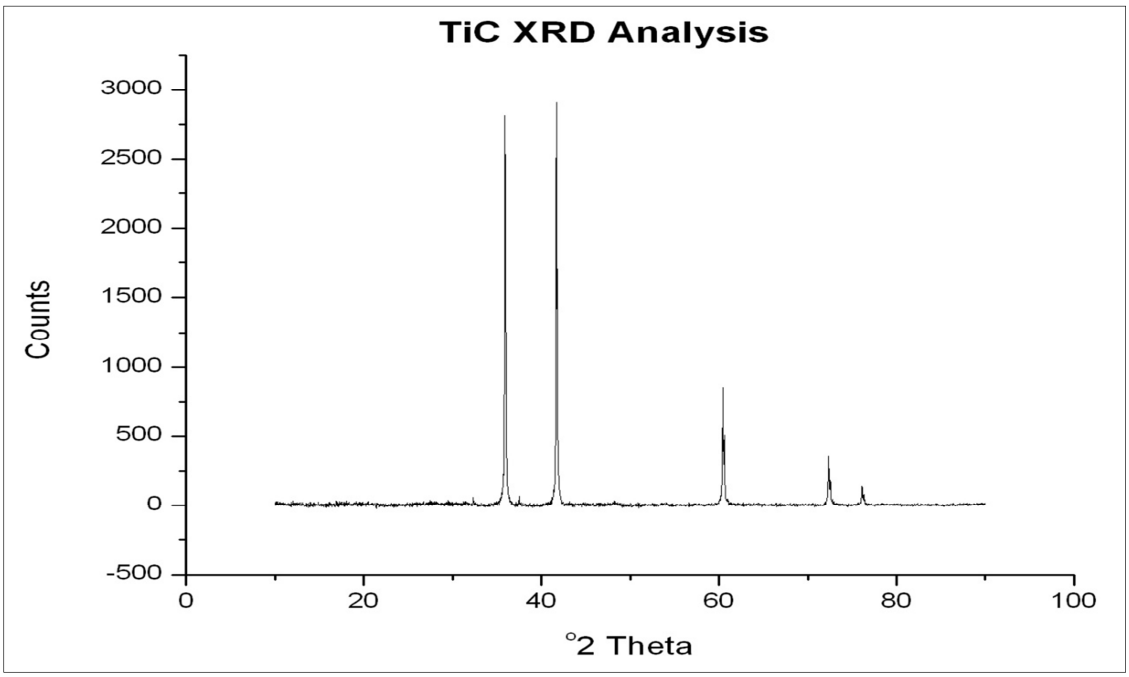


Figure 21:XRD analysis of pure titanium carbide µm-powder as obtained from supplier.

The XRD was analysed and found to be synthetic Khamrabaevite which has a chemical formula of TiC. The XRD pattern in Figure 22 was found for the titanium nitride µm-powder obtained from Element Six.

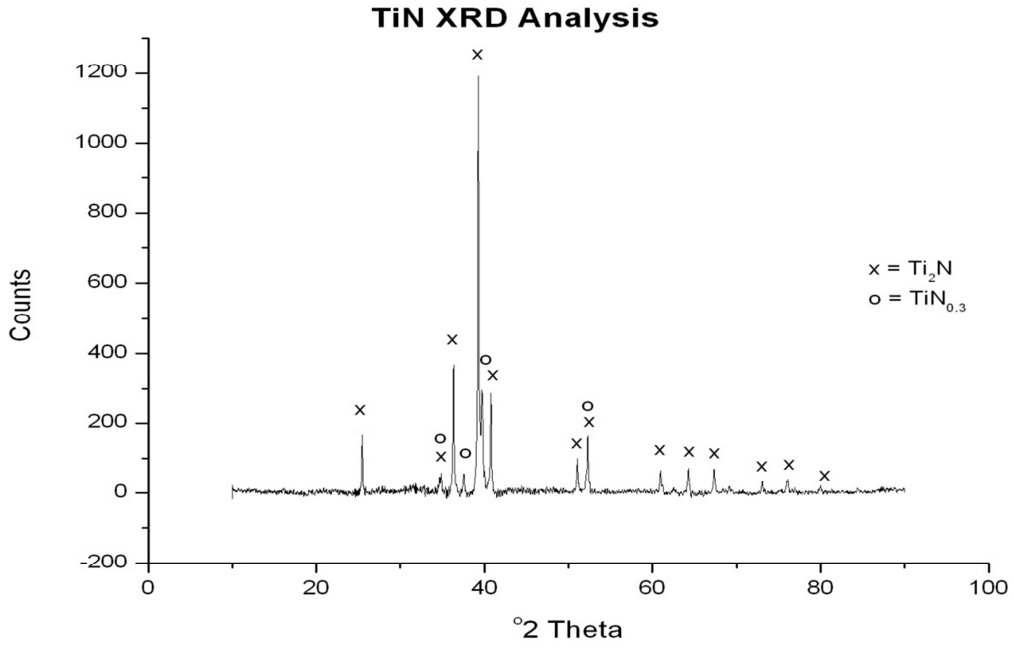


Figure 22:XRD analysis of titanium nitride powder as obtained from supplier.

The analysis of this XRD pattern showed the presence of titanium nitride with a chemical formula of Ti_2N and also titanium nitride with a chemical formula of $TiN_{0.3}$.

5.1.4. BET

The BET analysis that was carried out at the School of Chemistry at the University of the Witwatersrand, gave the following results for each of the µm-powders shown in Table 10.

Table 10: BET analysis on each of the course powders.

Sample	BET SA (m^2/g)
TiN	1.9
TiC	1.9
AKP-50Alumina	11.9

5.1.5. Dispersion

In order to perform the dispersion studies on the composite materials, a suitable dispersant had to be found. The dispersant had to meet the following criteria:

- Disperse each of the powders individually
- Be used in a solvent that would not result in oxidation of the non-oxide powders.

The dispersants investigated were Dolapix CE64, Polyethylene Glycol (PEG) 200, PEG 400, Darvan C and Lubrizol 2155. From these experiments, Lubrizol 2155 was the only dispersant that met the criteria detailed above.Lubrizol 2155 is a succinimide dispersant which has a density of 0.9-0.93 g/cm^3 and a flash point of 160°C. The succinimide group is an organic compound which is made up of a pyrole ring with two carbonyl substitutions and it has a chemical formula $C_4H_5NO_2$[57]. A schematic of the succinimide is shown in Figure 23.

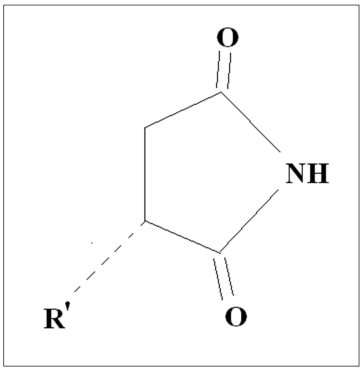
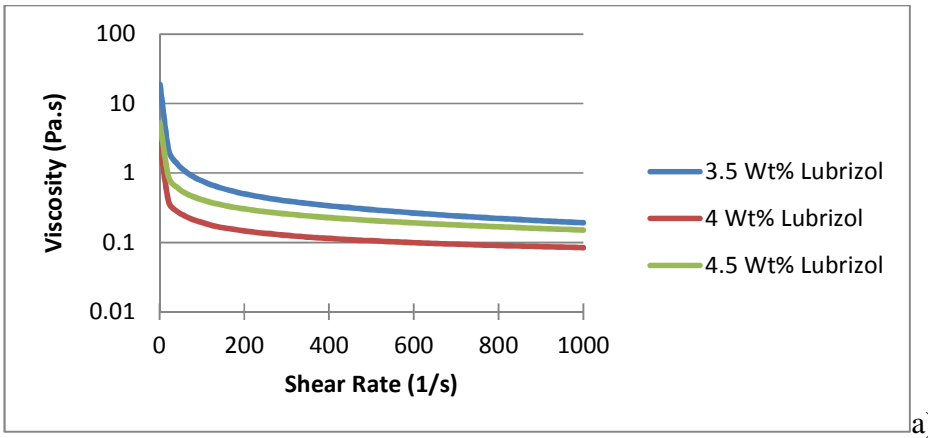


Figure 23: Schematic of a succinimide[58].

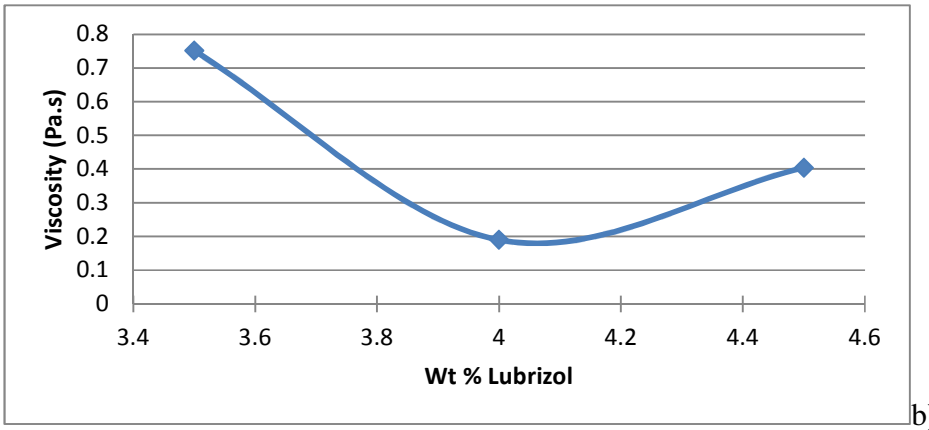
The organic solvent that was found suitable for use with the Lubrizol 2155 dispersant was hexane.

5.1.5.1. µm-Powder Rheology Studies

The rheology studies were then carried out on each of the individual powders. Various amounts of Lubrizol 2155 were added to each of the powders, using hexane as a solvent in order to form a suspension.The rheology studies on the AKP-50 Alumina were carried out using a 50% solids loading by volume with hexane as the dispersant. The Lubrizol 2155 additions to the suspension are shown in weight percent with respect to the solids in the system. The volume of the Lubrizol 2155 was also accounted for in the total volume of the system.



a)



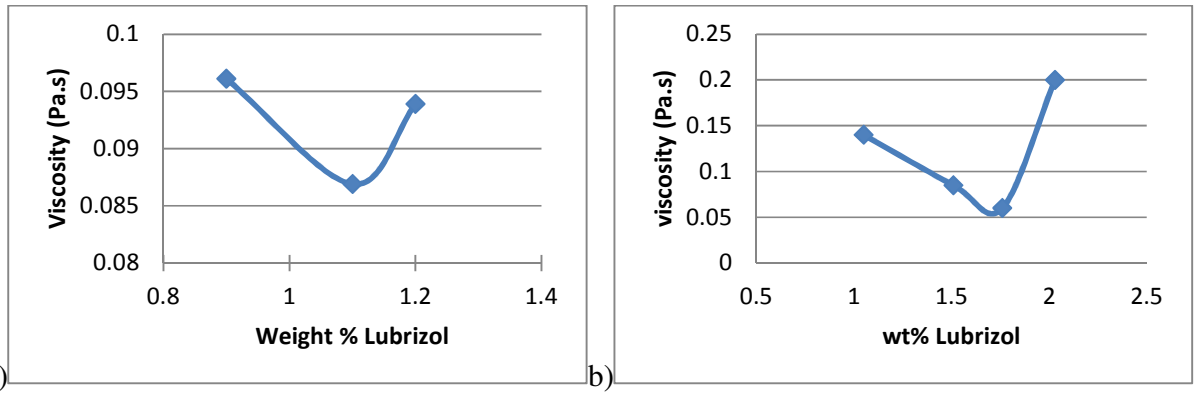
b)

Figure 24: Relationship between viscosity and a) shear rate for AKP-50 Alumina with various concentrations of Lubrizol 2155 and b)the amount of Lubrizol 2155 added at a shear rate of 100/s for the AKP-50 Alumina powder.

From the results shown inFigure 24a), it is possible to determine the optimum amount of dispersant, which results in the lowest viscosity of the suspension. The viscosity was plotted for

each of the Lubrizol 2155 additions at a fixed shear rate of 100/s and is shown in Figure 24b). The results reveal that the optimal amount of Lubrizol 2155 to achieve a stable suspension at these conditions is approximately 4 weight percent.

The rheology studies on the titanium carbide and titanium nitride µm-powders were also carried out using a 50% solids loading by volume with hexane as the dispersant. The Lubrizol 2155 additions to the suspension are shown in weight percent with respect to the solids in the system. The volume of the Lubrizol 2155 was also accounted for in the total volume of the system. The viscosity for each of the Lubrizol 2155 additions at a fixed shear rate of 100/s is shown in Figure 25a) and b).



a) b)

Figure 25: Relationship between viscosity and the amount of Lubrizol 2155 added at a shear rate of 100/s for a) the titanium carbide µm-powder and b) the titanium nitride µm-powder

These results revealed that the optimal amount of Lubrizol 2155 to achieve a stable suspension at these conditions for the titanium carbide µm-powder is approximately 1.1 weight percent, and for the for the titanium nitride µm-powderisapproximately1.7 weight percent.

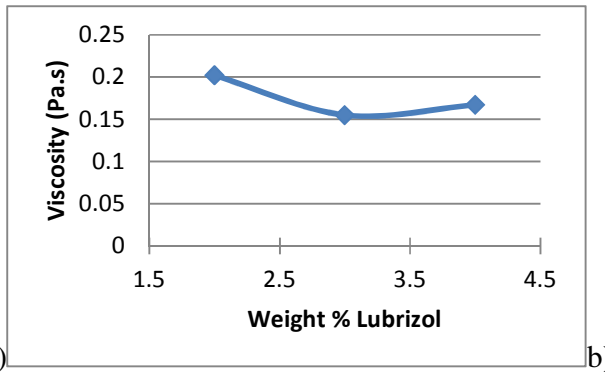
It must be noted that the viscosity values obtained,even at Lubrizol 2155 additions below the optimum, for both the titanium carbide and titanium nitride µm-powders are lower than those obtained for the AKP-50 Alumina powder when it is optimally dispersed.

5.1.5.2. Microcomposite Rheology Studies

The rheology studies on the Al_2O_3-50%TiC microcomposite materials and the Al_2O_3-50%TiN microcomposite materials were carried out using a 50% solids loading by volume with hexane as the dispersant. The Lubrizol 2155 additions to the suspension are shown in weight percent with respect to the solids in the system. The volume of the Lubrizol 2155 was also accounted for in the total volume of the system.

From the results obtained, the viscosity was plotted for each of the Lubrizol 2155 additions at a fixed shear rate of 100/s. The plots are given in Figure 26 a and b) for Al_2O_3-50%TiC and Al_2O_3-50%TiN respectively.

a)



b)

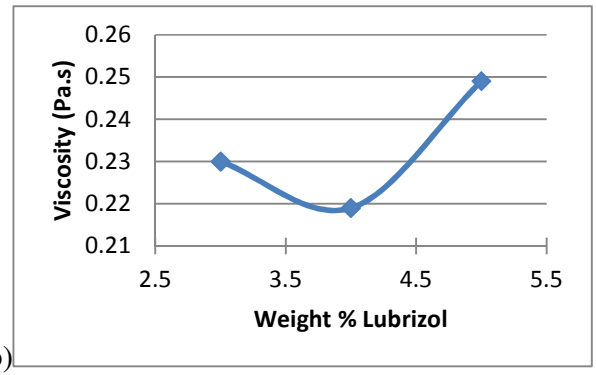


Figure 26: Relationship between viscosity and the amount of Lubrizol 2155 added at a shear rate of 100/s for the a) Al_2O_3-50%TiC microcomposite material and b) the Al_2O_3-50%TiN microcomposite material.

It can be seen from Figure 26 a) that the optimal amount of Lubrizol to achieve a stable suspension for Al_2O_3-50%TiC is approximately 3.2 weight percent. However at Lubrizol 2155 amounts below the optimum, there is not a big change in the viscosity and thus a lower amount of Lubrizol 2155 can be used. Figure 26 b) shows that the optimal amount of Lubrizol 2155 to achieve a stable suspension for Al_2O_3-50%TiN is ±3.5-4.5 weight percent.

5.2. Sintering and Characterization of the composite based µm-powders

The powders were mixed, dried, sieved and the dispersant was burnt off as per the experimental procedure. Once the samples were prepared the powders could then be sintered. Two samples for each of the composite materials being investigated (Al_2O_3-50%TiC and Al_2O_3-50%TiN) were sintered using the spark plasma sintering furnace. The samples all used a heating rate of 250°C/min, a pressure of 30 MPa and were held at the relevant sintering temperature for 5 minutes. The samples were sintered at two different temperatures for each of the composite materials. Table 11summarizes the sintering conditions used for each of the composites. Using the Archimedes' principle method, the density of the sintered samples were obtained, and these results are summarized in Table 12.The relative densities obtained for each of the samples shows that the samples were all acceptably densified using SPS sintering with these conditions.

Table 11: Sintering conditions used for µm-powdersamples.

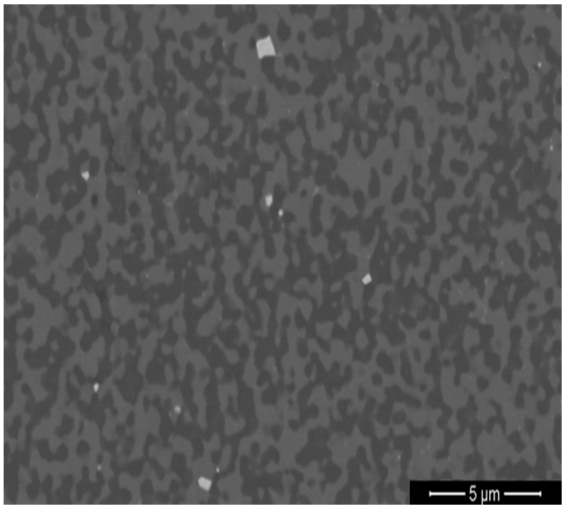
Sample	Volume of reinforcing material (%)	Temperature (°C)	Heating Rate (°C/min)	Pressure (MPa)	Dwell Time (min)
Al_2O_3-TiC	50	1700	250	30	5
Al_2O_3-TiC	50	1600	250	30	5
Al_2O_3-TiN	50	1500	250	30	5
Al_2O_3-TiN	50	1600	250	30	5

Table 12: Density results obtained for sintered samples.

Sample No.	Bulk Density (g/cm^3)	Open Porosity (%)	Relative Density (%)	Theoretical Density (g/cm^3)
1. Al_2O_3-TiC, 1700°C	4.43±0.02	0.53±0.12	99.4	4.46
2. Al_2O_3-TiC, 1600°C	4.44±0.00	0.10±0.03	99.7	4.46
3. Al_2O_3-TiN, 1500°C	4.64±0.01	0.33±0.06	99.0	4.69
4. Al_2O_3-TiN, 1600°C	4.67±0.02	0.10±0.01	99.5	4.69

5.2.1. SEM Analysis

SEM analysis was carried out on both the Al_2O_3-50%TiC and Al_2O_3-50%TiNcomposites in order toestablish the degree of dispersion of the various phases within the sintered samples. The micrographs obtained are shown inFigure 27. The SEM analysis reveals that the mixing of the µm-powders using Lubrizol 2155 as a dispersant for both the Al_2O_3-50%TiC and the Al_2O_3-50%TiN composites is sufficient. Therefore Lubrizol 2155 is an acceptable dispersant for use with the both of the composite materials being investigated. The bright phase that is present within the samples was found to be tungsten carbide contamination during the mixing process. XRD analysis of the Al_2O_3-50%TiN composite showed the presence of α-Al_2O_3 and Ti_2N.

a) 

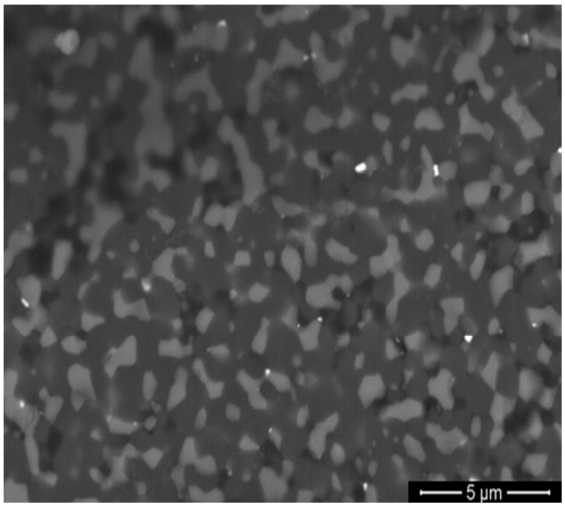
b) 

Figure 27: SEM images showing dispersion of the various phases for the a) Al_2O_3-50%TiC and the b) Al_2O_3-50%TiN composites.

5.2.2. Hardness and Fracture Toughness

Once the densities of the samples had been determined, they were cut, mounted and polished as per the procedures discussed in the experimental design. Hardness and fracture toughness tests were then performed using the Vicker's hardness testing equipment. The results of these tests are shown in Table 13.

Table 13: Summary of Hardness and Fracture Toughness Results

Sample	Relative Density	Hardness	Fracture Toughness
1. Al_2O_3-TiC, 1700°C	99.4	19.1±1.1	3.8±0.3
2. Al_2O_3-TiC, 1600°C	99.7	19.4±0.9	3.7±0.3
3. Al_2O_3-TiN, 1500°C	99.0	18.7±0.6	3.8±0.3
4. Al_2O_3-TiN, 1600°C	99.5	18.1±1.3	3.1±0.3

6. Discussion of the Results Concerning the µm-composites

6.1. Rheology of the suspensions

The particle size analysis curves for each of the materials correspond to each of the respective SEM micrographs of the pure powders. Thus the AKP-50 Alumina is over ten times smaller than both the TiN and TiC. The TiC and TiN powders are approximately the same size and this is confirmed with the BET analysis which shows them both to have a specific surface area (SSA) of 1.9 m^2/g. Due to the smaller size of the alumina powder the SSA is much higher at 11.9 m^2/g, as expected. As a result of this, it is expected that the alumina powder will require a larger amount of dispersant than the other materials as there is a larger surface area of particles that need to be coated by the dispersant in order to disperse the powders effectively. The Lubrizol 2155 requirements are also dependent on the force /degree of adsorption.The rheology results obtained from the Al_2O_3-50%TiC and Al_2O_3-50%TiN suspensions are shown in comparison to the pure alumina suspension in Figure 28.

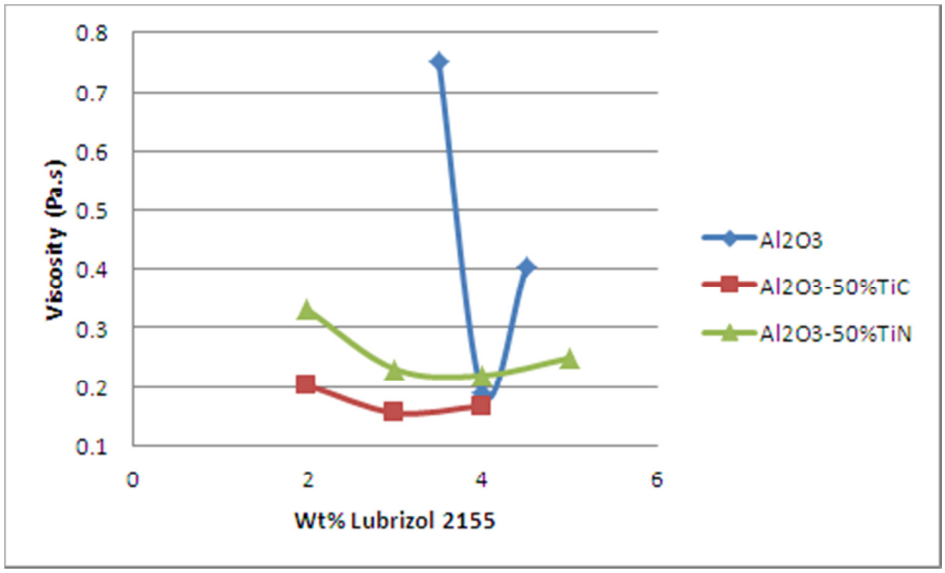


Figure 28: Comparison of the viscosity of the composites to the pure AKP50 alumina suspension.

It is evident that the addition of titanium carbide and titanium nitride into alumina each results in each of the suspensions requiring less Lubrizol 2155 in order to form a stable suspension. From this it was also clear that at lower additions of Lubrizol 2155 the viscosity was significantly lower in the mixtures compared to the pure alumina and also the curve was not as steep when approaching the minimum when working with the mixtures.

Table 14shows a comparison between the surface area of the powders used and the weight percentage of the dispersant Lubrizol at the minimum viscosity. This was then used to determine the mass of Lubrizol 2155 required per unit area of each of the powders.

Table 14: Comparison between the weight percentage of Lubrizol and the surface areas of the powders

Sample	BET SA (m^2/g)	Solid Loading (Volume %)	Lubrizol at minimum viscosity (wt %)	Mass Lubrizol per unit area powder (mg/m^2)
TiN	1.9	50	1.7	8.9
TiC	1.9	50	1.1	5.8
Alumina AKP-50	11.9	50	4	3.4

From these results, it is seen that as the surface area of the material increased there was a general trend that the amount of Lubrizol 2155 required also increased. It must be noted that the material itself also had an effect on the amount of Lubrizol 2155 that was required, as was evident from the fact that whereas TiC and TiN have the same specific surface area, the TiN required more Lubrizol 2155 than the TiC to produce a stable suspension. This was possibly due to the degree of adsorption of the Lubrizol 2155 onto the surface of the TiN being lower than that of the TiC at the same concentration.

6.2. Properties

From the hardness and fracture toughness results for the samples prepared from the µm-powders, it is evident that the hardness values for the materials correspond to those for samples of a similar composition in literature, as shown in Table 5, where the Al_2O_3-TiC containing composites have a hardness of 19 – 23 GPa and a fracture toughness of 3.6 - 4.5 MPa.$m^{0.5}$; the µm-composites sinteredin this work were seen to have a hardness of 19.6 GPa and a fracture toughness of 3.8 MPa.$m^{0.5}$.From Table 5 the Al_2O_3-TiN containing composites are reported to have a hardness of 17.7 – 22 GPa and a fracture toughness of 4 – 5.7 MPa.$m^{0.5}$, while the µm-composites sintered in this work were seen to have a hardness of 18.7 GPa and a fracture toughness of 3.8 MPa.$m^{0.5}$. The fracture toughness of the sintered composites are close to the lower limits of the values reported in literature. This is possibly due to the large starting particle size of the titanium carbide and titanium nitride µm-powders respectively.

From the SEM analysis of the sintered samples it is clear that the powders were sufficiently dispersed before sintering. As a result of this, Lubrizol 2155 appears to be an acceptable dispersant for this project.

7. Results of the investigation of the nanocomposites

7.1. Powder Processing

Once the powders were received, a number of characterisation steps were taken. Table 15 summarises the results obtained during the powder characterization stage and compares them to those that were provided by the suppliers.

Table 15: Summary of the properties of the powder obtained compared to those provided by the supplier.

Properties	Al_2O_3		TiC		TiN	
	Supplier	Obtained	Supplier	Obtained	Supplier	Obtained
Average Particle Size (nm)	100	95.1	40	39.4	20	25.4
Specific Surface Area (m^2/g)	14.5	14.7	25-35	23.7	40-55	61.3
Oxygen (%)	-	-	< 1	3.5	< 3	8.4

7.1.1. SEM Analysis

SEM analysis was performed on each of the powders being used in the nanopowder study prior to any processing had taken place in order to get an idea of the respective grain size of the materials. The SEM images are given in Figure 29.

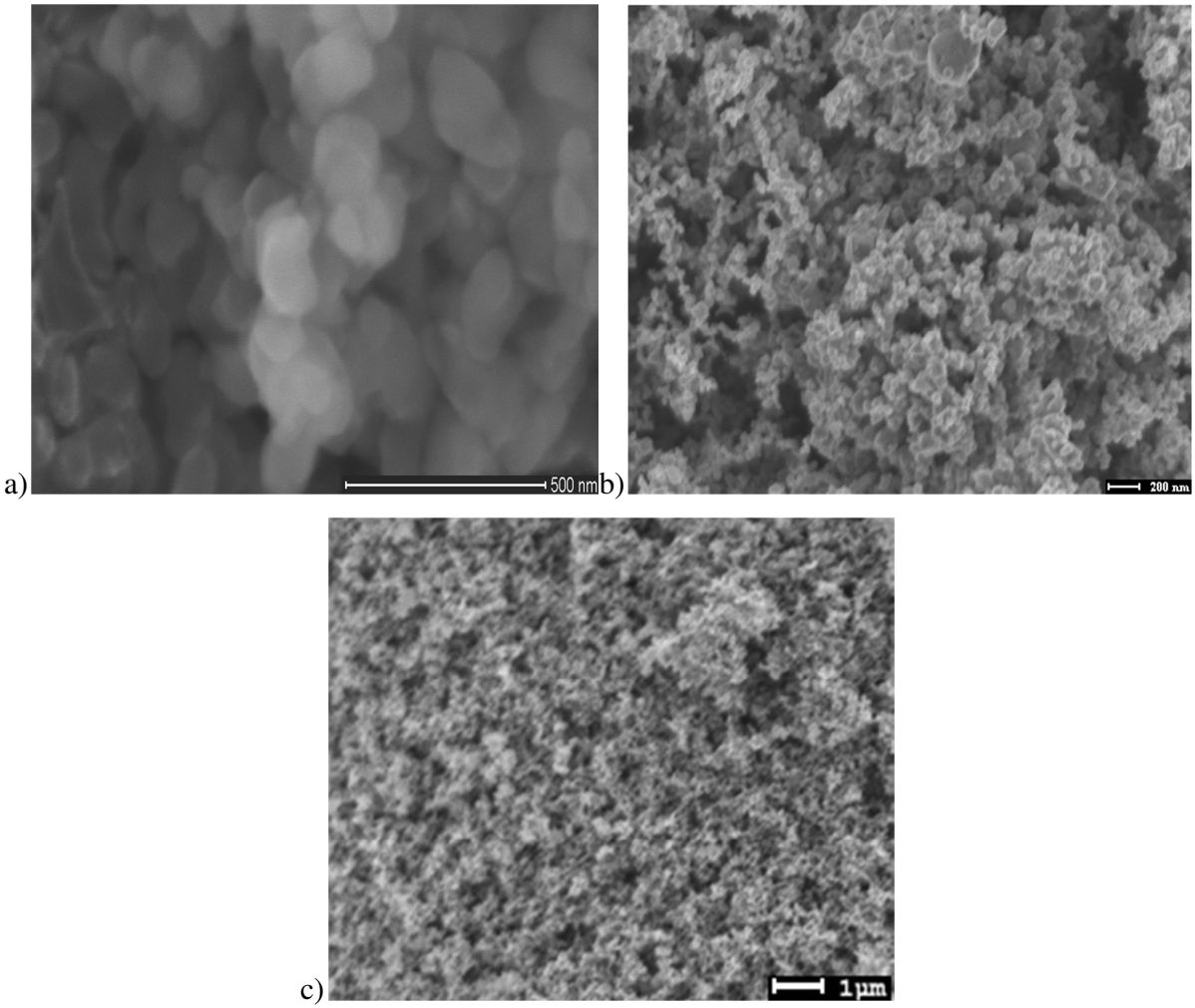


Figure 29:SEM micrograph of a) TM-DAR Alumina powder, b) ABCR AB255319 TiCnanopowder and c) ABCR AB255327 TiNnanopowder.

7.1.2. XRD analysis

XRD analysis was then performed on each of the nanopowders to be used in this project. Analysis of the TM-DAR alumina showed that the powder consisted only of α-Al_2O_3. Figure 30 shows the XRD diffractograms that were obtained from the analysis of the TiC and the TiN nanopowders. Analysis of these diffractograms showed that the TiC nanopowder contains only synthetic Khamrabaevite which has a chemical formula of TiC. It was also found that the TiN nanopowder contained only synthetic Osbornite which has a chemical formula of TiN.

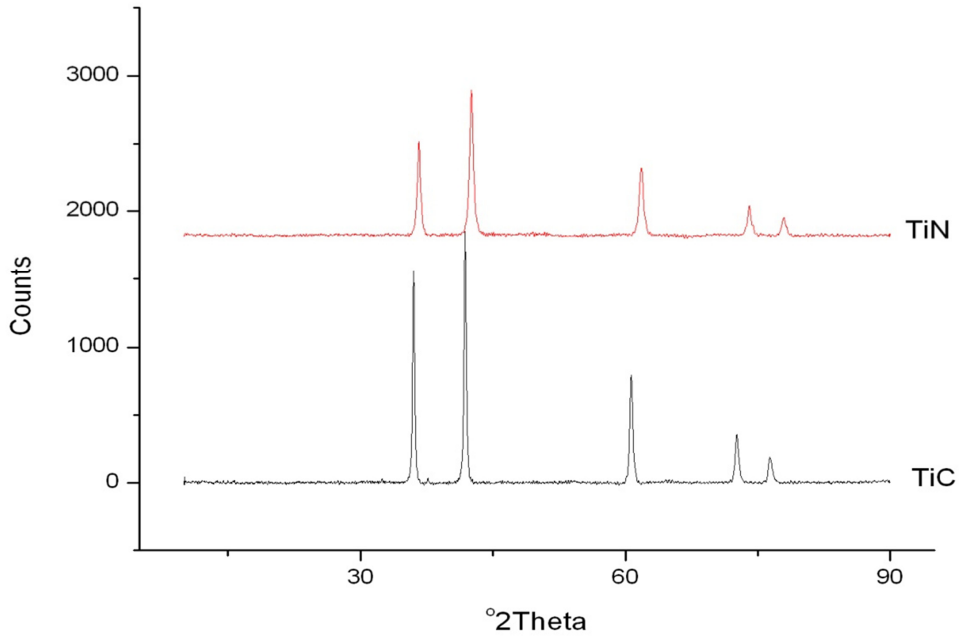


Figure 30:XRD analysis of the pure titanium carbide and titanium nitride nanopowders as obtained from the supplier.

7.1.3. BET

The BET analysis was carried out gave the results shown in Table 16.

Table 16: BET analysis on each of the nanopowders compared to the data received from the supplier.

Sample	Surface Area(m^2/g)	
	Obtained	**From Supplier**
Al_2O_3	14.7	14.5
TiC	23.7	25-35
TiN	61.3	40-55

It is evident from these results that the TM-DAR alumina powder has a SSA that is similar to that provided by the supplier, whilst the SSA of the TiC is lower and that of the TiN is higher than those provided by the supplier.

7.1.4. Particle Size Analysis

Particle size analysis was only performed after the dispersion studies as the powders needed to be properly dispersed in order to obtain an accurate particle size distribution from the Malvern Zetasizer. Table 17 shows the sizes of the particles measured using the zetasizer; this is also compared to the sizes claimed by the relevant suppliers. The duration that the powders were mixed for in order to fully disperse them is also shown. It is clear from these results that the particle sizes measured are all relatively close to those claimed by the various suppliers for each of the powders. It is also evident that the time required in order to fully disperse the powder increases as the particle size decreases. This is expected as the propensity for agglomeration increases with decreasing particle size as discussed previously.

Table 17: Comparison of measured d_{50}particle size to that claimed by the supplier.

Material	Particle Size (nm)		Time of dispersion (Hr)
	Measured	From Supplier	
Al_2O_3	95.1	100	2
TiC	39.4	40	3
TiN	25.4	20	4

7.1.5. Oxygen Content of the Powder

It was required to determine the amount of oxygen present in the starting titanium carbide and titanium nitride nanopowders as they are sensitive to oxygen contamination which will affect the expected densities of the materials. This was done by performing Leco oxygen sensitivity

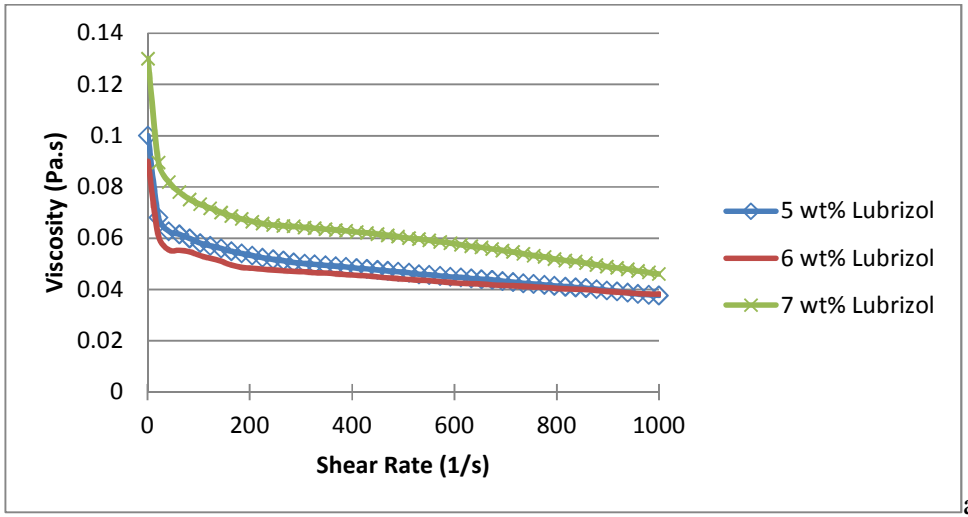
experiments on the powder; these tests were run at Anglo Research. From these results, the TiC powder was found to contain 3.54 weight percent oxygen and the titanium nitride powder 8.44 weight percent oxygen.

7.1.6. Preparation and Properties of the Dispersion

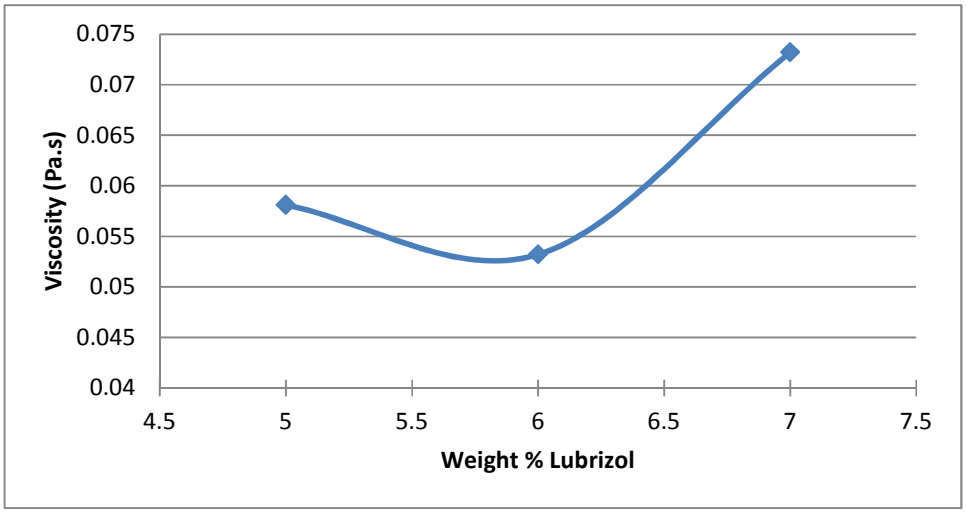
From the work on the µm-powders, Lubrizol 2155 was found to be a suitable dispersant for the materials being investigated. As a result, this was the only dispersant that was used to perform the rheological studies on the nanopowders.

7.1.6.1. Dispersion of individual nanopowders

Rheology studies were carried out on each of the individual nanopowder materials. The Lubrizol 2155 additions to the suspension are shown in weight percent with respect to the solids in the system; the volume of the Lubrizol 2155 was also accounted for in the total volume of the system. The rheology studies on the TM-DAR Al_2O_3suspension were carried out using a 40% solids loading by volume with hexane as the solvent and using Lubrizol 2155 as the dispersant.



a)



b)

Figure 31: a) Comparison of viscosity at shear rates up to 1000/s for various additions of Lubrizol 2155 for the TM-DAR alumina nanopowder and b) the relationship between viscosity and the amount of Lubrizol 2155 added at a shear rate of 100/s for the TM-DAR alumina powder.

In Figure 31 a), the viscosity is plotted for each of the Lubrizol 2155 additions as a function of shear rate.Figure 31 b) shows the viscosity plotted as a function of Lubrizol 2155 addition to the TM-DAR alumina suspension for a fixed shear rate of 100/s.

These results show that the optimum amount of Lubrizol 2155 for the TM-DAR Alumina is approximately 6 weight percent. It must be noted that the viscosities obtained for the suspension

at the various Lubrizol 2155 additions are approximately a factor of four lower than those obtained for the AKP-50 alumina that was investigated in the µm-powder study. It must however be noted that different solids loading amounts were used in each case. This does however suggest that even lower Lubrizol 2155 amounts can be used to disperse the alumina nanopowder to produce a similar result to that obtained for the AKP-50 alumina.

The rheology studies on the ABCR AB255319TiCand the ABCR AB255327 TiN nanopowders were carried out using a 15% solids loading and a 3.2% solids loading respectively. Once again the solvent used was hexane with Lubrizol 2155 as the dispersant. From the results of the rheology experiments, the viscosity was plotted for each of the Lubrizol 2155 additions at a fixed shear rate of 100/s for both the TiC and the TiN nanopowder suspensions (Figures 32a) and 32b) respectively).

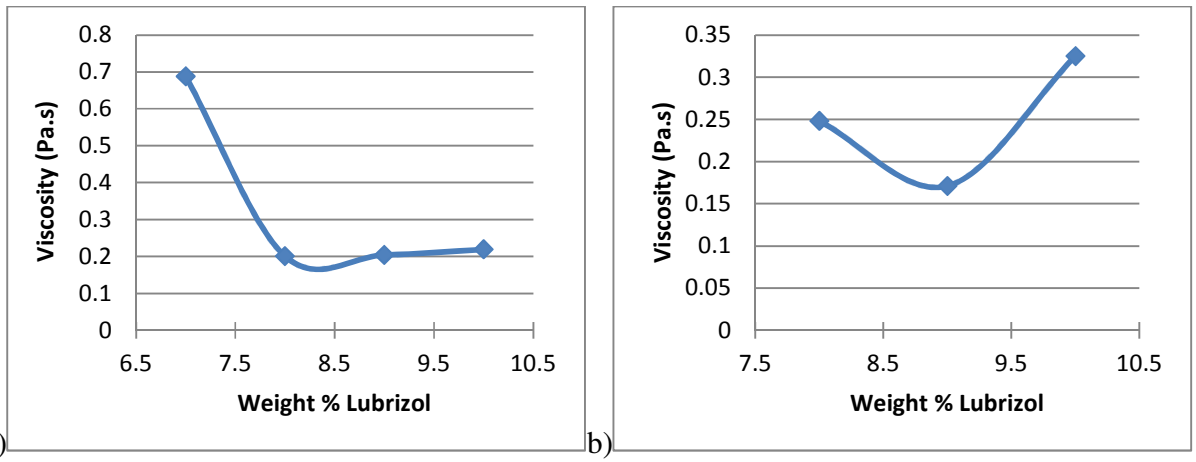


Figure 32: Relationship between viscosity and the amount of Lubrizol 2155 added at a shear rate of 100/s for the a) nanoTiC suspension and b)nanoTiN suspension.

From these results it is evident that the amount of Lubrizol 2155 required to optimally disperse the titanium carbide nanopowder is 8.3 weight percent; also from figure 32b) it is evident that the titanium nitride nanopowder suspension requires 9 weight percent of Lubrizol 2155.

7.1.6.2. Rheology of nanocomposite suspensions

For the studies on the Al_2O_3-TiC and the Al_2O_3-TiN suspensions, the expected amount of Lubrizol 2155 required was calculated to be the sum of the amount required for each of the individual powders in the suspension. An expected solid loading was also calculated using the solids loading used for the individual powders and weighting them with respect to their volume fraction in the composite suspension. The solids loadings were found to be too high in order to form suspensions for the rheology tests and as a result, the solid loadings of each of the systems was lowered in order to obtain a suspension that could be dispersed and the experiments performed.

7.1.6.2.1. Rheology of the Alumina – Titanium Carbide nanosuspensions

The rheology studies were carried out on the Al_2O_3-10% TiC and the Al_2O_3-50% TiC suspensions using a 30% and a 22.5% solids loading respectively. Lubrizol 2155was used as the dispersant and hexane as the solvent. Figure 33shows the viscosity of these suspensions as a function of added Lubrizol2155.It can be seen that when the fraction of titanium carbide is increased, a greater amount of Lubrizol 2155 is required in order to effectively disperse the powders. It is seen that the Al_2O_3-10% TiC suspension requires 6 weight percent Lubrizol 2155 and the Al_2O_3-50% TiC suspension requires 7.3 weight percent in order to be optimally dispersed. It must be noted that the optimal amount of Lubrizol 2155 required to disperse the Al_2O_3-10% TiC could be as low as 5 weight percent due to the errors associated with the experiments. However there was a significant increase in the viscosity when less than 5 weight percent dispersant was used.

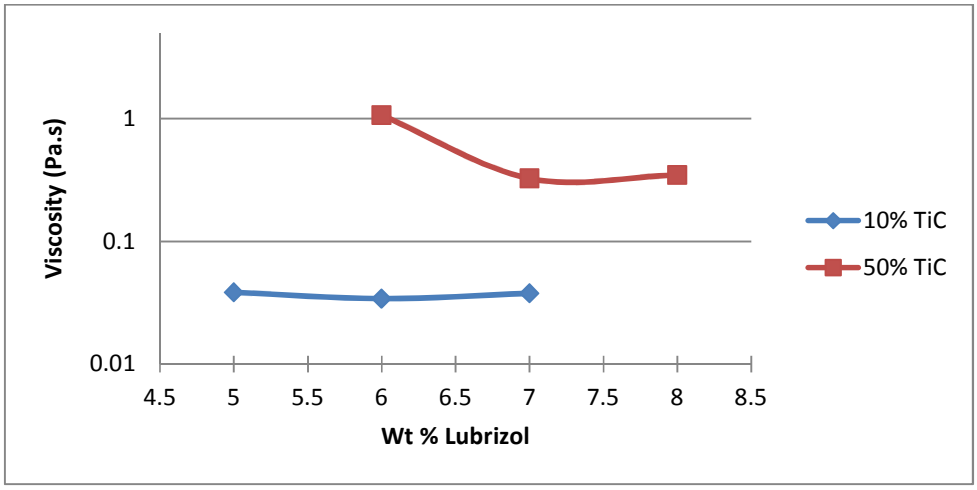


Figure 33: Relationship between viscosity and the amount of Lubrizol 2155 added at a shear rate of 100/s for both the Al_2O_3-10%TiC and the Al_2O_3-50%TiC composite suspensions.

7.1.6.2.2. Rheology of the Alumina – Titanium Nitride nanosuspension

The rheology studies on the Al_2O_3-10% TiN suspension and the Al_2O_3-50% TiN suspension were carried out using a 27.3% and a 5% solids loading respectively. The dispersant used was Lubrizol 2155 in conjunction with hexane as the solvent. Figure 34shows the viscosity of these suspensions, plotted as a function of the dispersant added, for a shear rate 100/s.

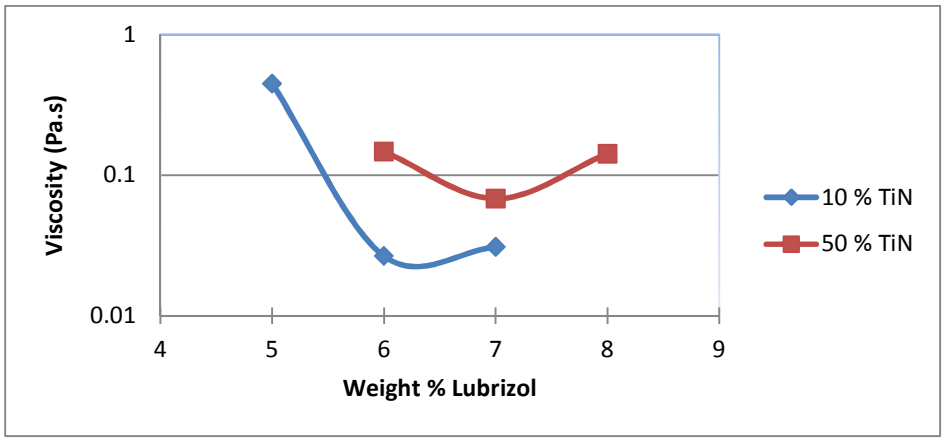


Figure 34: Relationship between viscosity and the amount of Lubrizol 2155 added at a shear rate of 100/s for both the Al_2O_3-10%TiN and the Al_2O_3-50%TiN composite suspensions.

These results show that the optimum amount of Lubrizol 2155 required to disperse the Al_2O_3-10% TiN suspension is approximately 6 weight percent and to disperse the Al_2O_3-50% TiN suspension, approximately 7 weight percent of Lubrizol 2155 is required. The results show that when the amount of titanium nitride is increased, a greater amount of Lubrizol 2155 is required in order to effectively disperse the powders. This is especially evident in the low solid loading that was required in order to disperse the Al_2O_3-50% TiN suspension.

7.1.7. Burning off of Dispersant

The samples were mixed, dried and sieved as per the experimental design. The Lubrizol 2155 dispersant that was remaining in the samples was then burnt off in the tube furnace as per the experimental design. The powders were weighed before and after burn-off in order to determine the effectiveness of the process. The change in weight was then compared to the original addition of Lubrizol 2155 to the suspension in order to determine the amount that was removed during the burn-off process. The main reason for this was to remove as much of the Lubrizol 2155 present as possible before the sintering process. If the burn-off of the dispersant was ineffective there was a risk of the sample outgassing during sintering, which would not only result in loss of the sample but could also cause failure of the dies during the sintering process.

A comparison between the Lubrizol 2155 burnt off in each of the titanium carbide and titanium nitride composites is shown in Figure 35.

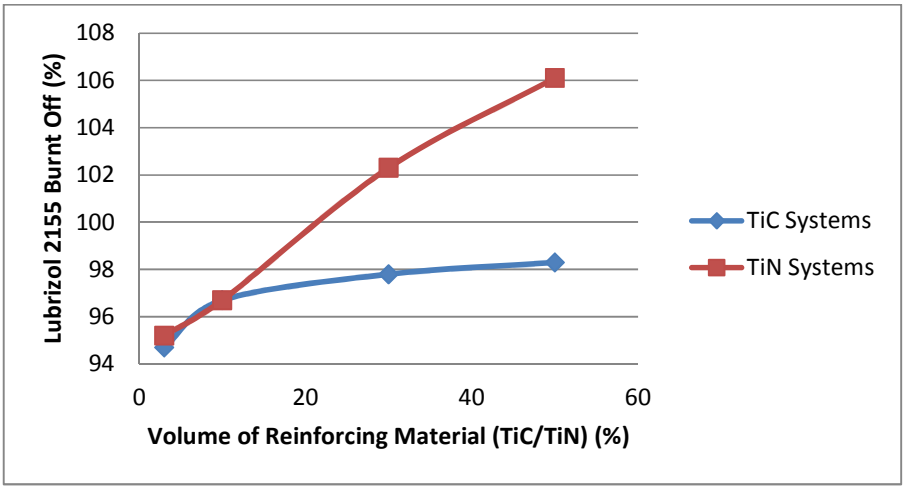


Figure 35: Comparison of effective Lubrizol 2155 burn-off between the Al_2O_3-TiC and Al_2O_3-TiN samples.

From this comparison between the TiC and TiN containing samples, it is obvious that for the samples with 3% and 10% of the reinforcing components (TiC/TiN), the amount of the Lubrizol 2155 burnt off is similar. However, it must be noted that there is a significant difference between the samples containing 30% and 50% of the reinforcing components. The Al_2O_3-30% TiN and the Al_2O_3-50% TiN powders show that over 100% of the dispersant is burnt off, but it is suspected that the actual amounts burnt off are similar to the Al_2O_3-30% TiC and the Al_2O_3-50% TiC powders. The results showing that over 100% of the Lubrizol 2155 is burnt off is suspected to be due to powder losses as a result of the gas flowing over the powder, removing some of the powder from the ceramic boat in which it is placed. This is due to the titanium nitride being very fine and "fluffy" powder.

7.2. Sintering and Characterization of the Alumina – Titanium Carbide nanocomposites

The samples were all sintered using a spark plasma sintering furnace. The sintering took place in the range of 1500°C and 1800°C, at pressures of 30 MPa and 50 MPa. The heating rate that was used in each case was 250°C/min. The sintered Al_2O_3-TiC samples were then characterized by

measuring the density, hardness and the fracture toughness of the materials. The results are shown in Table 18. SEM and XRD analyses were also carried out on the samples in order to better understand the properties of the various materials.

Table 18: Properties obtained for the Al_2O_3-TiC samples using various sintering conditions

Sample	Temperature (°C)	Pressure (MPa)	Bulk Density (g/cm^3)	Open Porosity (%)	Relative Density (%)	Hardness (GPa)	Fracture Toughness ($MPa.m^{1/2}$)
Al_2O_3-3% TiC	1600	30	3.99±0.01	0.03±0.02	99.1±0.2	19.0±0.7	2.7±0.2
Al_2O_3-3% TiC	1700	30	4.00±0.01	0.02±0.01	99.4±0.2	18.9±0.4	2.8±0.1
Al_2O_3-3% TiC	1800	30	4.00±0.01	0.03±0.00	99.2±0.2	18.8±0.2	3.0±0.2
Al_2O_3-3% TiC	1500	50	4.01±0.00	0.01±0.00	99.4±0.0	21.2±0.6	2.4±0.1
Al_2O_3-3% TiC	1600	50	4.00±0.01	0.01±0.01	99.4±0.2	20.3±0.5	2.5±0.1
Al_2O_3-3% TiC	1700	50	4.01±0.01	0.02±0.01	99.5±0.2	19.2±0.4	2.6±0.2
Al_2O_3-10% TiC	1600	30	4.04±0.01	0.03±0.02	98.6±0.2	20.3±0.4	2.6±0.1
Al_2O_3-10% TiC	1700	30	4.04±0.00	0.00±0.00	98.8±0.0	19.5±0.5	2.6±0.1
Al_2O_3-10% TiC	1800	30	4.05±0.01	0.01±0.01	98.8±0.2	17.9±0.1	3.1±0.3
Al_2O_3-10% TiC	1500	50	4.02±0.03	0.00±0.00	98.3±0.7	21.0±0.2	2.5±0.1
Al_2O_3-10% TiC	1600	50	4.05±0.02	0.00±0.02	98.9±0.5	20.0±0.2	2.7±0.2
Al_2O_3-10% TiC	1700	50	4.04±0.01	0.00±0.00	98.8±0.2	19.7±0.5	2.5±0.1
Al_2O_3-30% TiC	1600	30	4.03±0.02	3.85±0.21	94.2±0.5	15.7±0.4	2.9±0.2
Al_2O_3-30% TiC	1700	30	4.07±0.04	2.80±0.15	95.2±0.9	17.3±0.3	2.7±0.2
Al_2O_3-30% TiC	1800	30	4.08±0.02	2.42±0.07	95.4±0.5	18.3±0.2	2.7±0.1
Al_2O_3-30% TiC	1500	50	4.05±0.03	3.60±0.30	94.7±0.7	18.9±0.4	2.6±0.0
Al_2O_3-30% TiC	1600	50	4.12±0.01	1.27±0.07	96.2±0.2	20.0±0.2	2.7±0.2
Al_2O_3-30% TiC	1700	50	4.13±0.05	0.84±0.12	96.6±1.2	20.3±0.3	2.7±0.1
Al_2O_3-50% TiC	1500	50	4.10±0.03	5.54±0.26	91.7±0.7	13.5±0.2	2.2±0.1
Al_2O_3-50% TiC	1600	50	4.15±0.02	3.29±0.19	93.0±0.4	15.8±0.2	2.2±0.1
Al_2O_3-50% TiC	1700	50	4.18±0.05	2.66±0.08	93.6±1.1	23.1±0.3	2.6±0.1
Al_2O_3-50% TiC	1800	50	4.24±0.02	1.59±0.16	95.0±0.4	19±0.5	2.8±0.3

Once the samples were sintered, the first property investigated was the density of the relevant samples. This was then compared to the theoretical density of each of the composite samples. These were calculated as per the method described in the experimental procedure and are shown in Table 19. The theoretical density used for the alumina powder was 4 g/cm^3(Kim, 2009)[59]and that used for the titanium carbide nanopowder was 4.93 g/cm^3, as given by the supplier.

Table 19: Theoretical densities of the Al_2O_3-TiC samples not taking into account the oxygen content

Sample	Al_2O_3-3% TiC	Al_2O_3-10% TiC	Al_2O_3-30% TiC	Al_2O_3-50% TiC
Theoretical Density (g/cm^3)	4.028	4.093	4.279	4.465

The samples were cut, mounted and polished as per the experimental design. The finely polished samples then underwent hardness and fracture toughness tests in order to determine whether the properties of the materials were significantly improved when working with the nanopowders. The hardness and the fracture toughness values were then calculated as per the methods described in the experimental design using the Vickers indentation equipment.

From the results in Table 18, it is evident that all of the conditions used for sintering the Al_2O_3-3% TiC and the Al_2O_3-10% TiC composites produced samples that were fully dense. It is also seen that all of the conditions that were used to sinter the Al_2O_3-30% TiC samples produced samples with densities that appear to be insufficiently dense. The samples were sintered at 50 MPa since sintering pressures of 30 MPa gave samples which were even less dense.

7.2.1. XRD Analysis

XRD analysis was performed on each of the compositions of the sintered Al_2O_3-TiC samples. Figure 36 shows the results obtained for each of the Al_2O_3-TiC samples.

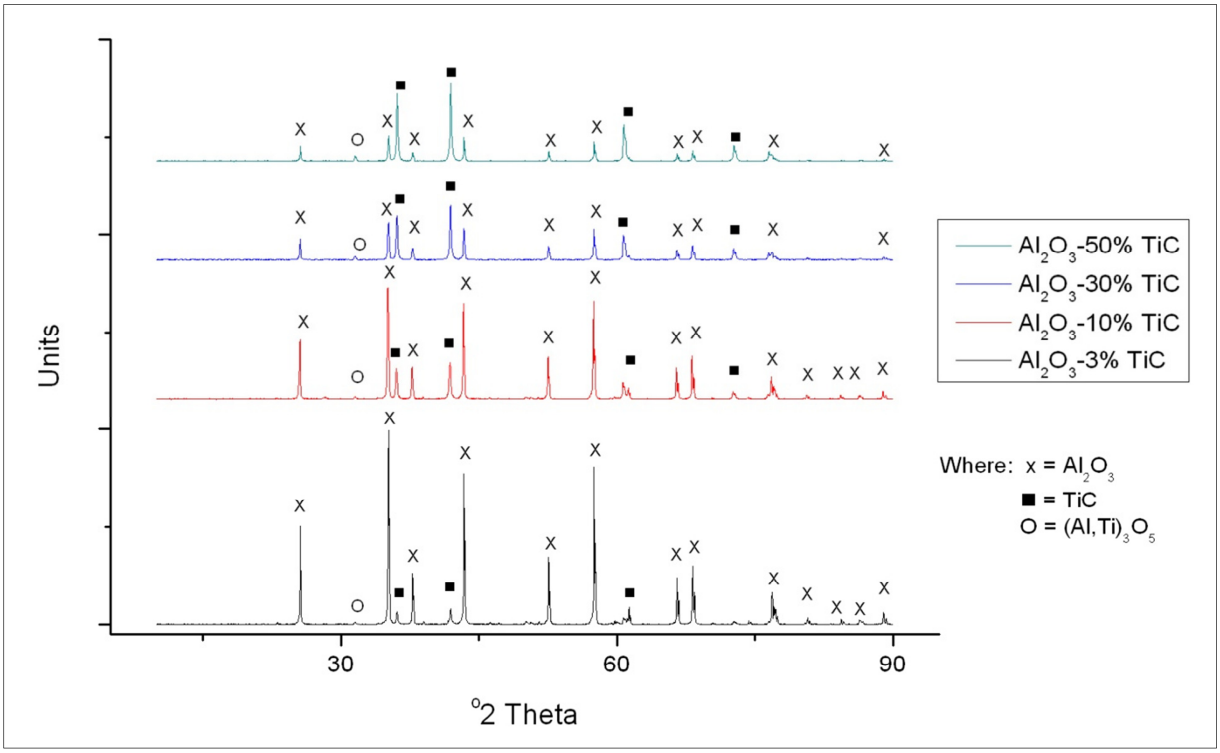


Figure 36: XRD analysis comparing each composition of Al_2O_3-TiC that was sintered at 1700°C and 50 MPa.

From these results, it is evident that there was a titanium oxide containing phase present in each of the sintered Al_2O_3-TiC samples. This was found to be a solid solution between Ti_3O_5 and $AlTi_2O_5$, and was determined to be $(Al,Ti)_3O_5$. The effect of increasing the TiC, which was determined to be synthetic Khamrabaevite, on the various composites is observed in Figure 36. As the amount of TiC was increased, the intensity of the α-Al_2O_3 begins to decrease as was expected. It is also clear from the XRD analysis that with increased TiC composition, the amount of $(Al,Ti)_3O_5$ that was present clearly increased.

The lattice parameters of the pure TiC powder and the TiC in the Al_2O_3-50%TiC composite sintered at 1700°C and 50 MPa, are shown in Figure 37. The lattice parameters were calculated as per the experimental procedure.

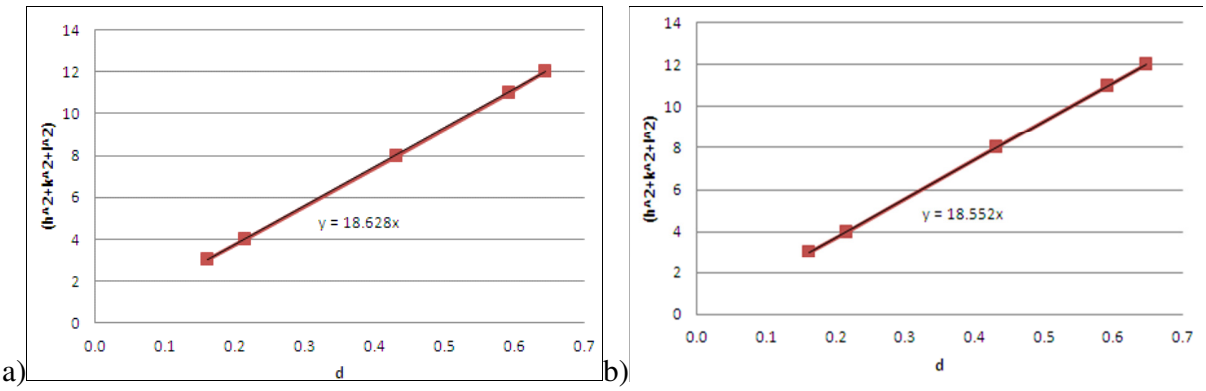


Figure 37: Calculation of the TiC lattice parameters in a) the pure TiC powder and b) the Al_2O_3-50%TiC composite sintered at 1700°C and 50 MPa.

By taking the square root of the gradients in each curve, it is possible to obtain the lattice parameters in each case. This showed that the TiC lattice parameter in the pure TiC powder was 4.316±0.005Å and in the Al_2O_3-50%TiC composite was 4.307±0.005Å. This was done in order to see the effects of the oxygen present on the structure of the TiC.

7.2.2. SEM Analysis

SEM analysis was carried out on selected samples in order to observe the effectiveness of the dispersing of the systems and to observe the microstructure of the materials in order to better understand the properties obtained for them. The samples were prepared for SEM analysis as per the experimental design.

The following micrographs represent the cross-section of the Al_2O_3-3% TiC composite that was sintered at 1700°C at a pressure of 50 MPa.

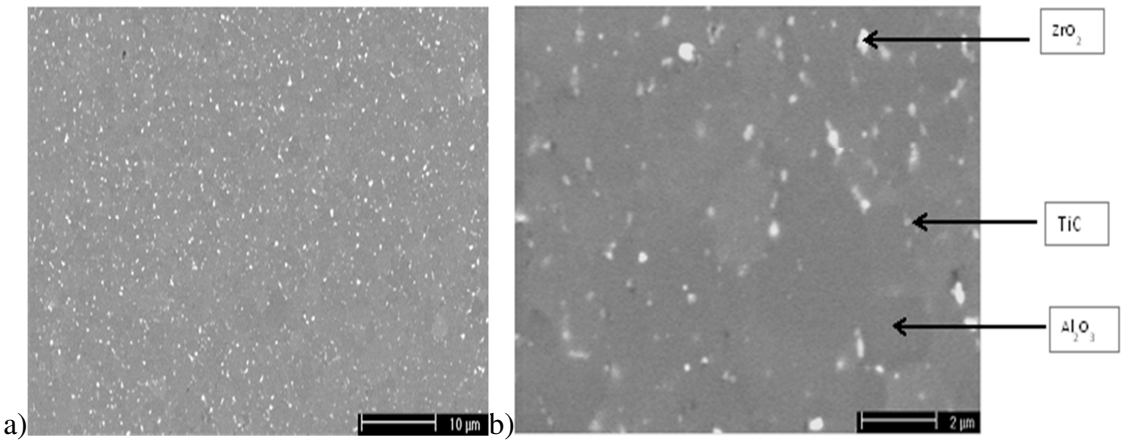


Figure 38:SEM micrographs of Al_2O_3-3% TiCsintered at 1700°C and 50MPa.

From Figure 38(a), it can be seen that the samples were well densified. It is clear however, that there is a relatively large amount of zirconia contamination (bright phase) as a result of the mixing process. Figure 38(b) shows that the majority of the zirconia contaminant and titanium carbide reinforcing materials are present at the grain boundaries of the alumina particles. There appears to have been significant grain growth of the alumina, which has an average grain size in the region of 1-1.5 µm.

The micrographs in Figure 39 summarise the structure of the Al_2O_3-30% TiC nanocomposite that was sintered at 1700°C at a pressure of 50 MPa.

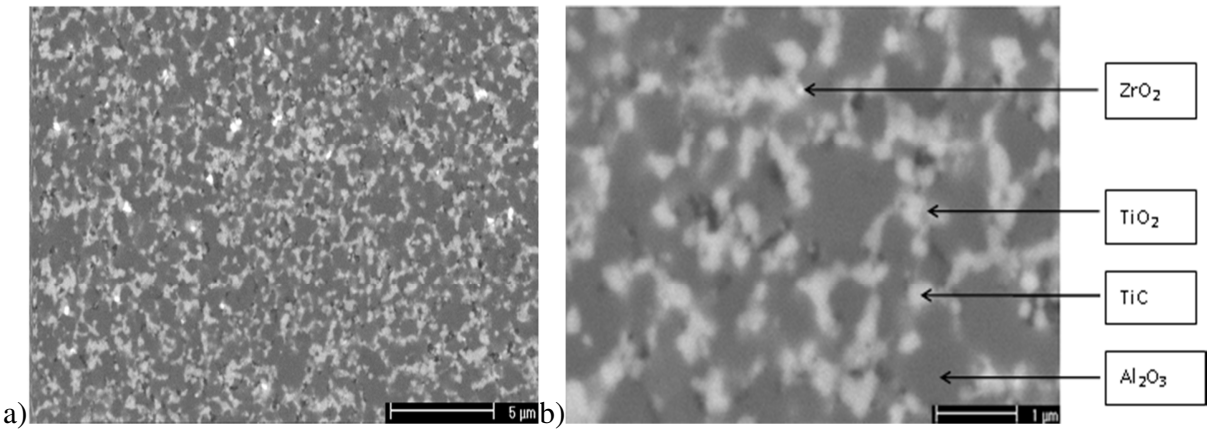


Figure 39:SEM micrograph of Al_2O_3-30% TiC sintered at 1700°C and a pressure of 50 MPa.

The phases were identified using EDS analysis and the spectra are shown in Figure 40.

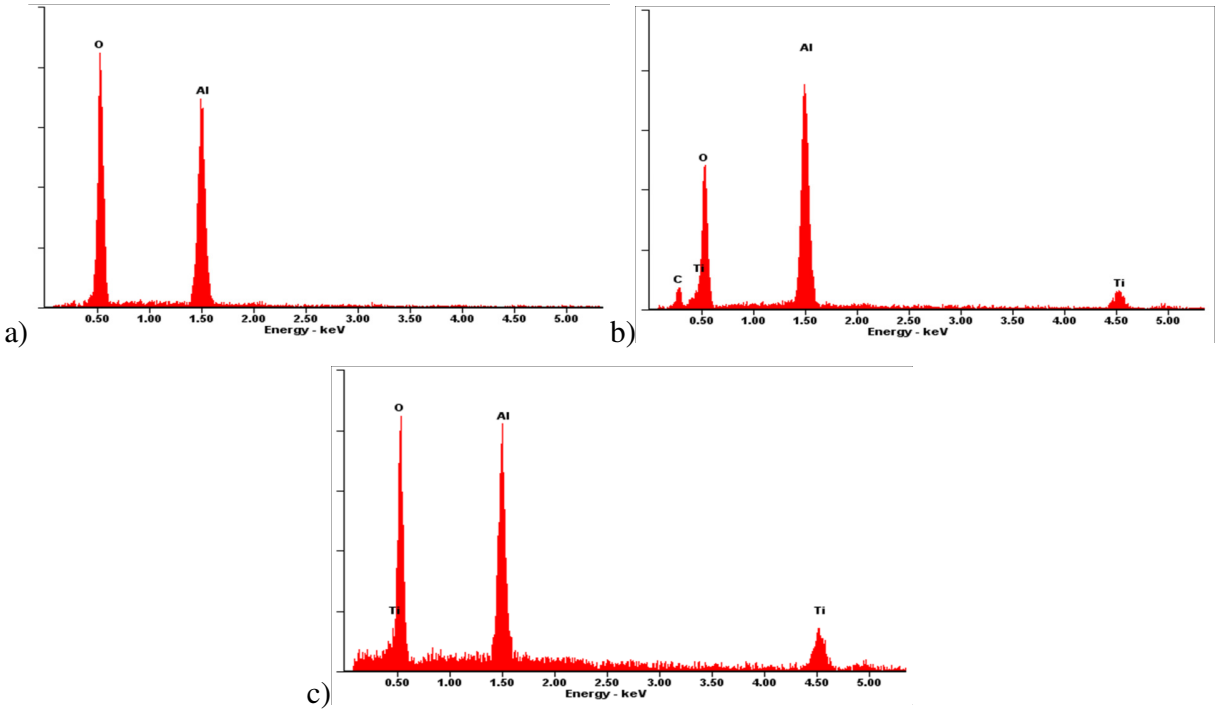


Figure 40:EDS spectra of the Al_2O_3-30% TiC composite showing a) the Al_2O_3phase, b) the TiC phase and c) the presence of a titanium oxide containing phase.

From Figure 39 (a) there appears to be less contamination from the milling process than there was for the samples that contained 3% and 10% TiC respectively. Figure 39 (b) shows that the titanium oxide phase was present. It is also clear that the growth of the alumina was less in comparison to the samples with a 3% and 10% TiC composition. The mean grain size of the alumina was roughly 500 nm.

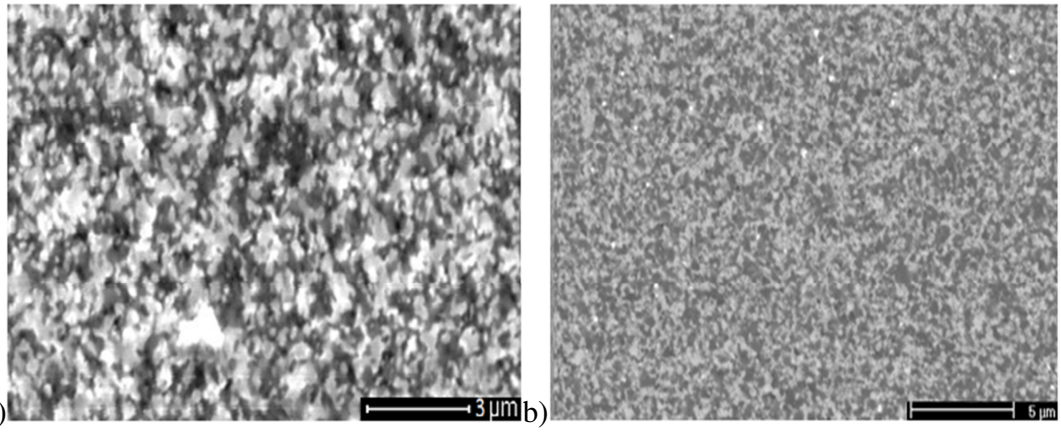


Figure 41:SEM micrograph of Al_2O_3-50% TiC sintered at a) 1600°C and 50 MPa and b) 1700°C and a pressure of 50 MPa.

From Figure 41, it is apparent that the higher temperatures produced samples with improved densification with the material shown in Figure 41 b) appearing to be almost fully dense. However, from the densification results, it is clear that the sample had a density of 93.6% and an open porosity of 2.66%. There was evidence of porosity near the surface of the sample; this was possibly a result of reduction due to the Al_2O_3 and TiC materials reacting with each other near the surface of these composites.

7.3. Densification and Characterization of the nano Alumina-Titanium Nitride materials

7.3.1. Density, Hardness and Fracture Toughness of the Al_2O_3-TiN Materials

The samples were all sintered using a spark plasma sintering furnace in an attempt to minimize grain growth during the sintering process thus keeping the grains within the nano range. Once the samples were sintered, the first property investigated was the density of the relevant samples. This was then compared to the theoretical density of each of the composite samples which were calculated as per the method described in the experimental procedure and are shown in Table 20. The theoretical density used for the alumina powder was 4 g/cm^3(Kim, 2009)[59] and that for the titanium nitride nanopowder was 5.4 g/cm^3 as given by the supplier.

Table 20: Theoretical densities of the Al_2O_3-TiN samples not taking into account the oxygen content

Sample	Al_2O_3-3% TiN	Al_2O_3-10% TiN	Al_2O_3-30% TiN	Al_2O_3-50% TiN
Theoretical Density (g/cm^3)	4.042	4.14	4.42	4.7

The samples were cut, mounted and polished as per the experimental design. The finely polished samples then underwent hardness and fracture toughness tests in order to determine the properties of the materials when working with the nanopowders. The hardness and the fracture toughness values were then calculated as per the methods described in the experimental design using the Vickers indentation equipment.

Table 21: Properties obtained for the Al_2O_3-TiN samples using various sintering conditions

Sample	Temperature (°C)	Pressure (MPa)	Heating Rate (°C/min)	Bulk Density (g/cm^3)	Open Porosity (%)	Relative Density (%)	Hardness (GPa)	Fracture Toughness ($MPa.m^{1/2}$)
Al_2O_3-3% TiN	1600	30	250	3.88±0.03	0.01±0.00	96.1±0.7	17.8±0.4	2.5±0.1
Al_2O_3-3% TiN	1700	30	250	3.93±0.02	0.32±0.07	97.2±0.5	18.3±0.2	2.4±0.2
Al_2O_3-3% TiN	1800	30	250	3.9±0.01	0.02±0.02	96.6±0.2	17.6±0.3	2.6±0.1
Al_2O_3-3% TiN	1600	50	250	3.97±0.02	0.02±0.01	98.2±0.5	18.6±0.4	2.7±0.2
Al_2O_3-3% TiN	1700	50	250	3.92±0.01	0.01±0.01	97.1±0.2	18.4±0.4	2.5±0.1
Al_2O_3-3% TiN	1800	50	250	3.92±0.04	0.01±0.00	96.9±1.0	18±0.2	2.4±0.1
Al_2O_3-10% TiN	1500	50	50	4.06±0.01	0.02±0.02	98.0±0.2	20.0±0.5	2.6±0.1
Al_2O_3-10% TiN	1600	50	50	3.96±0.06	0.91±0.15	95.7±1.4	18.6±0.3	2.7±0.1
Al_2O_3-10% TiN	1600	50	250	3.79±0.04	0.12±0.01	91.5±1.0	17.9±0.3	2.5±0.2
Al_2O_3-10% TiN	1700	50	250	3.76±0.05	0.20±0.05	90.8±1.2	17.6±0.3	2.6±0.1
Al_2O_3-30% TiN	1700	30	250	3.57±0.21	0.87±0.10	80.7±4.7	Too Porous for Vickers Testing	
Al_2O_3-30% TiN	1500	65	25	4.14±0.01	0.66±0.08	93.6±0.2	20.0±0.3	2.9±0.2
Al_2O_3-30% TiN	1500	65	100	4.14±0.02	1.34±0.14	93.6±0.5	20.6±0.6	2.7±0.4
Al_2O_3-30% TiN	1500	65	250	4.13±0.02	1.74±0.25	93.5±0.5	20.5±0.5	2.7±0.1
Al_2O_3-30% TiN	1600	50	250	4.03±0.04	1.48±0.09	91.1±0.9	19.6±0.5	2.6±0.1
Al_2O_3-30% TiN	1800	30	250	Die failure, no remaining sample.				
Al_2O_3-30% TiN	1700	50	250					
Al_2O_3-30% TiN	1800	50	250					
Al_2O_3-50% TiN	1500	60	50	4.24±0.03	0.78±0.07	90.3±0.6	13.5±0.6	2.8±0.1
Al_2O_3-50% TiN	1600	50	250	4.16±0.02	0.15±0.06	88.5±0.4	12.2±0.3	2.7±0.3
Al_2O_3-50% TiN	1700	60	50	4.31±0.04	1.23±0.22	91.8±0.9	16.0±0.5	2.8±0.1

Due to the low densification results obtained when sintering the Al_2O_3-10% TiN samples using a heating rate of 250°C/min, it was decided to lower the heating rate to 50°C/min. The effect of the lower heating rates on the densification of the samples isshown in Figure 42.

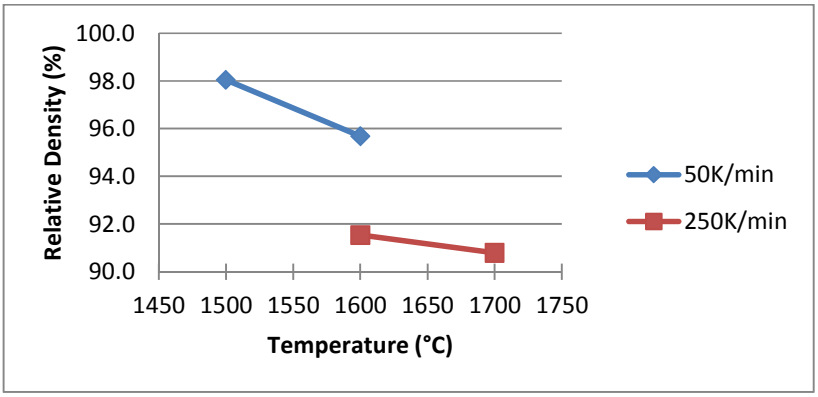


Figure 42: Comparison of densities of Al_2O_3-10% TiN sintered at various temperatures using different heating rates.

From these results, it is seen that at lower heating rates there was a significant improvement in the densification of the Al_2O_3-10% TiN samples. It is also clear that with increased sintering temperature there was a decrease in the densification of the samples. In order to better understand the reason for these results, the densfication curves for the samples were analysed and are shown in Figure 43.

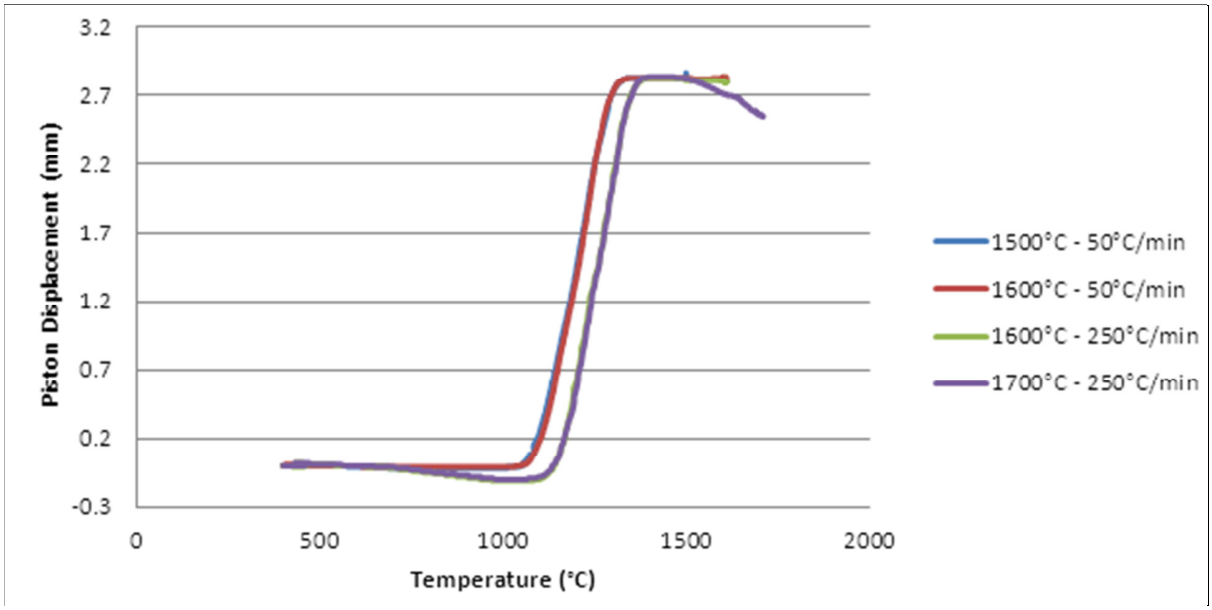


Figure 43: Comparison of densification curves for Al_2O_3-10% TiN sintered using a heating rate of 50°C/min and 250°C/min.

For the samples sintered using a heating rate of 50°C/min, it was clear that the piston displacement was almost identical. However, it was clear that for the sample sintered at 1600°C, the piston displacement began to decrease during the sintering temperature dwell period. For the samples sintered using a heating rate of 250°C/min, it was clear that the piston displacement was almost identical. However, it was clear that for the sample sintered at 1700°C, the piston displacement began to decrease drastically during the sintering temperature dwell period. When comparing the different heating rates, it was evident that the piston movement began at a lower temperature when using 50°C/min rather than 250°C/min. This was expected as the composite had more time to adjust as the temperature was increased. There were very slight differences in the piston displacement with the composite sintered at 1500°C and 50°C/min having the highest displacement. When comparing the piston displacement of the composites with the densification results that were obtained, it was evident that the samples that had the best densification results had the highest piston displacement respectively.

From Table 21 it was obvious that as the temperature of the system was increased the densification of the Al_2O_3-30% TiN composites began to decrease. It must be noted however, that the samples sintered at 1800°C (at pressures of 30 MPa and 50 MPa) and the samples sintered at 1700°C with a pressure of 50 MPa each having a heating rate of 250°C/min, resulted in catastrophic failure of the die. The heating rate of the samples was also varied in order to see the effect on the densification of the sample. The samples were sintered at 1500°C using heating rates of 25°C/min, 100°C/min and 250°C/min respectively. The results of this are shown in Figure 44.

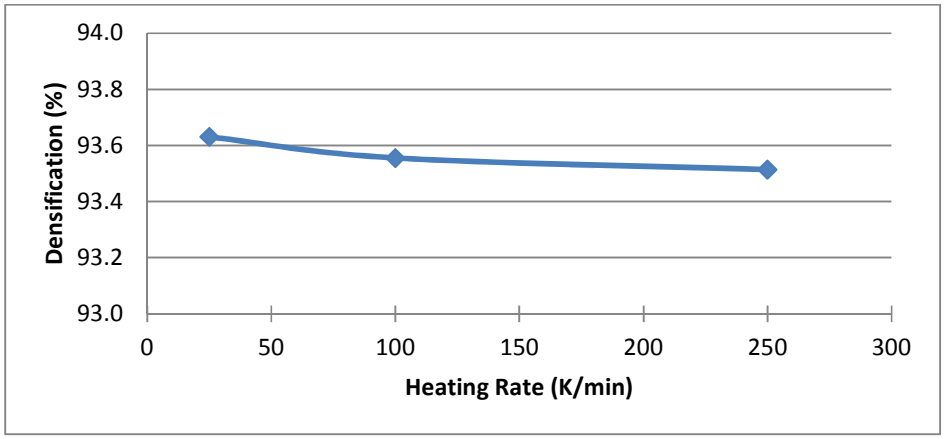


Figure 44: The effect of the heating rate used on the densification of Al_2O_3-30% TiN sintered at 1500°C and a pressure of 65 MPa.

It is clear from this that as the heating rate was increased, the densification decreased. However, the changes in densification for the Al_2O_3-30% TiN samples were small.

From the results in Table 21 it was evident that the Al_2O_3-50% TiN samples produced appeared to be insufficiently densified. It was evident that as the sintering temperature of the Al_2O_3-50% TiN samples was increased, there was an initial decrease in the density and then as the temperature was increased further, the density of the sample increased. However, it must be noted that the sample sintered at 1700°C had a mass that was less than half of the mass of the starting powder that was packed into the die.

7.3.2. XRD Analysis

XRD analysis was performed on each of the compositions of the sintered Al_2O_3-TiN nano composites. Figure 45 shows the results obtained for each of the Al_2O_3-TiN samples.

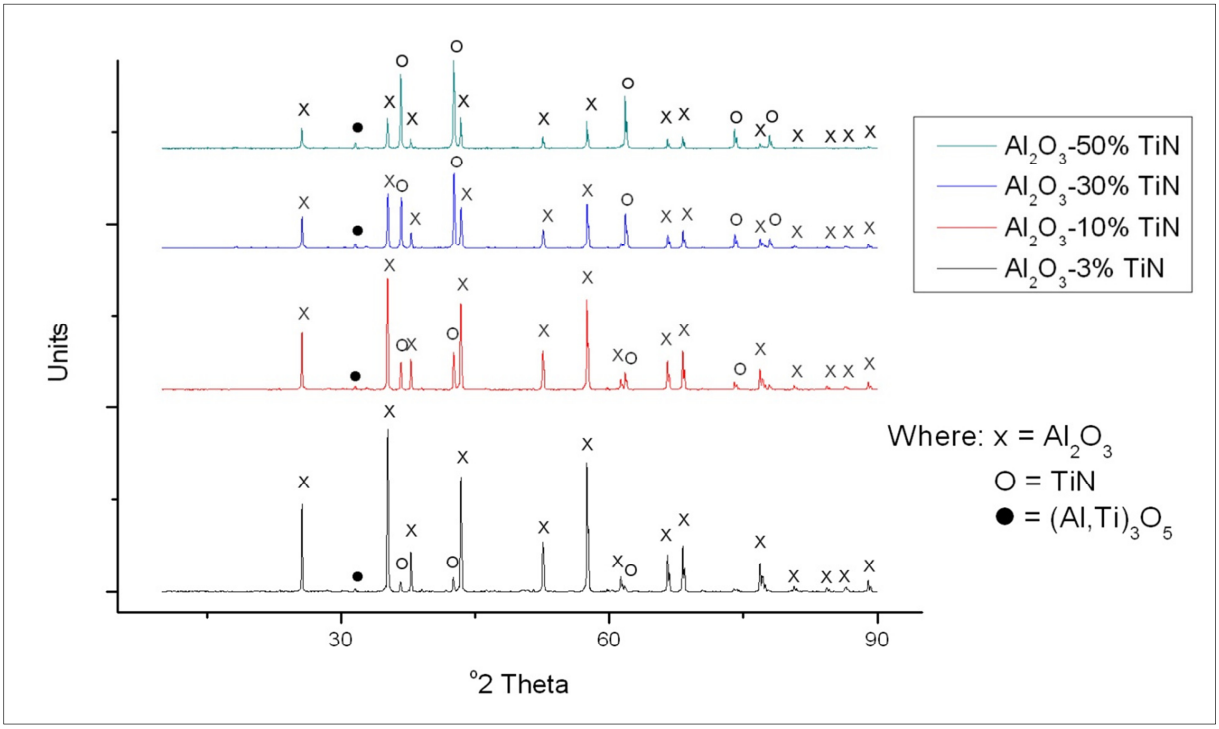
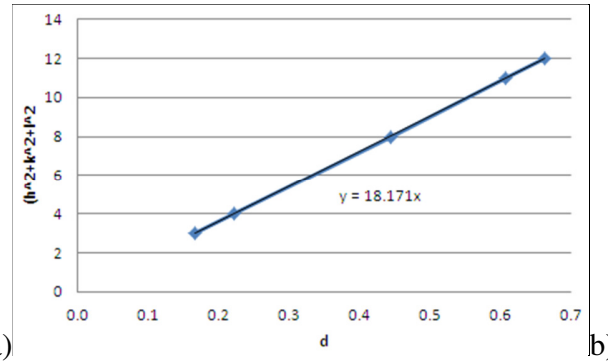


Figure 45:XRD analysis comparing each composition of Al_2O_3-TiN that nano composites that were sintered at 1600°C and 50MPa.

From these results, it is evident that there was a titanium oxide containing phase present in each of the sintered Al_2O_3-TiN samples. This was found to be a solid solution between Ti_3O_5 and $AlTi_2O_5$, namely $(Al,Ti)_3O_5$. The effect of increasing the TiN content, which was determined to be synthetic Osbornite, on the various compositions is observed in Figure 45. It was also clear from the XRD analysis that with increasing the TiN composition, the amount of $(Al,Ti)_3O_5$ that was present clearly increased.

The lattice parameters of the pure TiN powder and also the TiN in the Al_2O_3-50%TiN composite sintered at 1600°C and 50 MPa, are shown in Figure 46. The lattice parameters were calculated as per the experimental procedure.

a) 

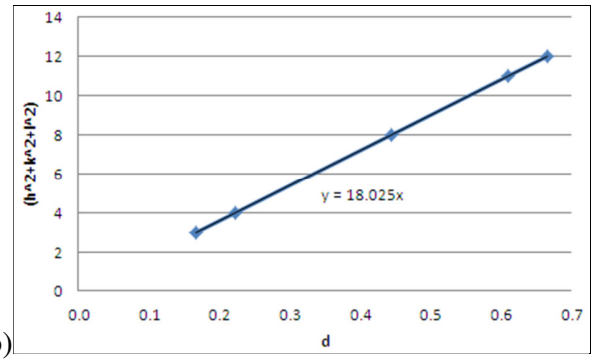
b) 

Figure 46: Calculation of the TiC lattice parameters in a) the pure TiN powder and b) the Al_2O_3-50%TiN composite sintered at 1600°C and 50MPa.

This showed that the TiN lattice parameter in the pure TiN powder was 4.263±0.005Å and in the Al_2O_3-50%TiN composite was 4.246±0.005Å.

7.3.3. SEM Analysis

SEM analysis was carried out on selected samples in order to observe the effectiveness of the dispersing of the systems and to observe the microstructure of the materials in order to better understand the properties obtained. The samples were prepared for SEM analysis as per the experimental design.

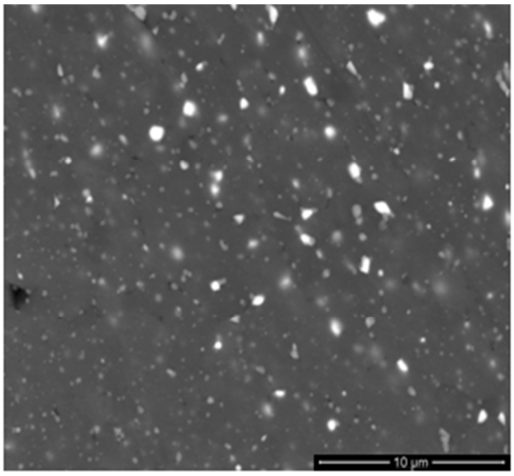


Figure 47: SEM micrograph of Al_2O_3-3% TiN sintered at 1600°C and 50 MPa

From the investigations on the Al_2O_3-3%TiN sample sintered at 1600°C and 50 MPa, it is seen that there was significant grain growth occurring in the alumina phase with the grains ranging between 1.5 µm and 2 µm. The TiN phase was also situated at the grain boundaries in the material as with the Al_2O_3-3%TiC sample. There was also a significant amount of zirconia from the milling media present as a result of the mixing of the materials. It is also evident that the phases within the sample were well dispersed.

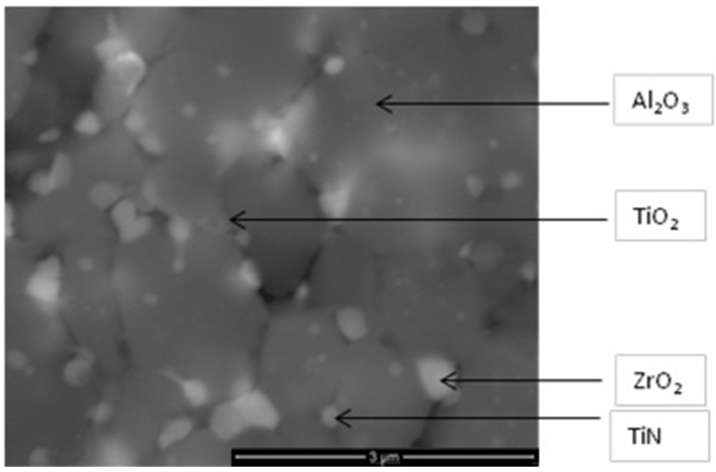


Figure 48: SEM micrograph of Al_2O_3-10%TiNsintered at 1500°C and a pressure of 50 MPa.

It is seen from this micrograph (Figure 48) that there was grain growth within theAl_2O_3-10% TiN sample, with the alumina grains being approximately 1 μm. The TiN was again present at the grain boundaries, and it is also evident that there was TiO_2 and zirconia contamination within the sample.

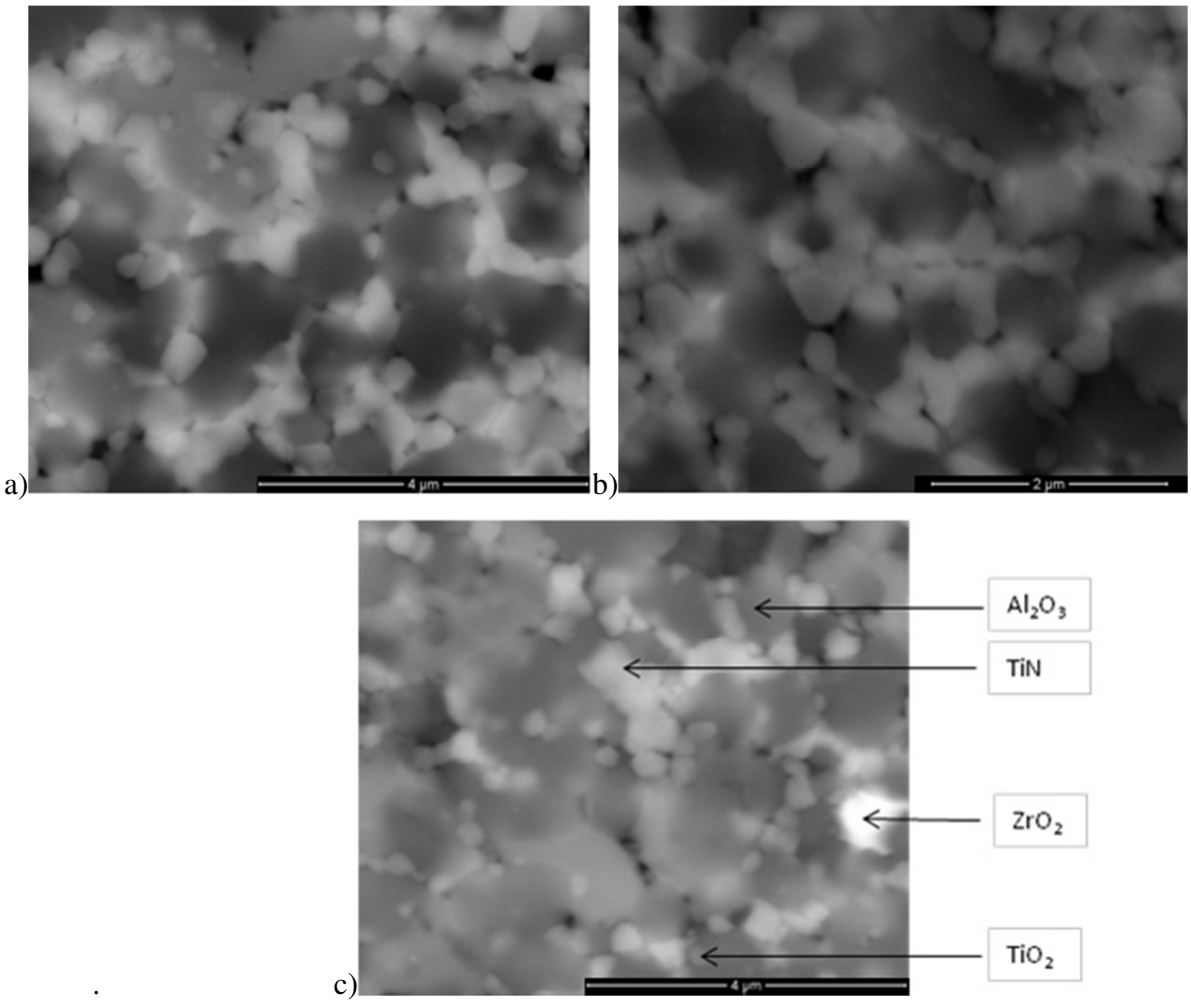


Figure 49: SEM micrograph of Al_2O_3-30%TiNsintered at 1500°C at a pressure of 65 MPa, using a heating rate of a) 50°C/min, b) 100°C/min and c) 250°C/min.

The phases were identified using EDS analysis and the spectra are shown in Figure 50.

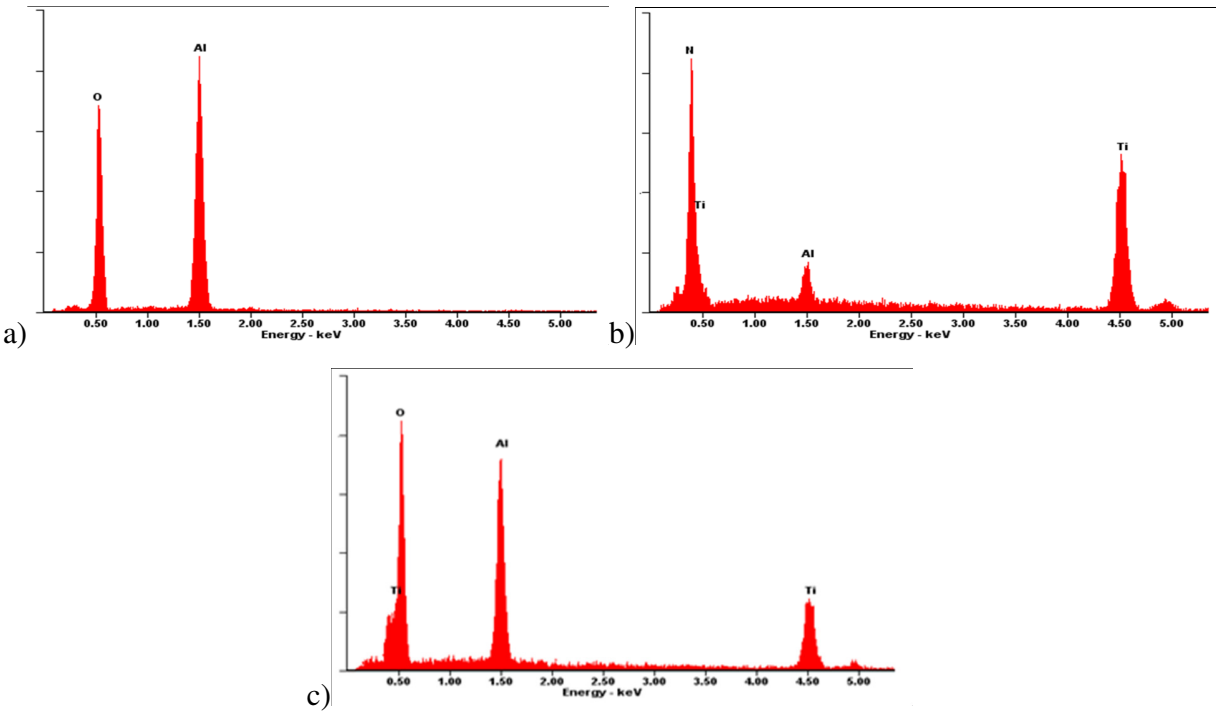


Figure 50:EDS spectra of the Al_2O_3-30% TiN composite showing a) the Al_2O_3 phase, b) the TiN phase and c) the presence of a titanium oxide containing phase.

The SEM micrographs in Figure 49comparing the Al_2O_3 30% TiN samples sintered using different heating rates show that there was similar grain growth in each of the composites. They also show that there was a significant amount of titanium oxide phase present in the samples.

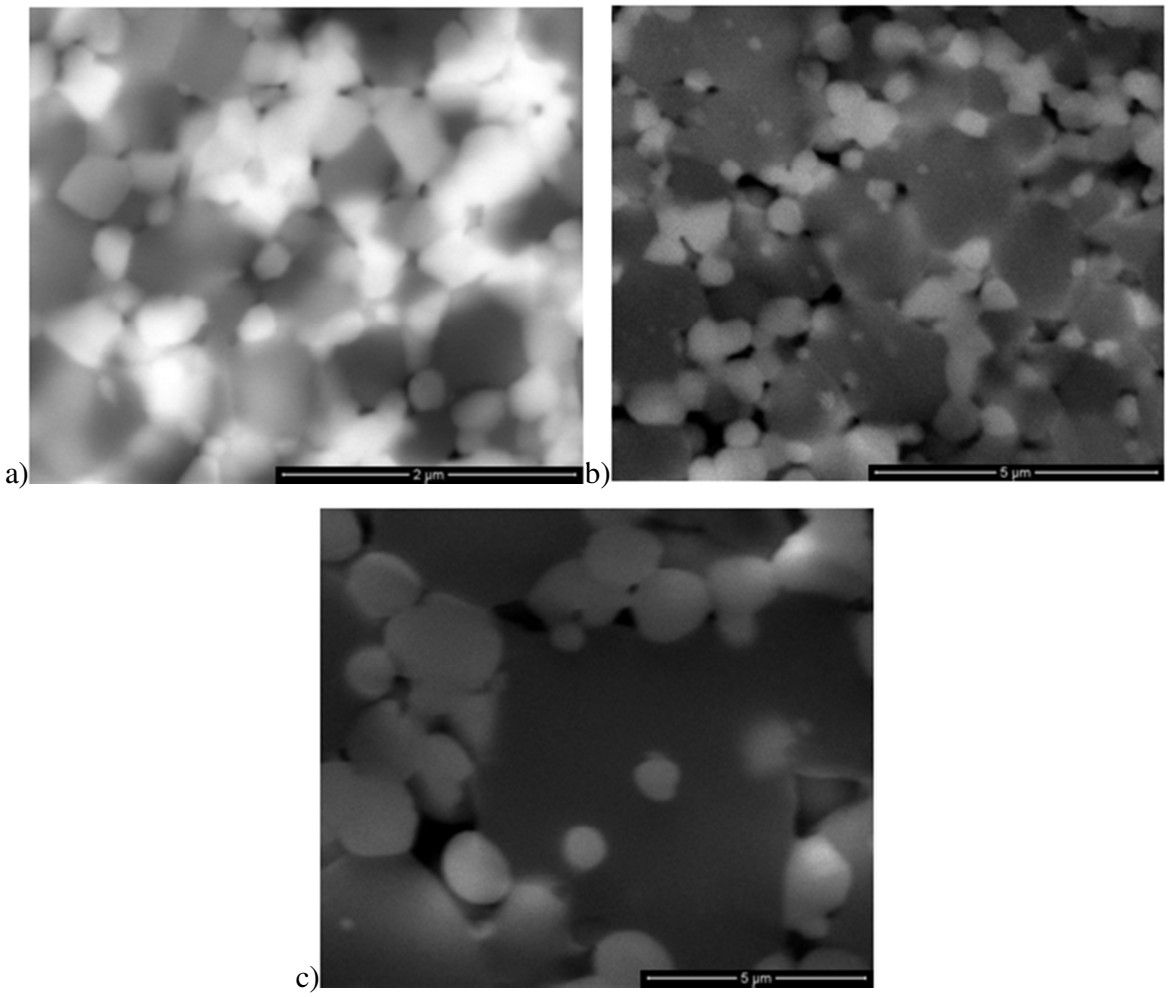


Figure 51: SEM micrograph of Al_2O_3-50%TiNsintered at a) 1500°C , b) 1600°C and c) 1700°C.

From the results shown in Figure 51 it is clear that when sintering the Al_2O_3-50%TiN samples, there was a significant increase in the porosity within the sample and there was also a very large amount of grain growth.

8. Discussion of preparation and properties of nanocomposites

8.1. Rheology of the Suspensions

From the SEM analysis and particle size analysis results, it was evident that each of the powders was approximately the size claimed by their respective suppliers. Due to the nano range of the powders, there was significant agglomeration of the materials. This agglomeration made particle size analysis using the zetasizer difficult as the materials needed to be properly dispersed. As a result of this it was decided to conduct the rheology studies in order to determine the optimum amount of dispersant needed to disperse each of the powders. The powders were then milled with the optimum amount of Lubrizol 2155 for various times and the particle size distributions were obtained. It must be noted that as the particle size of each of the materials decreased the times required to produce the dispersed suspensions for particle size analysis increased. This is evident in Table 17 which showed that the mixing time used to produce a dispersed suspension increased with decreasing particle size. This was expected as the extent of agglomeration in the finer powders is more significant[(5)]. As expected, the specific surface area of each of the individual powders increased with the decreasing particle size. Due to this increase in surface area, it was also expected that the amount of Lubrizol 2155 required to disperse the powders will then increase.

Table 22shows a comparison between the surface area of the powders used and the weight percentage of the dispersant Lubrizol at the minimum viscosity. This was then used to determine the mass of Lubrizol 2155 required per unit area of each of the powders.

Table 22: Comparison between the weight percentage of Lubrizol and the surface areas of the powders

Sample	Particle Size (nm)	Surface Area (m^2/g)	Solids Loading (Volume %)	Lubrizol at minimum viscosity (Wt %)	Mass Lubrizol per unit area powder (mg/m^2)
Al_2O_3	100	14.7	40	6	4.1
TiC	40	23.71	15	8.3	3.5
TiN	20	61.26	3.2	9	1.5

It is obvious from the results in Table 22 that as the surface area of the material increased there was a general trend that the amount of Lubrizol 2155 required also increased. Although the total amount of Lubrizol 2155 required increases, it was evident that the amount of Lubrizol 2155 per unit area decreases. This was evident when comparing the results from the µm-powder to the nanopowders, where the µm-TiC required 5.8 mg/m^2 (Table 14) and the nano-TiC required 3.5 mg/m^2 and also the µm-TiN required 8.9 mg/m^2(Table 14) and the nano-TiN required 1.5 mg/m^2 in order to be adequately dispersed. It is also possible that there was stronger adsorption as a result of the oxide phase present. The rheology results obtained from the Al_2O_3-TiC and Al_2O_3-TiN mixtures were then compared to those obtained from the pure alumina powder and are shown in Figure 52. Due to the amount of Lubrizol 2155 required to disperse the TiC and TiN being higher than that of the pure TM-DAR alumina, it was expected that in comparison to the pure alumina there would be an increase in the amount of Lubrizol 2155 required to disperse the systems.

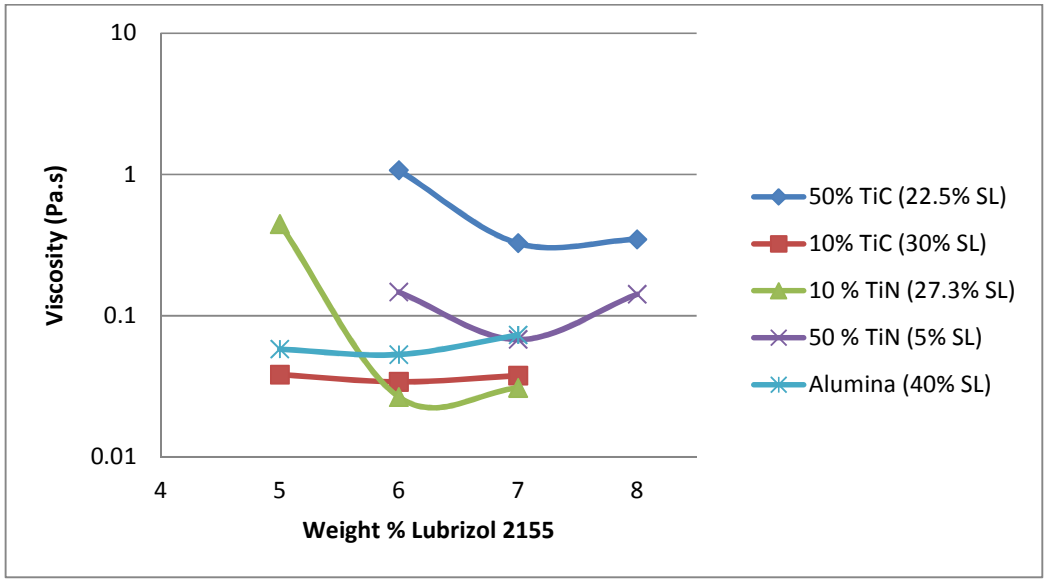


Figure 52: Comparison of mixtures containing 10% and 50% (by volume) of the respective reinforcing component (TiC/TiN) to pure alumina.

From Figure 52 it is clear that there was very little change in the amount of Lubrizol 2155 required to disperse the mixtures containing 10% of the reinforcing components when compared to the pure alumina. It must be noted that the solids loadings used in each case were lower than the pure alumina. In Al_2O_3-10% TiC, the addition of TiC had almost no effect on the amount of Lubrizol needed, but it does result in a lower viscosity than the pure alumina. The Al_2O_3-10% TiN shows an increase in the required amount of Lubrizol 2155 when compared to the pure alumina. It was also obvious that there was a significant increase in the amount of Lubrizol 2155 required to disperse the mixtures containing 50% of the reinforcing components when compared to the pure alumina, with the Al_2O_3-50% TiC requiring slightly more Lubrizol 2155 than the Al_2O_3-50% TiN suspension in order to be optimally dispersed. However, it must be noted that the viscosity of the Al_2O_3-50% TiC suspension was significantly higher than that of the Al_2O_3-50% TiN suspension. This was due to the solids loading of the Al_2O_3-50% TiC suspension being higher than that of the Al_2O_3-50% TiN suspension. Lower amounts of Lubrizol 2155 could be used to disperse both the alumina and the Al_2O_3-10% TiC suspensions due to the fact that the minimums obtained are not steep and thus similar viscosities can be obtained at lower Lubrizol 2155 additions.

It was expected that the TiN would have a bigger effect on the amount of Lubrizol 2155 required as it had a much larger specific surface area. From Figure 52 it would appear that this was the case, but although there was an increase in the Lubrizol 2155 required, the amount required for the Al_2O_3-50% TiN suspension was less than that for the Al_2O_3-50% TiC suspension. A reason for this is that the solid loadings that were used in order to perform the rheology test were not the same for each of the materials. This was a result of the properties of the materials and is evident in Table 22 which shows the specific surface area of each of the individual powders and in Table 23 which shows the dispersant estimated-and-used for the composite materials.

From the studies on the Al_2O_3-TiC and the Al_2O_3-TiN composite suspensions, the expected amount of Lubrizol 2155 required was calculated to be the sum of the amount required for each of the individual powders in the system. An expected solid loading was calculated in order to determine an initial solid loading to be used with the composite suspensions. This was calculated using the solid loadings used for the individual powders and weighting them with respect to their volume fraction in the composite suspension. However, from Table 23, it is clear that the actual solids loadings used in each case were lower than those used as the starting point. This was due to the fact that the viscosities of the initial suspensions were too high and as a result a rheology test could not be carried out on them. The Lubrizol 2155 required, in each case, was calculated with respect to the solid content of the suspension.

Table 23: Comparison between the expected and the actual amount of Lubrizol 2155 required and the solid loadings that were used

Matrix Material	Volume % Reinforcing Material	Actual Solid Loading (Vol %)	Actual Wt% Lubrizol	ExpectedSolid Loading (Vol %)	Expected Wt% Lubrizol
Al_2O_3	10% TiC	30	6	37.5	6.3
Al_2O_3	50% TiC	22.5	7.3	27.5	7.3
Al_2O_3	10% TiN	27.3	6.3	36.32	6.4
Al_2O_3	50% TiN	5	7	21.6	7.7

Due to the nature of the reinforcing powders it was not possible to create suspensions using the expected solid loadings. As a result, the solid loadings that were used had to be decreased in order to form a suspension that could be used for the rheology studies. As was suggested in the μm-powder work involving the rheology of the materials, the material that has the higher specific surface area once again appeared to have a bigger effect on the dispersal requirements of the systems. In the μm-powder investigation it was seen that the amount of dispersant required was higher than expected; there, the solids loading used for all the experiments was 50 volume %. It is suspected that this was also the case with the nanopowder suspensions; however, due to the decrease in the solid loadings (with respect to the expected solid loadings) the amount of dispersant used was found to be close with that which was expected. In the case of the Al_2O_3-50% TiN suspension where the solid loading was drastically decreased, the Lubrizol 2155 required to optimally disperse the suspension was significantly lower than that which was initially expected. The effect of the solids loading on the amount of dispersant needed was clear in the rheology studies carried out on the TiN nanopowder.

The rheology on the TiN system was initially performed using a solid loading of 15%, where the optimum amount of Lubrizol 2155 required to disperse the material was found to be 23 weight percent with respect to the solid content in the suspension. Due to the large Lubrizol requirement, the solid loading was decreased to 3.2% in order to determine if this would require a smaller amount of dispersant with respect to the solid content. This would result in any residue from the dispersant remaining in the powder after the burn-off process being less and as a result would have a smaller effect on the final properties of the sintered composites. Thus it was evident from these results that the solid loading of the suspension affects the concentration of the dispersant required to optimally disperse it, and thus the optimum Lubrizol 2155 addition corresponds to the chosen solid loading. This was also evident in work done on alumina suspensions by Tsetsekou et al. 2001[(60)]. However, it must be noted that in order to form the suspension, there had to be a sufficient number of particles present to prevent settling. The effect of this can be seen by comparing the micron and the nano TiN powders, where the μm-powder was able to support a 50 volume % solids loading, while in order to produce a suspension with the nanopowder the solids loading had to be lowered to 3.2 volume %. Due to the difference in

size of the particles, there will be a greater number of particles present in the nanopowder suspension than in the µm-powder suspension. This is particularly evident when the specific surface areas of the powders are considered, which show the SSA of the micron TiN to be 1.9 g/cm^2 and that of the nano TiN to be 61.26 g/cm^2.

8.2. Discussion of sintering behaviour and properties of theAl_2O_3-TiC nanocomposites.

The results obtained for the sintering process of the Al_2O_3-TiC samples were analysed and compared to one another. Figure 53 shows the densification curves of the Al_2O_3-TiC nanocomposites sintered at 1700°C and 50 MPa(Figure 53).

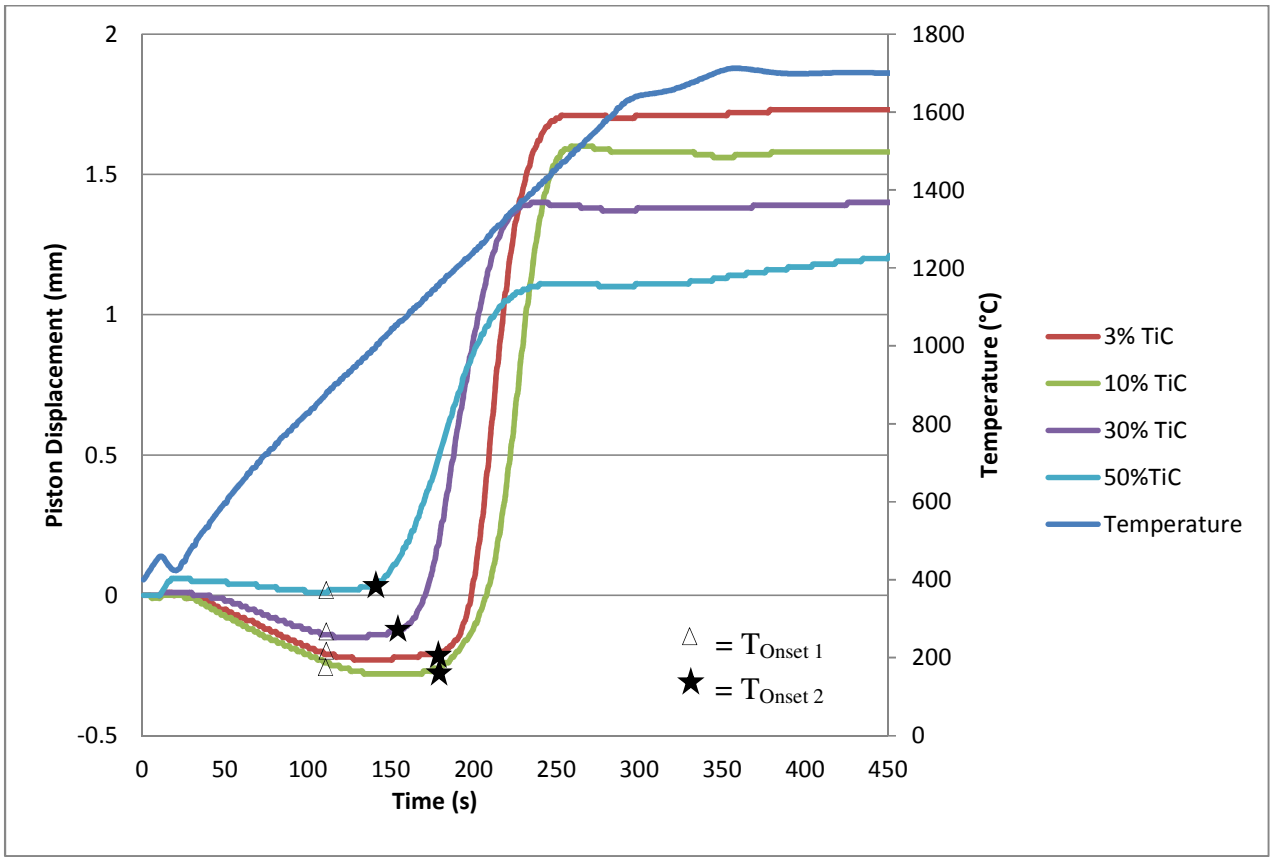


Figure 53: Densification curves for Al_2O_3-TiC sintered at 1700°C and a pressure of 50 MPa.

From these results it is evident that as the concentration of TiC in the composite was increased, the total piston displacement decreased. It is clear that the Al_2O_3-3%TiC, Al_2O_3-10%TiC,Al_2O_3-30%TiC and the Al_2O_3-50%TiC composites began sintering at approximately the same temperature at about 900°C, as shown in Figure 54. Although the initial onset temperature (T_{Onset1}) was approximately the same for each composition it is clear that the onset temperature, for the stage where there was intensive shrinkage (T_{Onset2}), decreased with increasing TiC content. This is shown more clearly in Figure 54. The shift to the lower temperature with increasing TiC content was likely due to the larger amount of the titanium oxide phase being present. The initial piston displacement ends before the final sintering temperature was reached for each of the composites. The sintering appeared to end at approximately 1500°C for both the Al_2O_3-3%TiC and the Al_2O_3-10%TiC composites and at about 1350°C for the Al_2O_3-30%TiC and the Al_2O_3-50%TiC composites. It was also evident that in the Al_2O_3-50%TiC composite there was a secondary movement of the pistons once the initial piston displacement had occurred.

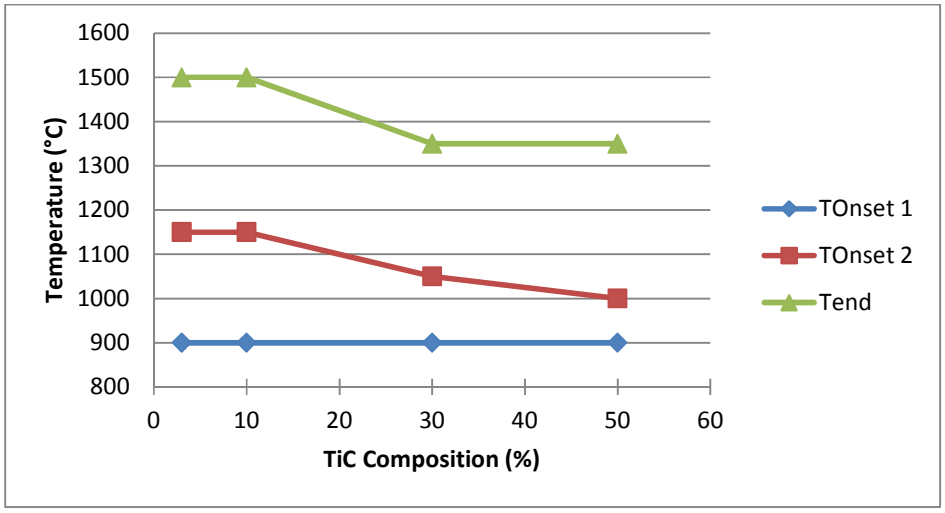


Figure 54: Onset temperatures for start of densification and the main densification and the end of densification with respect to the TiC concentration of the composites sintered at 1700°C and a pressure of 50 MPa.

8.2.1. Comparison of Densities

From the density results obtained for the Al_2O_3-TiC composites, particularly the Al_2O_3-30%TiC and the Al_2O_3-50%TiC it was seen that the densities were very low. These densities would be unacceptable, however upon polishing the composites it was noted that the samples found to have low densification results appeared to have better densities under the optical light microscope, than those calculated using Archimedes' principle. A possible explanation for this is that there was titanium oxide present in the starting powders which was lowering the density of the samples.

A possible cause of the theoretical density being incorrect would be that there was a significant amount of oxygen contamination of the titanium carbide powder. As a result of this, it was imperative to determine whether or not there was an oxide phase present in the sintered materials and also to determine the amount of oxygen present in the starting powder.This would result in the theoretical densities of the materials that were calculated being higher than they should be as a TiO_2 phase will have a lower density than that of TiC. The theoretical density used for the rutile TiO_2 phase present was 4.1 g/cm$^{3(61)(62)}$.

From the XRD analysis that was performed on the materials, it is shown that there was in fact an oxide phase [$(Al,Ti)_3O_5$] present in the samples. When the microstructures of the materials were investigated, a $(Al,Ti)_3O_5$phase was identifiable in the Al_2O_3-10% TiC, Al_2O_3-30% TiC and the Al_2O_3-50% TiC samples. Also, from the XRD analysis it was evident that there was a very small amount of $(Al,Ti)_3O_5$ present in the Al_2O_3-3% TiC, but due to the small amount of TiC present in that composite the phase could not be identified in the sample through SEM analysis.

The presence of the titanium oxide containing phase would result in the theoretical densities calculated for the materials being higher than those of the actual materials. This is due to the fact that the titanium oxide containing phase will have a lower density than the pure TiC. As a result

of this, a new theoretical density for the various composites had to be estimated in order to more accurately assess the extent of densification in the samples. It was decided to determine the density using the oxygen content associated with the starting TiC powder.

It was assumed that all the oxygen present in the titanium carbide powder was in the form of TiO_2 as this is the most stable form of titanium oxide at room temperature. Since the amount of oxygen present in the TiC powder is known, this allowed for the amount of oxygen that was present in the sample to be used to calculate the amount of TiO_2 that was present in the titanium carbide nanopowder. The Leco oxygen determination results revealed that the TiC powder contained 3.54 weight percent oxygen.

The calculations were made using the following equation in order to determine the mass of TiO_2 in each of the initial starting powders.

$$m_{Oxide} = M_{Oxide} \times \frac{x}{2 \times M_O} \qquad \text{Equation 1}$$

Where;

m_{Oxide} = Mass Percent of TiO_2 (%)

x = Weight % oxygen (%)

M_y= Molar mass of material Y (g/mol)

From the above equation, it was possible to directly obtain the relevant compositions of both the TiO_2 and TiC. From these calculations, the starting powder was found to contain 91.15 % TiC and 8.85% TiO_2.

Using this composition, it was then possible to recalculate the theoretical densities of each of the Al_2O_3-TiC materials as shown in Table 24. It must be noted however, that this calculation did not take into account any oxygen pickup during the processing of the powders (i.e. post-Leco analysis) and also no reduction of the TiO_2 by carbon in the TiC powder. This means that these density values calculated were a first approximation of the theoretical density.

Table 24: Recalculated theoretical density compared to the original theoretical density

Al_2O_3– TiC		
TiC Composition (%)	**Original Theoretical Density (g/cm^3)**	**Recalculated Theoretical Density (g/cm^3)**
3	4.028	4.026
10	4.093	4.086
30	4.279	4.256
50	4.465	4.425

It was clear from these results that the presence of the oxide material resulted in a decrease of the theoretical density. This would result in an increase of the relative density of all the materials sintered as shown in Table 25.

Table 25: Recalculated Relative densities with change in density

Sample	Temperature (°C)	Pressure (MPa)	Relative Density (%)	Recalculated Relative Density (%)	Change in Relative Density (%)
Al_2O_3-3%TiC	1600	30	99.1	99.2	0.1
Al_2O_3-3%TiC	1700	30	99.4	99.5	0.1
Al_2O_3-3%TiC	1800	30	99.2	99.3	0.1
Al_2O_3-3%TiC	1500	50	99.4	99.5	0.1
Al_2O_3-3%TiC	1600	50	99.4	99.5	0.1
Al_2O_3-3%TiC	1700	50	99.5	99.6	0.1
Al_2O_3-10%TiC	1600	30	98.6	98.8	0.2
Al_2O_3-10%TiC	1700	30	98.8	98.9	0.1
Al_2O_3-10%TiC	1800	30	98.8	99.0	0.2
Al_2O_3-10%TiC	1500	50	98.3	98.5	0.2
Al_2O_3-10%TiC	1600	50	98.9	99.0	0.1
Al_2O_3-10%TiC	1700	50	98.8	98.9	0.1
Al_2O_3-30%TiC	1600	30	94.1	94.7	0.6
Al_2O_3-30%TiC	1700	30	95.2	95.7	0.5
Al_2O_3-30%TiC	1800	30	95.4	96.0	0.6
Al_2O_3-30%TiC	1500	50	94.7	95.2	0.5
Al_2O_3-30%TiC	1600	50	96.2	96.8	0.6
Al_2O_3-30%TiC	1700	50	96.6	97.1	0.5
Al_2O_3-50%TiC	1500	50	91.7	92.6	0.9
Al_2O_3-50%TiC	1600	50	93.0	93.8	0.8
Al_2O_3-50%TiC	1700	50	93.6	94.4	0.8
Al_2O_3-50%TiC	1800	50	95.0	95.9	0.9

From these results it is clear that as the amount of titanium carbide in the composites was increased, the change in the relative density of the material also increased. This was due to the larger amount of the oxide material being present in the sample which lowered the theoretical density. The Al_2O_3-3%TiC samples were sufficiently dense with all the densification values increasing with all the density values above 99% with respect to the recalculated theoretical density of the TiC powder. The Al_2O_3-10% TiC samples were also sufficiently dense with the

densification reaching 99%. However, it must still be noted that the densification for the materials were still decreasing with increasing amount of titanium carbide within the samples. The recalculated densification of the Al_2O_3-30%TiC showed that when considering the oxide phase within the samples, the densification passes the threshold of what is considered sufficiently dense, i.e. 97% of theoretical density. As a result it can be said that the Al_2O_3-30%TiC material had in fact been sufficiently densified. The maximum densification in the Al_2O_3-50%TiC composite was 95.9% when taking into account the recalculated relative densities. This suggests that these samples were still not sufficiently dense.

It was seen that for each of the Al_2O_3-3% TiC, Al_2O_3-10% TiC, Al_2O_3-30% TiC composites that sintering at 50 MPa applied pressure typically produced higher densification results than when 30 MPa was used(Figure 55).This effect was minimal in the Al_2O_3-3% TiC and Al_2O_3-10% TiC composites, however it was significant in the Al_2O_3-30% TiC composites.

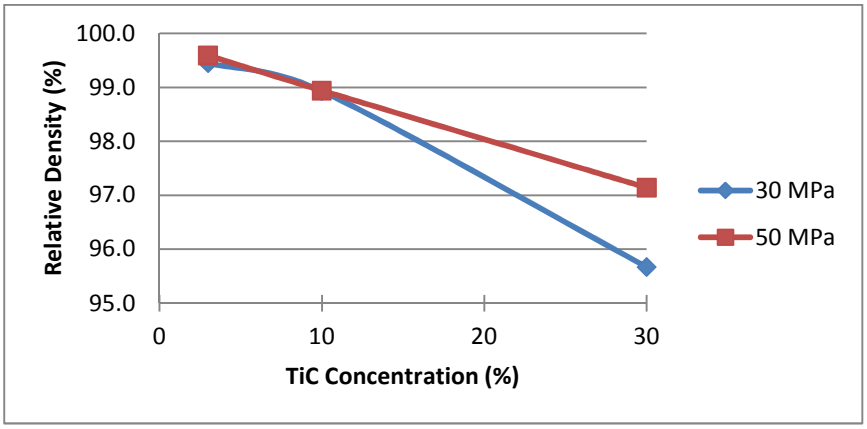
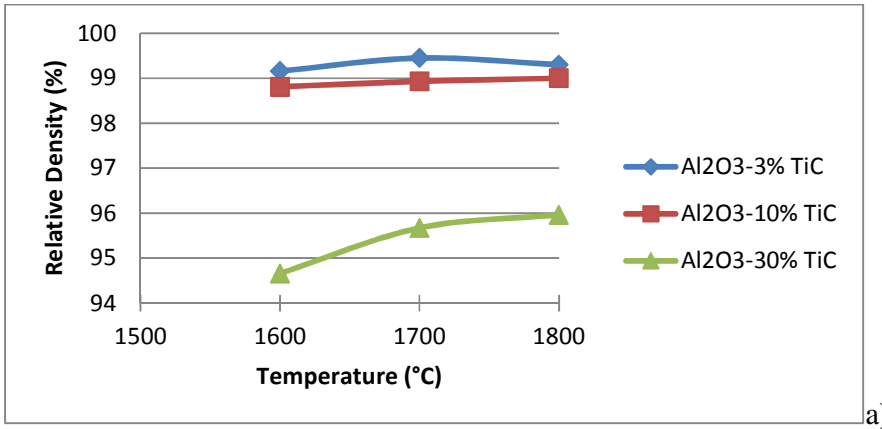


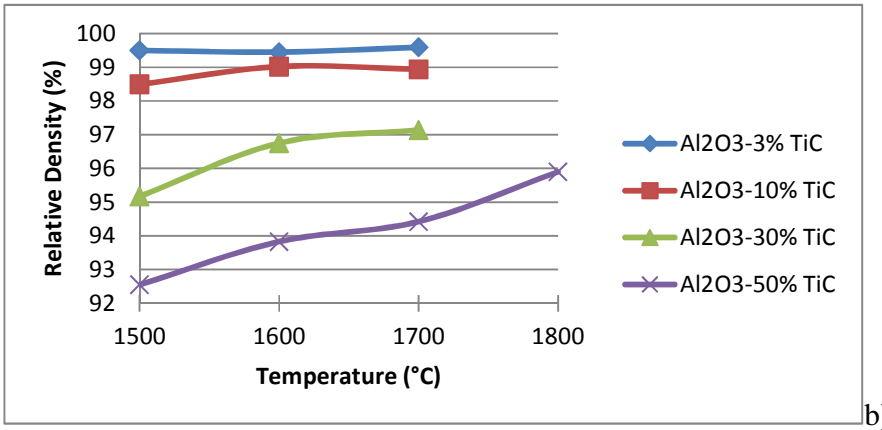
Figure 55: Effect of reinforcing component and sintering pressure on the relative densities obtained for Al_2O_3-TiC composites sintered at 1700°C.

The densification results obtained for the Al_2O_3-TiC samples with different TiC compositions were compared to one another in order to determine the effects of the changing composition on

the densification properties of the materials. Figure 56shows the comparison of the densities for the samples sintered at 30 MPa and 50 MPa as a function of the sintering temperature.



a)



b)

Figure 56: Comparison of the densities obtained for the various compositions sintered using a pressure of a) 30 MPa and b) 50 MPa.

Due to the noticeable decrease in the densification of the samples, and since sintering at 50 MPa had resulted in superior densification of the Al_2O_3-30% TiC samples, it was decided to only sinter the Al_2O_3-50% TiC samples using a pressure of 50 MPa. In both cases (sintering at 30 MPa and 50 MPa) the relative density of the samples decrease with increasing titanium carbide content.

The densification results tended to plateau with increased temperature for the Al_2O_3-10% TiC and Al_2O_3-30% TiC when a pressure of 50 MPa was used. This also suggests that there was no further densification taking place and as a result, it was possible that the samples had a density higher than that calculated using Archimedes' principle. The increase in densification of the Al_2O_3-50% TiC sample when sintering at 1800°C would suggest that this is not the case, however it is suspected that this increase is due to the presence of the titanium oxide phase which begins to be reduced at the high temperatures, rather than further densification taking place.

Figure 57 shows the relationship between the densification results obtained and the amount of titanium carbide present in the samples for samples sintered at 1700°C and 50 MPa.

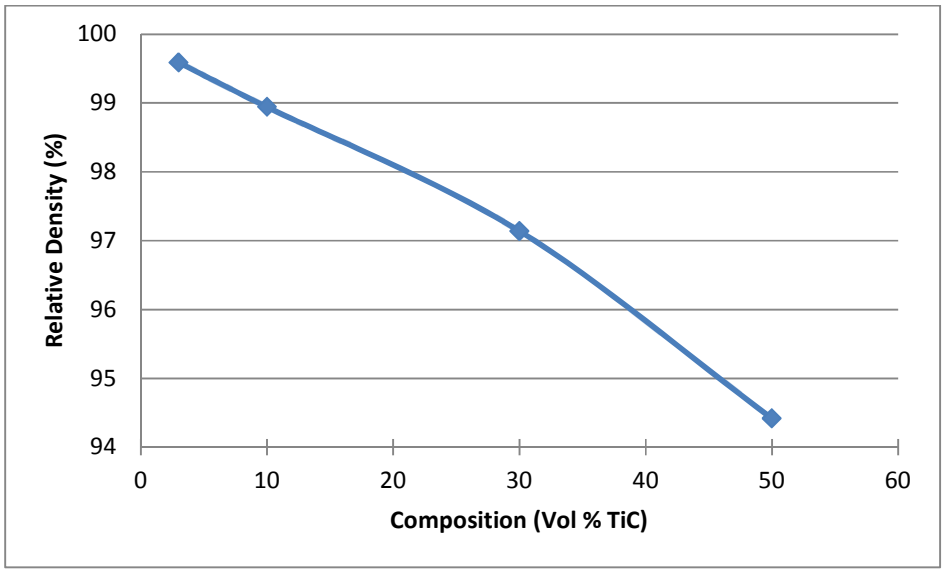


Figure 57: Relationship between the relative density and increasing TiC content for composites sintered at 1700°C and 50 MPa.

From these results, it was clear that with increasing the titanium carbide composition of the sample, the relative density decreased. If it was only the fact that the amount of oxide present in the starting powders was resulting in the materials having densities lower than the recalculated theoretical densities, one would expect that the relative density of the samples would decrease

linearly with respect to the TiC composition. However, this was not the case as it was clear that as the TiC composition was increased to 50% the trend is no longer linear. This suggests that it was not only the amount of oxygen in the starting powders that was affecting the densification results obtained.

Two suggestions for this decrease are:

- During processing of the powders there was more oxygen picked up by the powders.
- Due to the material surpassing the percolation limit, the ability to sinter the materials with a high TiC content was reduced[63].

If the decrease in densification was a result only of oxygen being picked up during the powder preparation phase, then in order for the Al_2O_3-50% TiC composite sintered at 1700°C and 50 MPa to actually be considered fully dense, it was calculated that the TiC powder would then need to have a composition (by weight) of 19.6% TiC and 80.4% TiO_2. This is shown in Table 26 below, which also shows the change in composition with decreasing the densification.

Table 26: Estimated composition of TiC in order for the following densification values to be obtained.

Densification (%)	Wt % TiC	Wt % TiO_2
100	19.6	80.4
99	25.4	74.6
98	31.1	68.9
97	36.8	63.2

From the XRD and SEM analysis of the samples, it was seen that this was not the case and that the amount of titanium carbide present was greater than that of the TiO_2. As a result although there may be further oxygen pick up during the powder processing stage, this was not sufficient to produce samples with a minimum density of even 97%.

Thus there must be other factors affecting the densification of the samples. The surpassing of the percolation limit may explain this. With the increased TiC compositions, the ability for the alumina to plastically deform and grain growth was greatly reduced as a result of the pinning effect associated with the secondary phase in the composite[64]. This was supported by the SEM analysis performed which shows that with increasing TiC content, there was a significant reduction in the amount of grain growth that occured during the sintering process. During sintering the ability of the larger alumina grains to move between the finer titanium carbide powder is much less than at lower TiC compositions, resulting in lower densification results being obtained. As was seen in Figure 53, very little densification was occurring towards the end of the sintering process. It is also possible that there was a diffusion of carbon from the carbide towards alumina[65][66], this would result in reduction in the surface region of the sample. Possible reactions that could have occurred:

$$Al_2O_3 + TiC \rightarrow TiC_{1-X} + Al_2O + CO$$

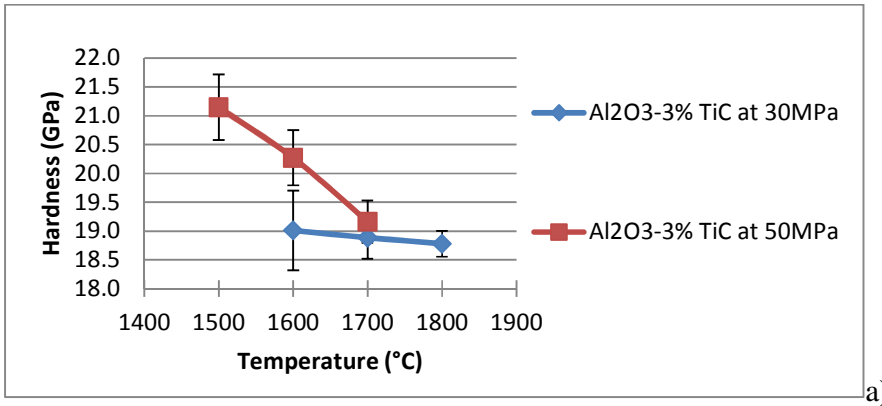
$$Al_2O_3 + 2C \rightarrow Al_2O + 2CO$$

It would appear that this was the case, particularly in the Al_2O_3-30% TiC and the Al_2O_3-50% TiC composites where there was evidence of porosity near the surface. If there was any residual carbon in the TiC powder, this would also result in a decrease in the density.

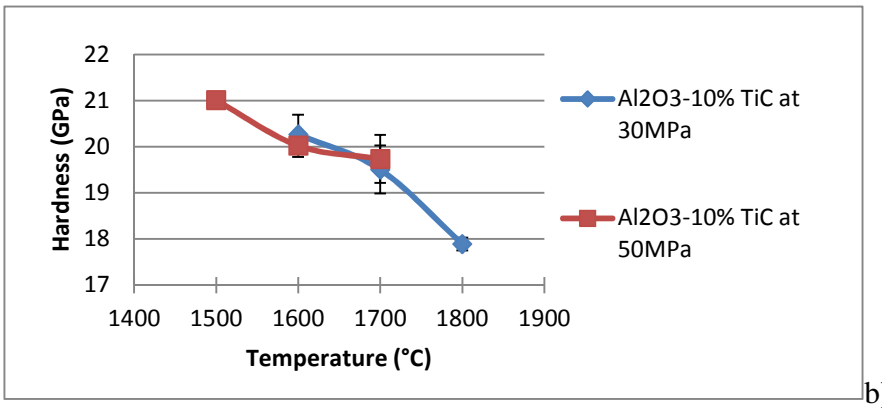
The lattice parameters of the pure TiC and the Al_2O_3-50%TiC nanocomposite sintered at 1700°C and 50 MPa were calculated and showed that there was no shift between the two. This suggests that the presence of the oxygen did not result in a distortion of the TiC lattice, which then would also have affected the density.

8.2.2. Comparison of Hardness and Fracture Toughness Results

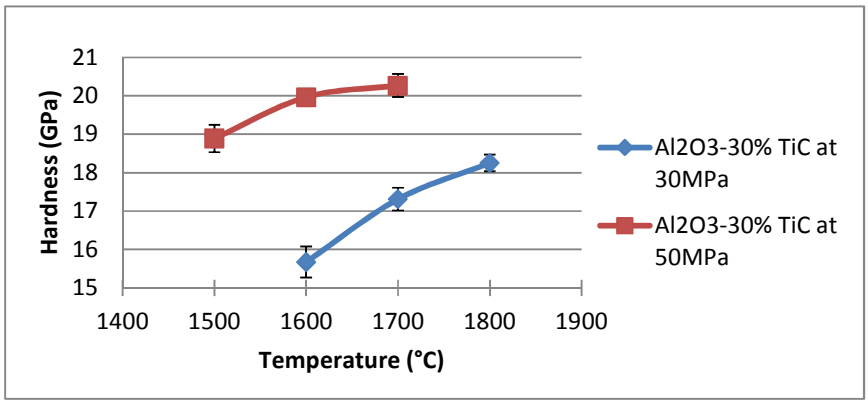
The hardness and fracture toughness values obtained for the Al_2O_3-3%TiC, Al_2O_3-10%TiC and Al_2O_3-30%TiCare given in Figure 58.



a)



b)



c)

Figure 58: Comparison of hardness of a) Al_2O_3-3% TiC, b)Al_2O_3-10% TiC and c)Al_2O_3-30% TiC sintered at various temperatures and pressures.

From Figure 58 a), it is clear that for the Al_2O_3-3% TiC samples, as the sintering temperature was increased the hardness of the materials began to decrease. It was also obvious that the samples sintered at 50 MPa have a higher hardness than those sintered at 30 MPa at the same temperatures. Figure 58 b) shows that for the Al_2O_3-10% TiC samples, as the sintering

temperature was increased the hardness of the materials began to decrease. It was also clear that the pressure at which the samples were sintered, at the same temperatures, results in similar hardness values for the samples. It is clear from Figure 58 c) that for the Al_2O_3-30% TiC samples, as the sintering temperature was increased the hardness of the materials began to increase. It is also clear that the hardness of the samples sintered at 50 MPa is at least 3 GPa higher than that for the samples sintered at 30 MPa. The hardness of the materials sintered using 50 MPa begins to plateau with increasing sintering temperature, which once again suggests that no further densification is taking place during the sintering of the samples with further increasein temperature, or that the densification is compensated by grain growth as there is still a 0.4% increase in the density.

Figure 59 shows the comparison of the hardness values for the samples sintered at 30 MPa.

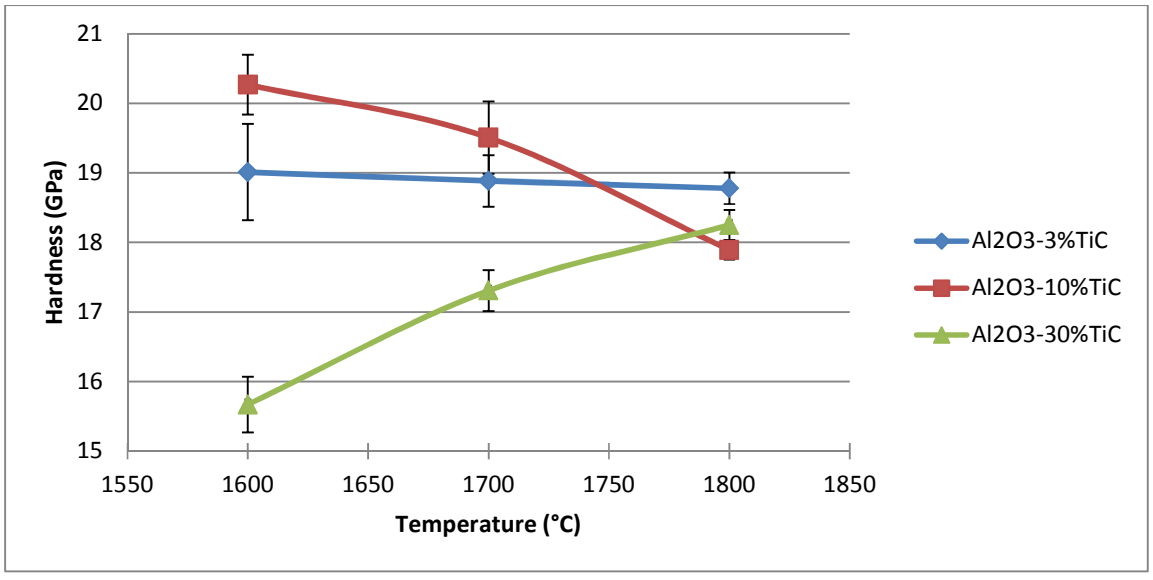


Figure 59: Comparison of the hardness values obtained for the various compositions sintered using a pressure of 30 MPa.

The hardness of the Al_2O_3-3% TiC and the Al_2O_3-10% TiC samples tended to decrease with increased temperature. The decrease was much greater in the Al_2O_3-10% TiC sample which suggests the greater amount TiC present has a significant effect on the properties of the materials

when the temperature was increased. This was due to the samples being fully dense at the lower temperatures and as a result increasing the temperature further resulted in grain growth within the sample. The hardness of the Al_2O_3-30% TiC increases with increasing temperature which suggests that there was still densification taking place and the effect of the better densification was greater than the effect of any grain growth that was occurring. When the hardness of the Al_2O_3-30% TiC sample tends to plateau, this could be due to the sample being densified and grain growth occurring or that the effect of the growing grains had started to have a greater effect than further densification. Figure 60 shows the comparison of the hardness values for the samples sintered at 50 MPa.

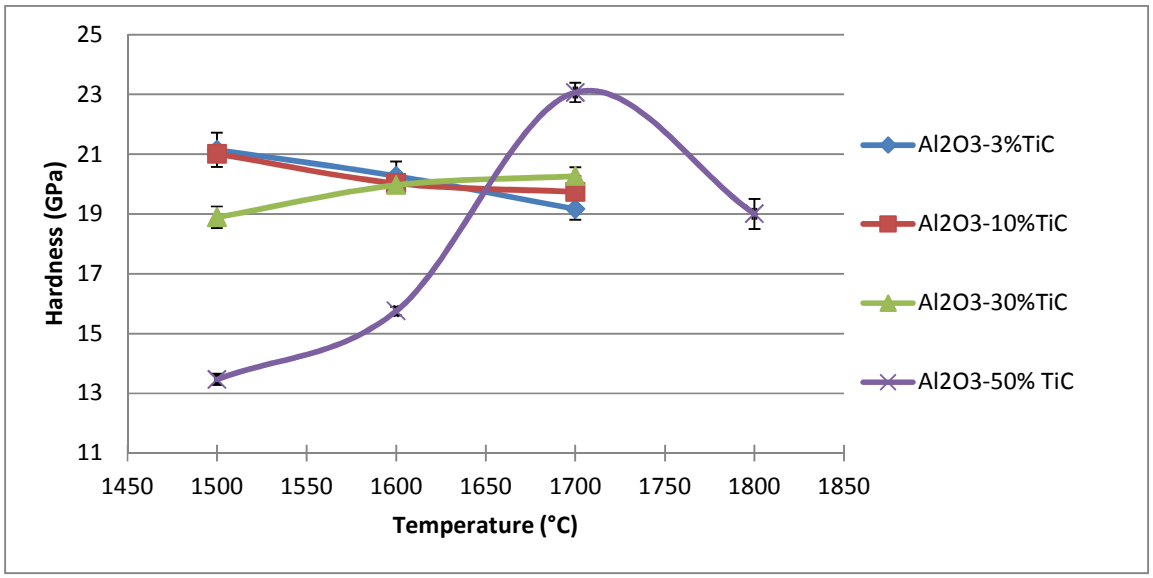


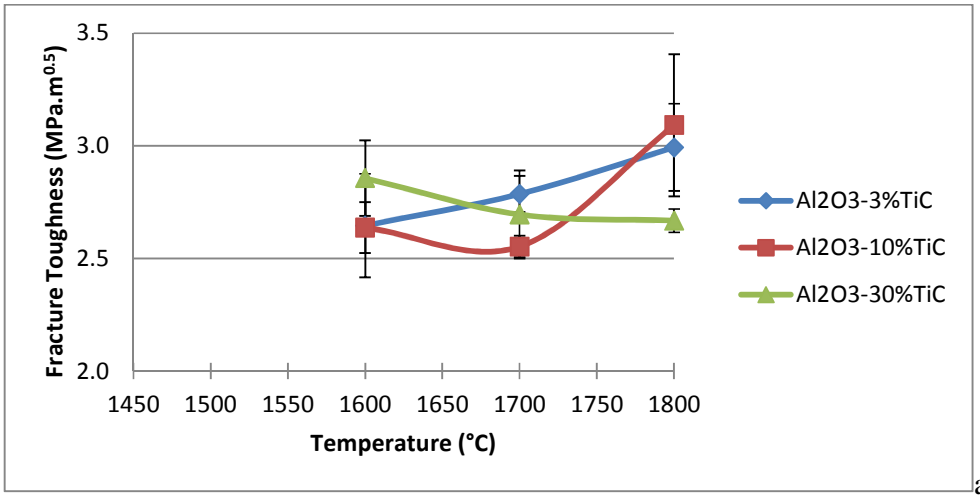
Figure 60: Comparison of the hardness values obtained for the various compositions sintered using a pressure of 50 MPa.

Once again, due to the Al_2O_3-3% TiC and the Al_2O_3-10% TiC being fully densified at the low temperatures, there will be grain growth in the samples with increasing temperature. This effect was evident in work done by Krell[67], thus once again, the Hall-Petch relationship results in the larger grain size causing the materials produced to have lower hardness values.

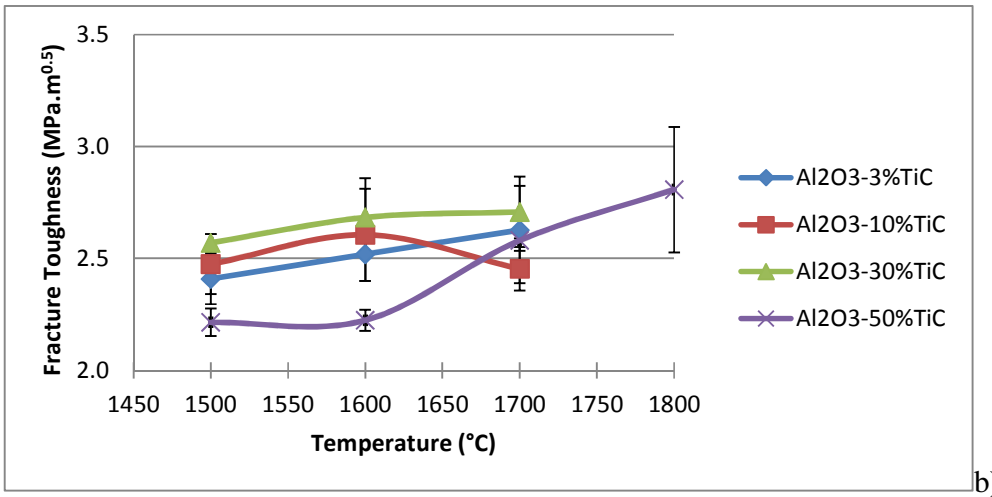
When the hardness of the Al_2O_3-30% TiC sample tends to plateau, this could be due to no further densification taking place in the sample and grain growth occurring or that grain growth has started to have a greater effect than the further densification of the sample. The oxide phase that was present in the materials will also result in the materials having a lower than expected hardness as it was softer than the TiC and alumina phases and as a result will lower the hardness. The hardness results of the Al_2O_3-50% TiC composites show that the hardness initially increases with increasing temperature from 1500°C to 1700°C where the hardness reaches a maximum. A further increase in the sintering temperature shows a significant decrease in the hardness of the material.

From the typical hardness values for Al_2O_3-TiC at various compositions obtained from literature shown in Table 5, it is seen that the hardness ranges between 19 and 23 GPa, with the higher hardness values obtained at the higher TiC compositions. Thus, although the hardness values obtained are slightly lower than expected they are still within the range of those found in literature for the samples that obtained the highest hardness values at each respective TiC composition.

When considering the standard deviation in the measurement of the fracture toughness of the Al_2O_3-TiC nanocomposites, there was little to no difference in the values obtained when sintering at 30 MPa and 50 MPa. Figure 61 a) shows the comparison of the fracture toughness values for the samples sintered at 30 MPa and Figure 61 b) for 50 MPa.



a)



b)

Figure 61: Comparison of the fracture toughness values obtained for the various compositions sintered using a pressure of a) 30 MPa and b) 50 MPa.

It is evident from Figure 61 a) that the fracture toughness of the Al_2O_3-3% TiC and the Al_2O_3-10% TiC tends to increase with increasing sintering temperature, however in the case of Al_2O_3-30% TiC this property decreases with increasing sintering temperature. This was possibly due to porosity in the sample at lower temperatures contributing to the toughness of this material.

From Figure 61 b) it is clear that as the sintering temperature was increased for materials sintered at 50 MPa their fracture toughness tends to increase, although the values tended to plateau and in the case of the Al_2O_3-10% TiC it began to decrease. The fracture toughness of the Al_2O_3-

50%TiC increases with increasing temperature. There was very little change in fracture toughness between 1500°C and 1600°C, but increasing the temperature further shows improved fracture toughness of the composites. From Figure 62, it was observed that for composites sintered using 50 MPa, the higher sintering temperature only affects the fracture toughness of the Al_2O_3-50%TiC composites where the fracture toughness is higher at the higher temperature.

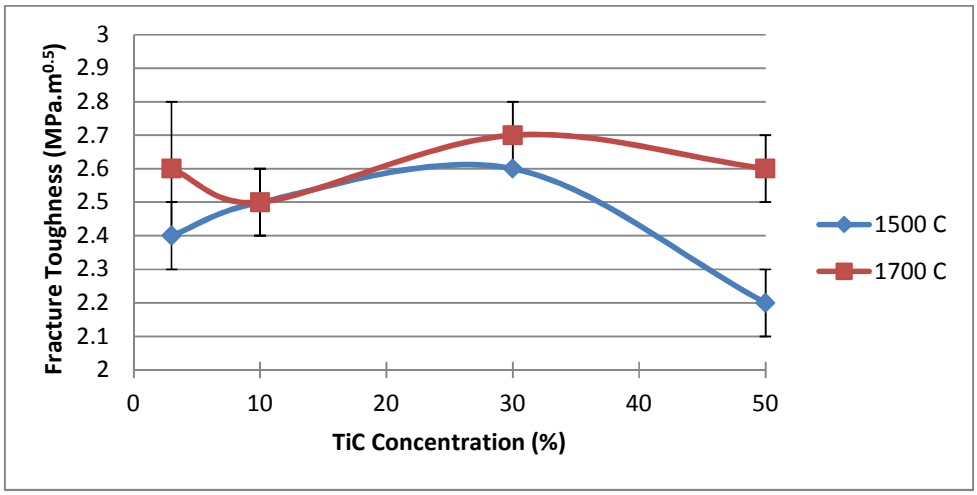


Figure 62: Effect of temperature on the fracture toughness values obtained for the various Al_2O_3-TiC compositions sintered using a pressure of 50 MPa.

From the typical fracture toughness values for Al_2O_3-TiC at various compositions obtained from literature and shown in Table 5, it was seen that the fracture toughness ranges between 3.6 and 6 $MPa.m^{0.5}$. Thus, the fracture toughness values obtained are lower than expected for each of the samples.

8.3. Discussion of sintering behaviour and properties of the Al_2O_3-TiN nanocomposites

The results obtained for the Al_2O_3-TiN composites were then analysed and compared to one another.

From the densification curves comparing the Al_2O_3-TiN nanocomposites sintered at 1600°C using a pressure of 50 MPa (Figure 63), it was clear that the Al_2O_3-3% TiN and the Al_2O_3-10% TiN materials reach a point where there is little to no movement of the pistons. As a result of this, very little to no densification was occurring by the end of the sintering experiment. In the case of the Al_2O_3-30% TiN and Al_2O_3-50% TiN samples it was seen that their densification appears to plateaus before beginning to increase again, once the final sintering temperature of 1600°C has been reached. However, this is due to thermal expansion of the composite with low densification rates during heating.

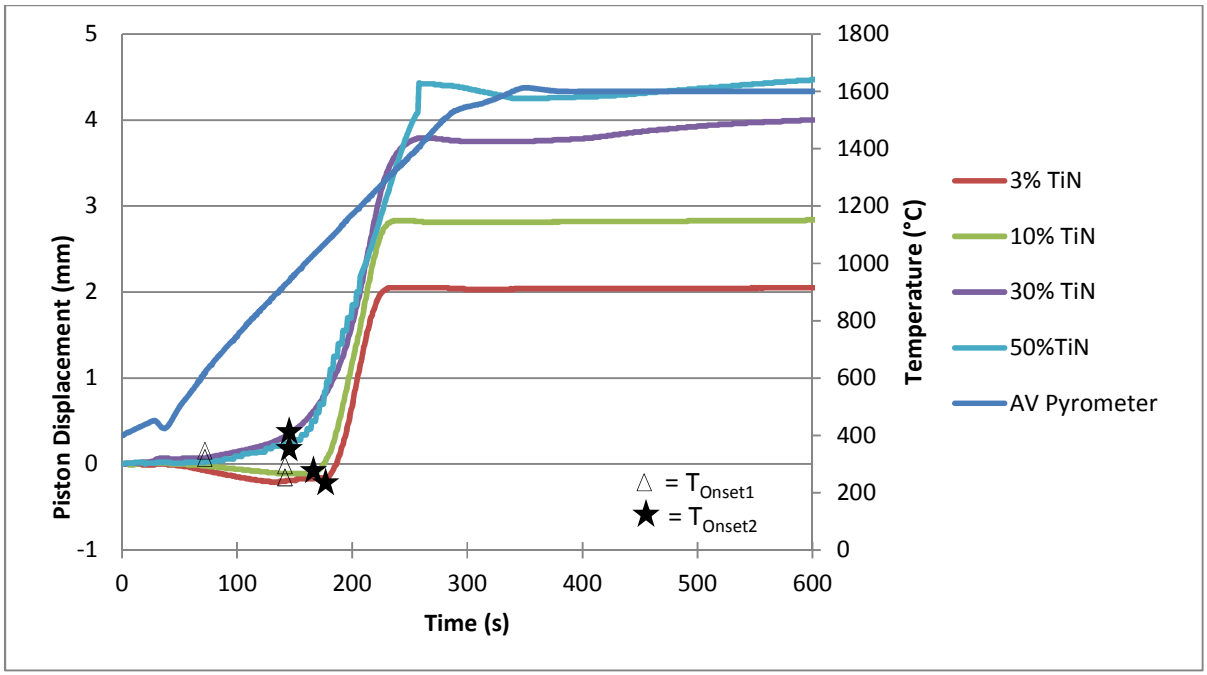


Figure 63: Densification curves for Al_2O_3-TiN sintered at 1600°C and a pressure of 50 MPa.

It is evident from these results that as the concentration of TiN in the composites was increased, there was an increase in the final piston displacement. The densification of the Al_2O_3-3%TiN and the Al_2O_3-10%TiN composites appeared to begin (T_{Onset1}) at approximately 950°C whilst those of the Al_2O_3-30%TiN and the Al_2O_3-50%TiN composites appeared to begin (T_{Onset1}) at approximately 650°C. It was evident from Figure 64 that the onset temperature, for the stage where there is intensive shrinkage (T_{Onset2}), decreases with increasing TiN content. The shift to the lower temperature with increasing the TiN content was likely due to the larger amount of the titanium oxide phase being present. The sintering appeared to end at approximately 1300°C for both the Al_2O_3-3%TiN and the Al_2O_3-10%TiN composites and at about 1450°C for the Al_2O_3-30%TiN and the Al_2O_3-50%TiN composites.

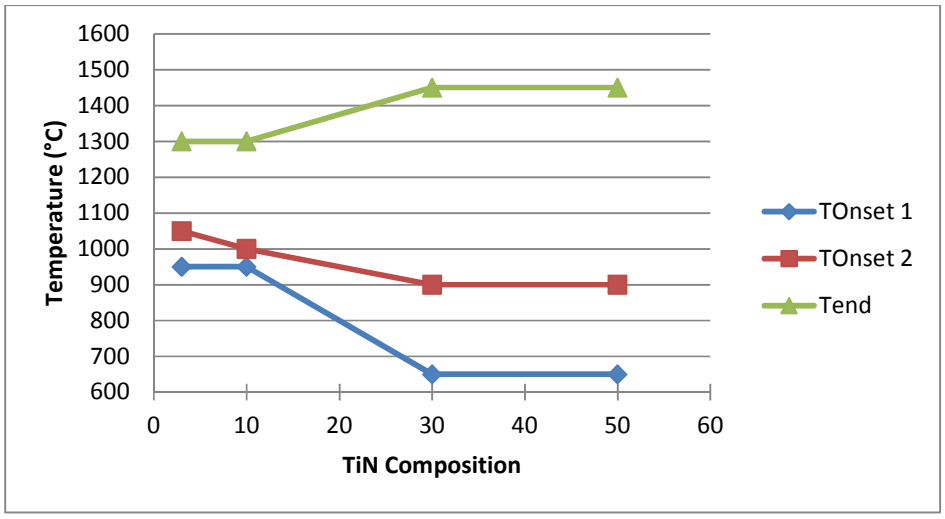


Figure 64: Onset temperatures for start of densification and the main densification and the end of densification with respect to the TiN concentration of the composites sintered at 1600°C and a pressure of 50 MPa.

8.3.1. Comparison of Densities

As seen with the Al_2O_3-TiC composites, the relative densities of the materials were too low and were recalculated taking into account the oxygen present in the starting powder. From the Leco oxygen analysis the titanium nitride powder was found to contain 8.44 weight percent oxygen.

The amount of TiO_2 was then calculated as with the Al_2O_3-TiC composites using equation 1 shown in section 8.2.1. From these calculations it was evident that the starting powder to contained 78.9% TiN and 21.1% TiO_2.

This enabled the theoretical density of the TiN powder to be recalculated and was found to be 5.06 g/cm^3, showing a decrease from the previous 5.4 g/cm^3 that was used for the pure powder. Using the new theoretical density for the TiN powder, it was then possible to recalculate the theoretical densities of each of the Al_2O_3-TiN materials as shown in Table 27.

Table 27: Recalculated theoretical density compared to the original theoretical density

Al_2O_3 - TiN		
TiN Composition (%)	**Original Theoretical Density (g/cm^3)**	**Recalculated Theoretical Density (g/cm^3)**
3	4.042	4.034
10	4.140	4.112
30	4.420	4.333
50	4.700	4.548

It is clear from these results that the presence of the oxide material resulted in a decrease of the theoretical density. This would result in an increase of the relative density of all the materials sintered as shown in Table 28.

Table 28: Recalculated Relative densities with change in density.

Sample	Temperature (°C)	Pressure (MPa)	Heating Rate (°C/min)	Original Relative Density (%)	Recalculated Relative Density (%)	Change in Relative Density (%)
Al_2O_3-3%TiN	1600	30	250	96.1	96.3	0.2
Al_2O_3-3%TiN	1700	30	250	97.2	97.4	0.2
Al_2O_3-3%TiN	1800	30	250	96.6	96.8	0.2
Al_2O_3-3%TiN	1600	50	250	98.2	98.4	0.2
Al_2O_3-3%TiN	1700	50	250	97.1	97.3	0.2
Al_2O_3-3%TiN	1800	50	250	96.9	97.2	0.3
Al_2O_3-10%TiN	1500	50	50	98.0	98.7	0.7
Al_2O_3-10%TiN	1600	50	50	95.7	96.3	0.6
Al_2O_3-10%TiN	1600	50	250	91.5	92.2	0.7
Al_2O_3-10%TiN	1700	50	250	90.8	91.4	0.6
Al_2O_3-30%TiN	1700	30	250	80.7	82.4	1.7
Al_2O_3-30%TiN	1500	65	250	93.5	95.4	1.9
Al_2O_3-30%TiN	1500	65	100	93.6	95.4	1.8
Al_2O_3-30%TiN	1500	65	25	93.6	95.5	1.9
Al_2O_3-30%TiN	1600	50	250	91.1	93.0	1.9
Al_2O_3-50%TiN	1500	60	50	90.3	93.3	3.0
Al_2O_3-50%TiN	1600	50	250	88.5	91.5	3.0
Al_2O_3-50%TiN	1700	60	50	91.8	94.8	3.0

From these results it was clear that as the amount of titanium nitride in the composites was increased, the change in the relative density of the material also increases. This was due to the larger amount of the titanium dioxide material being present in the sample thus lowering the theoretical density. It was seen that when comparing the original and the recalculated relative densities, the density increases linearly with increasing the TiN composition of the sample. The Al_2O_3-3% TiN and the Al_2O_3-10% TiN samples obtain densification values that are considered sufficiently high. Densification values over 98% were obtained following the recalculation of the theoretical density of the TiN powder. As with the Al_2O_3-TiC samples, it was observed that densification still decreases with increasing titanium nitride content. The recalculated densities of

the Al_2O_3-30%TiN showed that when taking into consideration the oxide phase within the samples, a densification of 95.5% at best was obtained. The maximum densification in the Al_2O_3-50%TiN composite is taken as 93.3% (due to the partial loss of sample mass when sintering at 1700°C where the density is 94.8%) when taking into account the recalculated relative densities. This suggests that these samples are still not sufficiently dense. It must also be noted that the Al_2O_3-30%TiN composites sintered at 1700°C/50 MPa and at 1800°C/30 MPa and the Al_2O_3-50%TiN composite sintered at 1800°C/50 MPa each using a heating rate of 250°C/min resulted in die failure. This was a result of the oxide phase present being strongly reduced, resulting in sample loss and eventually failure of the die.

The densification results for the Al_2O_3-TiN nanocomposites show that similar to the Al_2O_3-TiC nanocomposites, the densities obtained for the sintered materials tended to decrease with increasing the TiN concentration within the materials. They differ from the TiC containing composites in that superior densification results were obtained at the lower temperatures. This holds for each of the compositions, with the effect being much greater in the materials containing larger amounts of TiN.

It is important to note that when using lower heating rates during sintering, the densification results obtained were better than when the samples were heated at 250°C/min. This is due to the various Al_2O_3-TiN composites having more time to adjust during the sintering procedure. It was found that when the sintering temperature was increased for the Al_2O_3-30% TiNand the Al_2O_3-50% TiN, there was failure of certain dies and also there were large weight changes in the material being sintered. It was suspected that reduction of the oxide phases was to blame, and this was possibly the reason for the decrease in the densities of the samples as the temperature was increased. Surface decomposition was clearly visible within these samples, resulting in the material appearing layered throughout the cross-section.

The decomposition during the densification was due to reduction of the titanium oxide phase. This was possibly due to the samples becoming conducting at the time the displacement began to increase, which resulted in the temperature within the sample increasing rapidly and being higher than expected. This could cause the oxide phases to start being reduced, which would result in gases being produced. This could then introduce porosity within the sample, explaining the failure of the dies and also the loss of sample during the sintering process. Due to the TiO_2 present in the TiC starting powder being much less than that in the TiN powder, this effect was suspected to have been subdued in the Al_2O_3-TiC composites.

Figure 65 shows the relationship between the densification results obtained and the amount of titanium nitride present in the samples for samples sintered at 1600°C and 50 MPa.

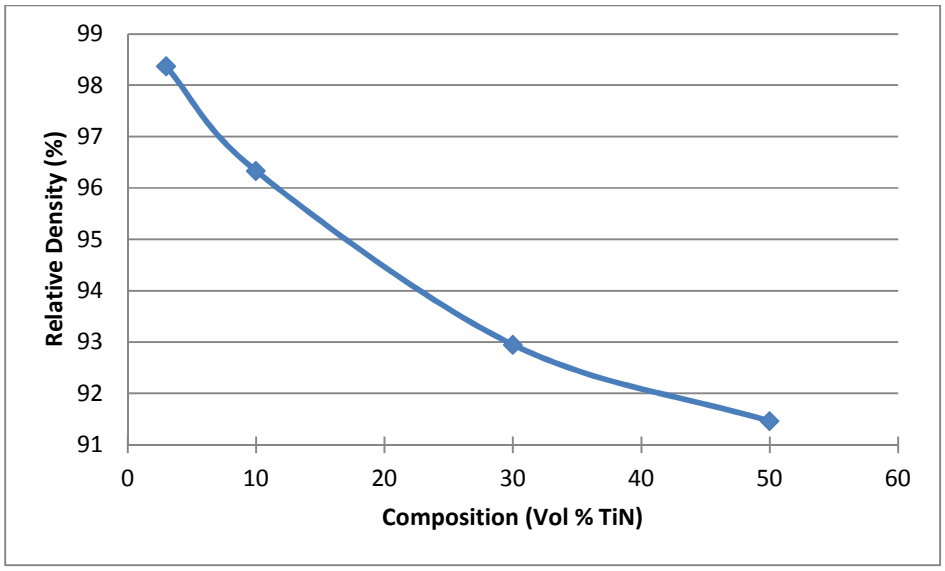


Figure 65: Relationship between the relative density and increasing the TiN concentration when using the recalculated theoretical density for the composites densified at 1600°C using a pressure of 50 MPa.

From these results, it was clear that with increased titanium carbide content within the sample, the calculated relative density decreased. As with the titanium carbide samples, we have explained most of the low densities obtained by correcting for the presence of oxides in the TiN

starting powder. However, if that were the only cause, one would expect that the relative density of the samples would decrease linearly with increasing TiN content. This was not the case because at TiN content of 50vol% there was pronounced deviation from linearity in the density vs composition graph of Figure 65. This suggests that it was not only the amount of oxygen in the starting powders that was affecting the densification results obtained.

It was again seen that if the decrease in densification was a result only of oxygen pick up, then the TiN powder in the composite would have to consist almost entirely of TiO_2. From the XRD and SEM analysis of the samples, it was seen that this is not the case and that the amount of titanium nitride present was greater than that of the titanium oxide containing phase which was found to be $(Al,Ti)_3O_5$. As a result, although there may be further oxygen pick up during powder processing, this was not sufficient to produce samples with a minimum density of even 97%.

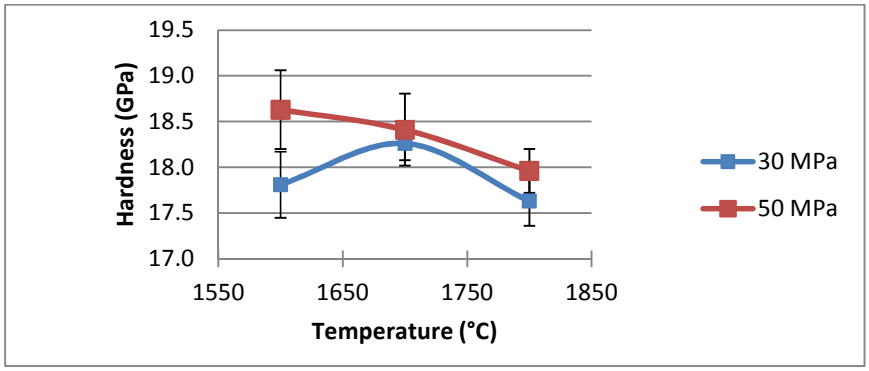
Thus, there must be other factors affecting the densification of the samples and the surpassing of the percolation limit may again explain this. When looking at Figure 65however, if it was only the percolation limit causing this deviation from linearity, one would expect the densities of the Al_2O_3-10%TiN composites to have been higher with a sharper decrease in relative density when moving to the Al_2O_3-30%TiN composites. With the increased TiN compositions, the ability for the alumina grains to grow was greatly reduced as a result of the pinning effect associated with the secondary phase in the composite[(64)]. However, it must be noted that although the growth of the alumina grains appeared to have decreased, there is significantly more growth associated with the TiN grains. This is supported by the SEM analysis which shows that with increasing TiN content in the samples, there was a significant reduction in the grain size of the Al_2O_3 and growth of the TiN. The TiN being finer and also containing more oxygen than the TiC could then explain why the densities of the Al_2O_3-TiN composites are lower than those of the Al_2O_3-TiC composites.

The decomposition of the Al_2O_3-30%TiN and the Al_2O_3-50%TiN composites when sintering at the higher temperatures would suggest that there was in fact reduction of the oxide phase occurring within the sample during sintering. This would result in porosity being introduced due to gases being produced during the reduction process. This would also suggest that a Ti_3O_5 phase would form, however this was not evident from the XRD analysis.

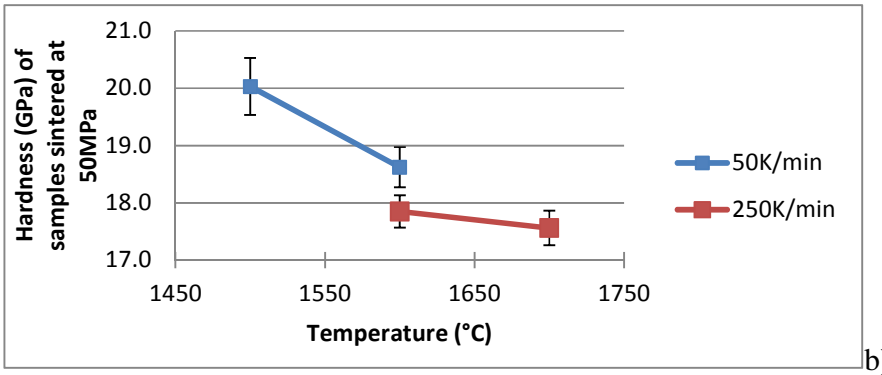
Concerning the lattice parameters of the TiN phase, it was established that this parameter was 4.246±0.005 Å for the Al_2O_3-50%TiNcomposite as opposed to 4.263±0.005 Å for TiN. This shows that there was a small shift in the lattice parameters which could also result in a change in the density of the materials.

8.3.2. Comparison of Hardness and Fracture Toughness Results

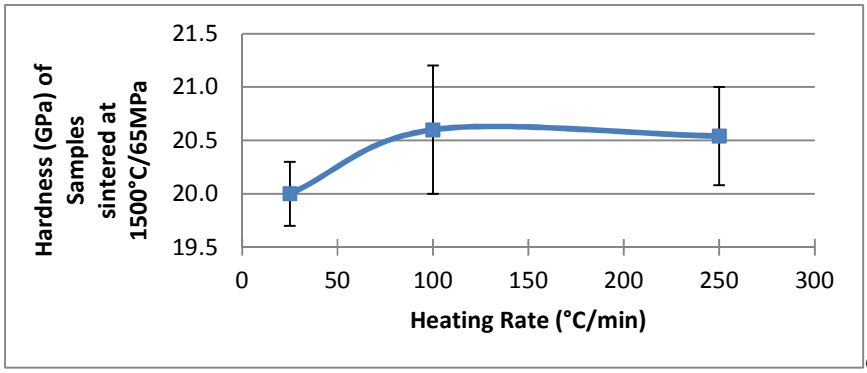
The hardness and fracture toughness results obtained were typically lower than those obtained for the Al_2O_3-TiNcomposites with the same concentrations of the reinforcingphases.



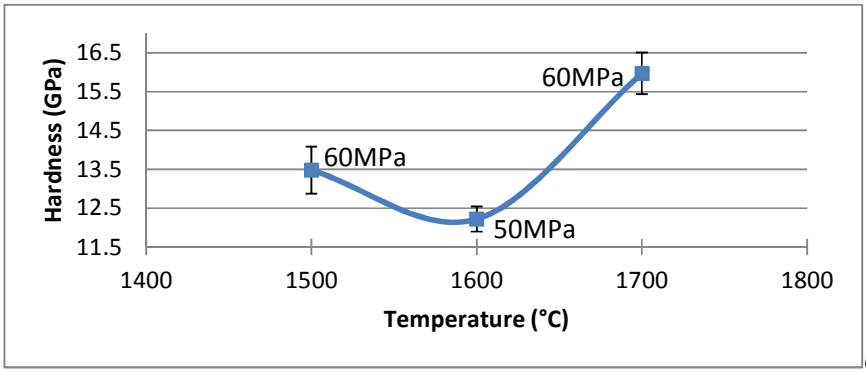
a)



b)



c)



d)

Figure 66: Comparison of thehardnessofa) Al_2O_3-3% TiN, b) Al_2O_3-10% TiN, c)Al_2O_3-30% TiNand d)Al_2O_3-50% TiN sintered under various conditions.

From the results shown in Figure 66(a), it is seen that the hardness of the Al_2O_3-3% TiN samples sintered using a pressure of 50 MPa decreased with increasing temperature in line with the densification of these samples which was also found to decrease with increasing the sintering temperature. The hardness of the samples sintered at 30 MPa increases before decreasing again. This was possibly due to the densification of the samples sintered at 30 MPa initially increasing and then decreasing with increasing temperature ($\rho_{1600°C}$=96.2 g/cm^3, $\rho_{1700°C}$=97.3 g/cm^3 and $\rho_{1800°}$C=96.7 g/cm^3). In both cases (30 and 50 MPa) the samples that achieved the highest densification had the highest hardness values.

The relationship between the hardness results obtained for the samples and the sintering temperature was investigated for the Al_2O_3-10% TiN materials and is shown in Figure 66(b), for the samples sintered using two different heating rates. It was evident from the results that the hardness of the materials was better when using lower heating rates. It was also seen that as the sintering temperature for the samples was increased there was a decrease in the hardness of the materials. It was again evident that the composites that achieved better densification results were the composites with the more favourable hardness values. The extent to which densification affected the hardness was evident in the materials sintered using a heating rate of 50°C/min, when the temperature was increased from 1500°C to 1600°C, there was a 2.4% decrease in the relative density and a 1.4GPa decrease in hardness.

A comparison of the hardness results obtained and the heating rate used was investigated and is shown in Figure 66(c), for the Al_2O_3-30% TiN samples sintered at 1500°C. This shows that as the heating rate was increased, the hardness of the materials initially increased between the heating rates of 25 and 100°C/min. However, it was also seen that there was a slight decrease in hardness when the heating rate was increased from 100°C/min to 250°C/min.

The relationship between the hardness results obtained for the Al_2O_3-50% TiN samples and the sintering temperature was investigated and is shown in Figure 66(d). The hardness results

obtained for the Al_2O_3-50% TiN samples that were sintered show that there was once again an initial decrease in the hardness of the materials before the hardness increases again with increasing the temperature from 1500°C to 1700°C.

The hardness values for each of the composites can be related to the density of the samples as the samples with the best densities are also those which have the highest hardness results. This was true for all the composition except for the Al_2O_3-30% TiN where the samples were sintered at the different heating rates in order to investigate this effect on the densification of the samples. Here for the samples sintered at 1500°C and 65 MPa, the sample with the heating rate of 25°C/min had a slightly higher densification than that for the sample sintered at 100°C/min and yet the hardness value of 20.0 GPa obtained was 0.6 GPa lower. This suggests that grain growth was occurring within the sample and the SEM analysis comparing these samples supports this. This effect was evident in work done by Krell et al. (1998)[67], which showed that with increasing grain size the hardness of the materials being investigated tended to decrease. Table 29 shows the best hardness values that were obtained for each of the Al_2O_3-TiN compositions sintered, irrespective of the sintering conditions that were used in order to produce the samples.

Table 29: Best hardness results obtained for each composition of the Al_2O_3-TiN samples that were sintered.

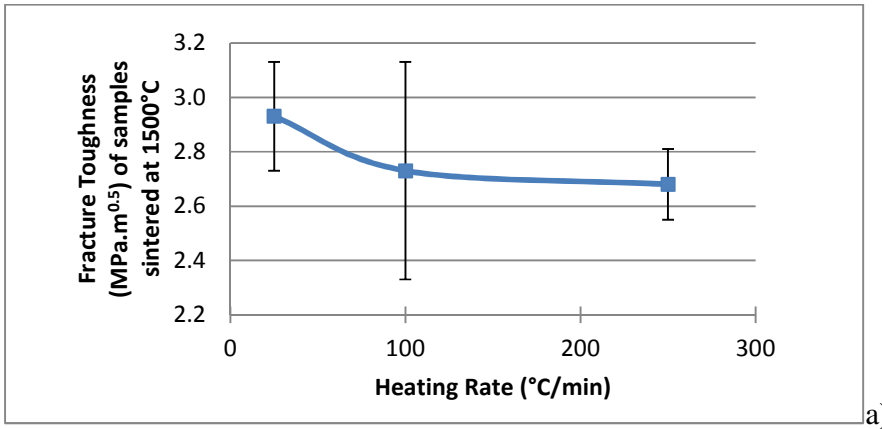
Sample	Temperature (°C)	Pressure (MPa)	Heating Rate (°C/min)	Relative Density (%)	Hardness (GPa)
Al_2O_3-3%TiN	1600	50	250	98.4	19.3±0.4
Al_2O_3-10%TiN	1500	50	50	98.7	20.0±0.5
Al_2O_3-30%TiN	1500	65	100	95.4	20.6±0.6
Al_2O_3-50%TiN	1700	60	50	94.8	16.0±0.5

It was clear from these values that the hardness values increased up to the 30% TiN composition, however there was a significant decrease in the hardness at the 50% TiN composition. This was again suspected to be due to the poor densification of the samples.

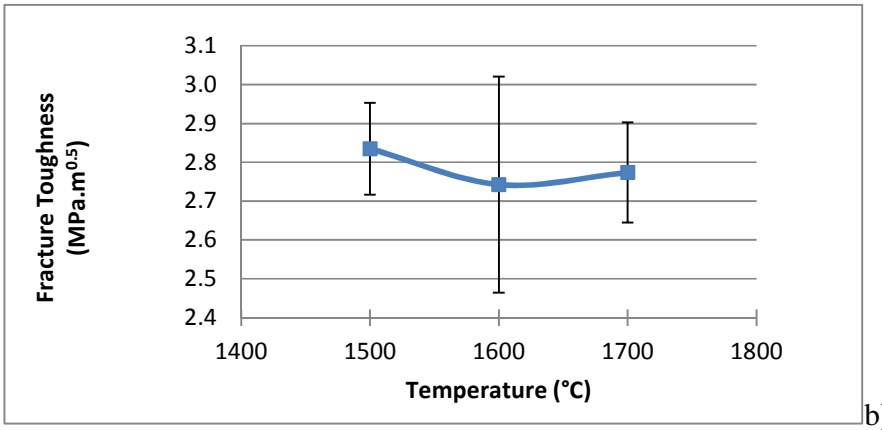
The Al_2O_3-50% TiN sample sintered at 1700°C was found to have the highest density and hardness. However, due to the mass loss experienced with this sample these values are not an accurate representation of the system being investigated. Further evidence of this is seen from the SEM analysis on the sample, which shows separation of the materials and also excessive grain growth of both the alumina and titanium nitride in the sample.

All the hardness values are slightly lower than expected; this also suggests the presence of the titanium oxide phase. The TiO_2 phase is softer than that of TiN and therefore it would result in a decrease in the hardness of the materials. From the typical hardness values for Al_2O_3-TiN at various compositions obtained from literature and shown in Table 5 it was seen that the hardness ranges between 17.7 and 22 GPa, with the higher hardness values obtained at the higher TiN compositions. Thus, although the hardness values obtained were slightly lower than expected they were still within the range of those found in literature for samples with a composition up to 30% TiN. The 50% TiN containing sample was well below that which was obtained from literature.

The fracture toughness values, on average, tend to increase with increasing TiN content. The difference in this increase was relatively small and the values for the materials are not as high as was expected for the nanomaterials. It is also possible that the porosity of the samples is responsible for the increase in fracture toughness as the pores will hinder crack propagation. As with the Al_2O_3-TiC nanocomposites, it was again evident that when the measurement error is taken into account, there was little to no difference in the fracture toughness when sintering using different conditions for the same composite.



a)



b)

Figure 67: Comparison of fracture toughness a) Al_2O_3-30% TiNand b)Al_2O_3-50% TiN sintered under various conditions.

The relationship between the fracture toughness results obtained for the samples and the heating rate used was investigated and shown in Figure 67 (a), for the Al_2O_3-30% TiN composites sintered at 1500°C. Figure 67 (b) shows the relationship between the fracture toughness results obtained for the Al_2O_3-50% TiN composites and the sintering temperature. This showed that there was very little change in the fracture toughness of the Al_2O_3-30% TiN composites with varying heating rate and of the Al_2O_3-50% TiN composites with increasing temperature. Figure 68 shows that with increasing the TiN concentration within the composites sintered at 1600°C using a heating rate of 250°C/min and a pressure of 50 MPa, there is little to no change in the fracture toughness of the composites.

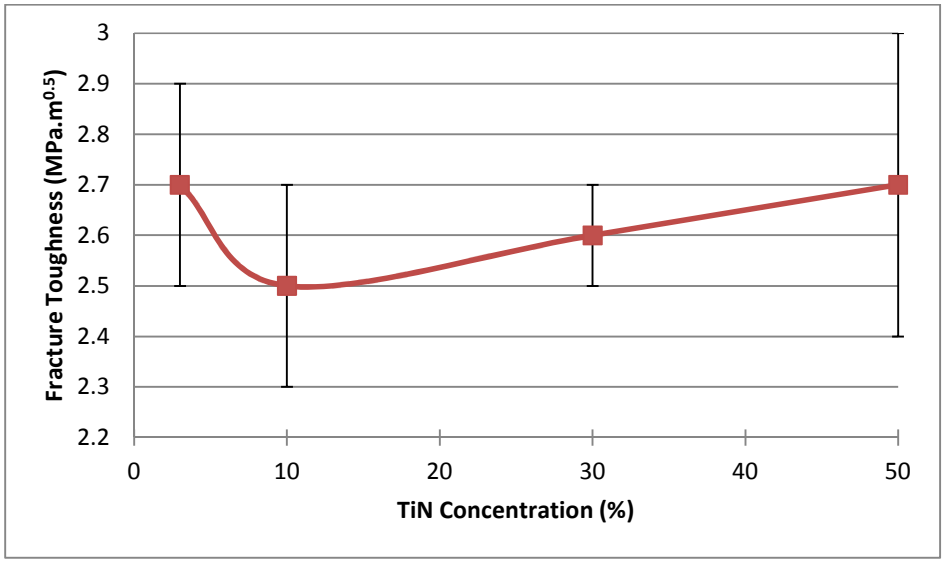


Figure 68: Effect of increasing TiN concentration on the fracture toughness of the Al_2O_3-TiN composites sintered at 1600°C and 50 MPa.

Table 30shows the highest fracture toughness values that were obtained for each of the Al_2O_3-TiN compositions made, irrespective of the sintering conditions used.

Table 30: Best fracture toughness results obtained for each composition of the Al_2O_3-TiN samples that were sintered.

Sample	Temperature (°C)	Pressure (MPa)	Heating Rate (°C/min)	Relative Density (%)	Fracture Toughness ($MPa.m^{1/2}$)
Al_2O_3-3%TiN	1600	50	250	98.40	2.7±0.2
Al_2O_3-10%TiN	1600	50	50	96.33	2.7±0.1
Al_2O_3-30%TiN	1500	65	25	95.51	2.9±0.2
Al_2O_3-50%TiN	1500	60	50	93.31	2.8±0.1

It was seen that there was very little change in the highest fracture toughness values obtained for the Al_2O_3-3% TiN and Al_2O_3-10% TiN samples. There was however some increase when

looking at the Al_2O_3-30% TiN and Al_2O_3-50% TiN samples which could be caused by the porosity in the sample as discussed above.

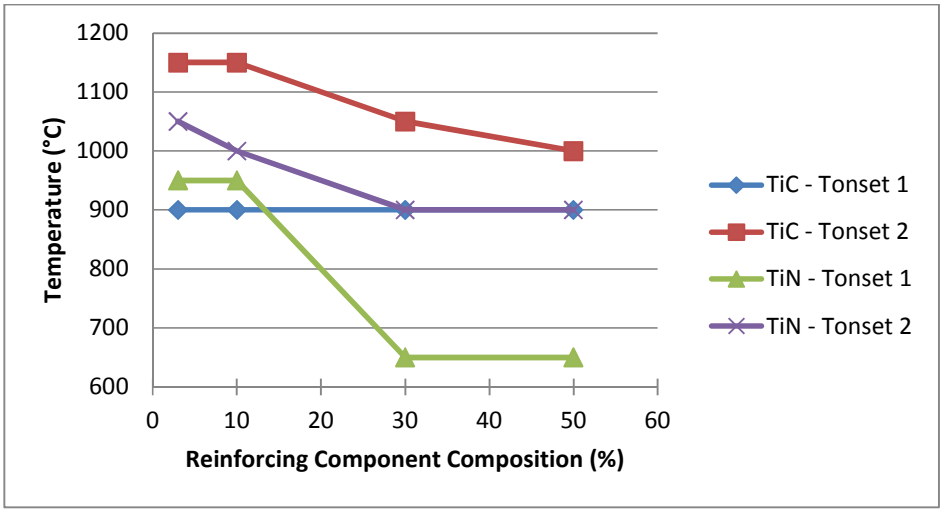
From the typical hardness values for Al_2O_3-TiN at various compositions obtained from literature and shown in Table 5 it was seen that the fracture toughness ranges between 4 and 5.7 MPa.$m^{0.5}$. Thus, the fracture toughness values obtained in this work were lower than expected for each of the samples.

8.4. Comparison of the Al_2O_3-TiC and the Al_2O_3-TiN nanocomposites

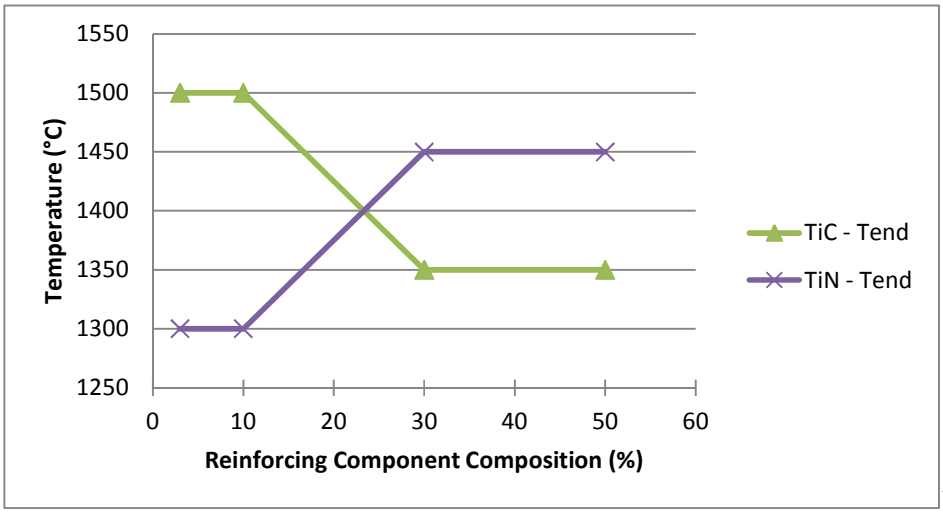
In order to objectively analyse the nanocomposites and compare them, the following comparisons of the materials were made in order to determine which of the composites achieved the most favourable properties. In order to compare the materials the best properties obtained for each of the materials for the various compositions sintered were taken into account. The properties analysed were densification, hardness and fracture toughness. The best values obtained for each of the above mentioned properties were used irrespective of the conditions under which they were obtained.

When comparing the densification curves it was seen that the initial sintering temperature (T_{Onset1}), as is shown in Figure 69 (a), for the Al_2O_3-TiC composites was approximately the same for each composition. The $T_{Onset1}$for Al_2O_3-3%TiC and Al_2O_3-10%TiC begins at lower temperatures than that for Al_2O_3-3%TiN and Al_2O_3-10%TiN however, there is a sharp decrease in the temperature for the Al_2O_3-30%TiN and the Al_2O_3-50%TiN composites. For the stage where there was rapid consolidation of the composites, the temperature at which this began (T_{Onset2}) typically decreased with increased concentration of the reinforcing component. This was suspected to be due to the presence of the titanium oxide phase present in the starting powder. The titanium oxide phase requires lower temperatures to sinter and thus as the amount was increased, there was a shift in the starting temperature of the sintering process. The fact that the

T_{onset2} temperature for each of the Al_2O_3-TiN composites was lower than the Al_2O_3-TiC composites with the corresponding concentration again suggests that this is the case as it was known that the TiN powder contained a great deal more (4.9 wt %) oxygen. When comparing the temperatures at which sintering appears to end (T_{end}), as shown in Figure 69 (b), between the Al_2O_3-TiCand the Al_2O_3-TiN composites it was evident that the Al_2O_3-3%TiC and the Al_2O_3-10%TiC have a higher end temperature than the Al_2O_3-3%TiN Al_2O_3-10%TiN. This was reversed however for the Al_2O_3-30%TiC and the Al_2O_3-50%TiC where the end temperatures are lower than the Al_2O_3-30%TiN and the Al_2O_3-50%TiN composites.



a)



b)

Figure 69: Comparison of (a) onset temperatures for start of densification and the main densification and (b) the end of densification with respect to the reinforcing component concentration for both the Al_2O_3-TiC and the Al_2O_3-TiN composites.

The first property that was compared was the densification that occurred within the various samples sintered. Table 31shows the best densification results that were obtained for each of the Al_2O_3-TiC and the Al_2O_3-TiN composites and the conditions at which they were achieved. The densification results that were used for the comparison are those that take into account the effect of the oxygen contamination within the TiC and TiN nanopowders respectively.

Table 31: Best densification results obtained for each composition of both the Al_2O_3-TiCand Al_2O_3-TiN samples that were sintered.

Sample	Temperature (°C)	Pressure (MPa)	Heating Rate (°C/min)	Relative Density (%)
Al_2O_3-3%TiC	1700	50	250	99.6
Al_2O_3-10%TiC	1600	50	250	99.0
Al_2O_3-30%TiC	1700	50	250	97.1
Al_2O_3-50%TiC	1800	50	250	95.9
Al_2O_3-3%TiN	1600	50	250	98.4
Al_2O_3-10%TiN	1500	50	50	98.7
Al_2O_3-30%TiN	1500	65	25	95.5
Al_2O_3-50%TiN	1500	60	50	93.3

From these results it was clear that the relative density of the Al_2O_3-TiC samples was higher than that of the Al_2O_3-TiN for each of the compositions that were investigated. The Al_2O_3-10% TiN and the Al_2O_3-10% TiC samples have densification results that are comparable, however it must be noted that the heating rate that was used for the TiN containing sample was reduced from 250°C/min to 50°C/min. It was only once this change in the heating rate was implemented that the densification results for the Al_2O_3-10% TiN composites became reasonable. Thus it is clear that in general the TiN containing composites are harder to densify than those that contain TiC. It was suspected that this was a result of the TiN particles being half the size of the TiC particles and this significantly decreased the extent of densification that occurred within the samples. It was suspected that the size and nature of the reinforcing materials resulted in the alumina grains

being pinned[64]. As a result, the ability of the alumina matrix to plastically deform during sintering is reduced, which decreases relative densification in comparison to the TiC containing composites. In both of the composite materials the densification decreases with increasing amount of the reinforcing component. In the composites with 30 and 50% of the relative reinforcing components added this was suspected to be due to the percolation limit being exceeded, which as mentioned above, results in the alumina not being able to plastically deform. At the higher concentrations of the reinforcing components, this effect was exaggerated because of grain growth in the alumina material being reduced. This was evident in the SEM images for both the composite materials systems investigated in this work. It must be noted however, that in the Al_2O_3-TiN composites in which there was significant decomposition of the titanium oxide-containing phases (Al_2O_3-30%TiN and Al_2O_3-50%TiN sintered at 1700°C and 250°C/min), there was significant growth of the TiN grains.

Table 32 shows the best hardness values that were obtained for each of the materials that were sintered. These materials are also compared with respect to their relative densification as shown in Figure 70.

Table 32: Best hardness results obtained for each composition of both the Al_2O_3-TiCand Al_2O_3-TiN samples that were sintered.

Sample	Temperature (°C)	Pressure (MPa)	Heating Rate (°C/min)	Relative Density (%)	Hardness (GPa)
Al_2O_3-3%TiC	1500	50	250	99.5	21.1±0.6
Al_2O_3-10%TiC	1500	50	250	98.5	21.0±0.2
Al_2O_3-30%TiC	1700	50	250	97.1	20.3±0.3
Al_2O_3-50%TiC	1700	50	250	94.4	23.1±0.3
Al_2O_3-3%TiN	1600	50	250	98.4	19.3±0.4
Al_2O_3-10%TiN	1500	50	50	98.7	20.0±0.5
Al_2O_3-30%TiN	1500	65	100	95.4	20.6±0.6
Al_2O_3-50%TiN	1700	60	50	94.8	16.0±0.5

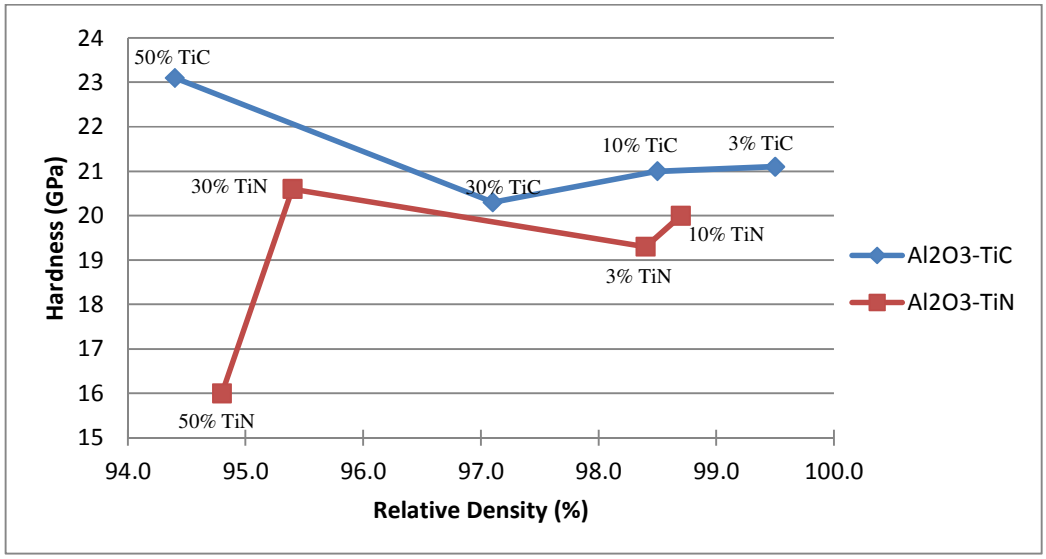


Figure 70: Comparison of hardness values obtained with respect to their relative density, for the samples as shown in Table 32.

It was evident from the comparison of the hardness values obtained for the two types of composites that typically the titanium carbide containing materials have slightly higher hardness. This is also evident in the composites sintered at 1600°C using a heating rate of 250°C/min and a pressure of 50 MPa, as shown in Figure 71. This was expected since TiC is a harder material than TiN, with hardness between 28 and 35 GPa while TiN has hardness between 18 and 21 GPa (Pierson, pp190)[68]. It must be noted however, that due to the presence of oxygen within these materials the hardness will be lower than expected; furthermore, the TiN powder had a significantly higher amount of oxygen than the TiC. The main difference observed when comparing the hardness of the two systems was that the hardness for the Al_2O_3-50% TiC significantly increased and the hardness of the Al_2O_3-50% TiN significantly decreases as the reinforcing component is increased to 50 vol.%. The porosity of the samples will result in the hardness values being lower than expected as seen in work done by Krell et al. (2001)[69]. When comparing the hardness values obtained to those in literature (Table 34), it was seen that the composites had hardness values comparable to those from literature, except for the Al_2O_3-50% TiN composite which has hardness slightly lower than the range found in literature.

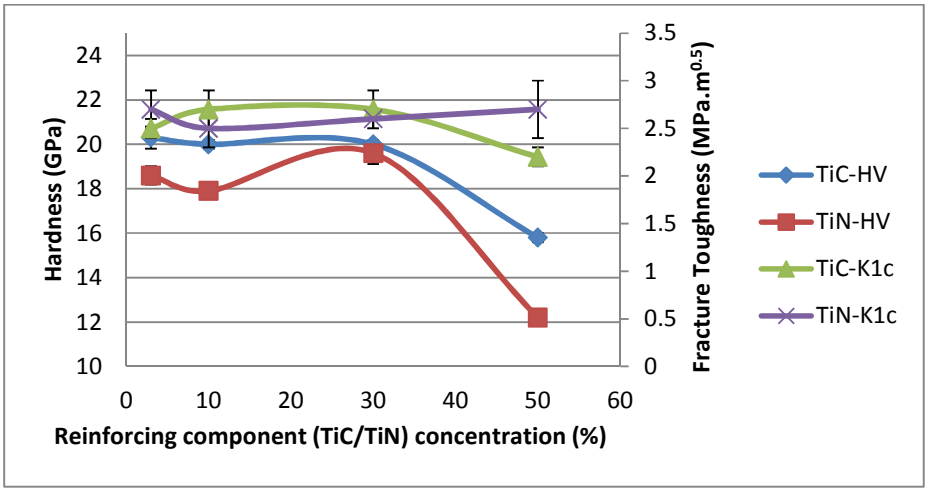


Figure 71: Comparison of hardness and fracture toughness values obtained with respect to the reinforcing component concentration for composites sintered under the same conditions at 1600°C and 50 MPa.

Table 33 shows the best fracture toughness values that were obtained for each of the composites sintered in this work.

Table 33: Best fracture toughness results obtained for each composition of both the Al_2O_3-TiCand Al_2O_3-TiN samples that were sintered.

Sample	Temperature (°C)	Pressure (MPa)	Heating Rate (°C/min)	Relative Density (%)	Fracture Toughness ($MPa.m^{1/2}$)
Al_2O_3	1500	50	250	99.1	3.0±0.3
Al_2O_3-3%TiC	1800	30	250	99.3	3.0±0.2
Al_2O_3-10%TiC	1800	30	250	99.0	3.1±0.3
Al_2O_3-30%TiC	1600	30	250	94.7	2.9±0.2
Al_2O_3-50%TiC	1800	50	250	95.9	2.8±0.3
Al_2O_3-3%TiN	1600	50	250	98.40	2.7±0.2
Al_2O_3-10%TiN	1600	50	50	96.33	2.7±0.1
Al_2O_3-30%TiN	1500	65	25	95.51	2.9±0.2
Al_2O_3-50%TiN	1500	60	50	93.31	2.8±0.1

From this comparison it was clear that at lower concentrations of the reinforcing components (3% and 10%), the Al_2O_3-TiC samples have a slightly higher fracture toughness than the Al_2O_3-TiN samples and all other TiC-containing composites studied in this work. It was seen however, that for the samples containing 30% and 50% of the respective reinforcing components, the fracture toughness values for both the Al_2O_3-TiC and the Al_2O_3-TiN composites at the same compositions were roughly the same. From Figure 71 it is evident that for the composites sintered under the same conditions there was little to no difference in the fracture toughness between samples containing TiC and TiN. When comparing the fracture toughness values obtained to those in literature (Table 34), it was seen that all of the composites had fracture toughness lower than those previously reported. Also the addition of the secondary phase showed no improvement in fracture toughness when compared to a pure alumina sample that was sintered for comparison.

Table 34: Hardness and fracture toughness results from Table 32 and Table 33 respectively compared to values from literature as shown in Table 5 and those obtained from the sintered µm-composites.

Material	Obtained (nano)		Literature (Table 5)			Sintered µm composites	
	Hardness (GPa)	Fracture Toughness ($MPa.m^{0.5}$)	Size Range	Hardness (GPa)	Fracture Toughness ($MPa.m^{0.5}$)	Hardness (GPa)	Fracture Toughness ($MPa.m^{0.5}$)
Al_2O_3-TiC	21.1-23.1	2.8-3.0	µm	19-23	3.6-6	19.1-19.4	3.7-3.8
			nano	≈21	≈3.9		
Al_2O_3-TiN	16-20.6	2.7-2.9	µm	17.7-22	4-5.7	18.1-18.7	3.1-3.8
			nano	18-22	≈5.7		

9. Conclusion

From the work done on the composite materials produced from µm ranged powders, it was found that the Al_2O_3-TiC and the Al_2O_3-TiN composites could be dispersed using Lubrizol 2155 dispersant and hexane as the solvent. The effect of the surface area of the powders on the amount of dispersant required was also evident in that the alumina with the larger SSA required more dispersant than the TiN and TiC powders which had both a smaller SSA. It was also evident that the amount of Lubrizol 2155 required was material dependent as the TiC and TiN µm-powders had similar SSA's but the TiN powder required more Lubrizol in order to be optimally dispersed.

The properties obtained for the materials produced from µm-range powders showed that the Al_2O_3-50% TiC samples had higher hardness values, reaching 19.4 GPa, compared to the Al_2O_3-50% TiN composites which reached 18.7 GPa. Both the Al_2O_3-50% TiC and the Al_2O_3-50% TiN had fracture toughness values reaching 3.8 $MPa.m^{0.5}$. Thus it was evident when comparing the µm-composites to the nanocomposites that the hardness value for the Al_2O_3-50% TiC µm-composite was lower than that of the nanocomposite (23.1 GPa) however, the fracture toughness of the µm-composite (3.8 $MPa.m^{0.5}$) was superior compared to that of the nanocomposite (2.6 $MPa.m^{0.5}$). Both the hardness and the fracture toughness values obtained for the Al_2O_3-50% TiN µm-composite were superior to the Al_2O_3-50% TiN nanocomposite which had a hardness of 16.0 GPa and a fracture toughness of 2.8 $MPa.m^{0.5}$.

The investigation of the Al_2O_3, TiC and TiN nanopowders revealed that the larger the SSA of the powder the more difficult they were to disperse. It was seen that the solids loading of the suspension had an effect on the amount of Lubrizol required to adequately disperse the powders. It was found that as the total amount (weight % with respect to the solid content) of Lubrizol 2155 required increased, the amount of this dispersant per unit area decreased with increasing surface area; this was evident when comparing the results from the µm-powder to the

nanopowders. The µm-TiC required 5.8 mg/m^2while the nano-TiC required 3.5 mg/m^2. Furthermore, the µm-TiN required 8.9 mg/m^2 and the nano-TiN required 1.5 mg/m^2 in order to be adequately dispersed. It must be noted that the µm-TiN was not a pure TiN phase and consisted primarily of Ti_2N.

The properties obtained from the sintered materials showed that there was a decrease in the relative density of both the Al_2O_3-TiC and the Al_2O_3-TiN nanocomposite materials when the reinforcing component (TiC/TiN) concentration was increased. A big disadvantage of the nanopowders was the oxygen content. The TiC nanopowder was found to contain 3.5 weight % oxygen and the TiN nanopowder 8.4 weight %. When taking the oxygen content into account for the density calculations, the Al_2O_3-50% TiC, Al_2O_3-30% TiN and the Al_2O_3-50% TiN nanocomposites were found to have relative densities of 95.9%, 95.5% and 94.8% respectively. Therefore, these composites were considered to be insufficiently dense. From the relationship between the reinforcing component composition and the densities obtained for both the Al_2O_3-TiN and Al_2O_3-TiC nanocomposites, it was evident that more than the oxygen contamination in the starting powders was influencing the densification behaviour of the materials.

For the Al_2O_3-TiN and the Al_2O_3-TiC composites possible influences on the composites were deemed to be:

- Further oxygen contamination during the powder processing stage
- Exceeding the percolation limit, which caused the alumina to be restricted by the reinforcing component to plastically deform and move between the reinforcing component to produce a fully dense sample.

In the Al_2O_3-TiC and Al_2O_3-TiN with more than 30% of the reinforcing component added, it was also suggested that with increasing sintering temperature the oxide materials began to reduce, this resulted in porosity within the composite and thus lowered the density of the material. It was shown that for the composites to have a relative density of 97%, a large portion of the reinforcing

component in the respective composites would have to be TiO_2. From the XRD and SEM analysis of the materials it was clear that this was not the case. As a result, although there may be some oxygen contamination during the powder processing stages, this was insufficient to lower the densities of the samples to their respective relative densities as calculated using Archimedes' principle.

Thus it was expected that the percolation limit of the materials was the major cause of the lack of densification in the materials with 30% and higher concentrations of the TiC or TiN. From literature it has also been shown that titanium carbide and titanium nitride additions impede densification[70]. It was observed that materials with high concentrations of such reinforcing components (≥30 vol%) added to Al_2O_3, high densities were more difficult to achieve. This can have a negative effect on the hardness of the material[66].The densification of Al_2O_3-TiC composites was also limited by chemical reactions between $A1_2O_3$ and TiC[65][66]. Pinning of the alumina grains by the reinforcing component occurs which limits grain growth of the alumina matrix. This results in a decrease of the mobility of the grain boundaries during the sintering process. This effect has been observed in a number of composite materials[64][65][71]. There is evidence of reduction of the oxide phases present in the composites; this is expected to have introduced porosity into the sample, lowering the densification. The pinning effect was significantly noticeable in the Al_2O_3-30%TiC composite.

The hardness values of the Al_2O_3-TiC nanocomposite materials typically were found to be higher than those of the Al_2O_3-TiN nanocomposites. The Al_2O_3-TiC nanocomposites were found to have hardness values of up to 21.1 GPa, 21 GPa, 20.3 GPa and 23.1 GPa for the 3%, 10%, 30% and 50% TiC containing composites respectively. In the Al_2O_3-TiN nanocomposites, hardness values of 19.3 GPa, 20.0 GPa, 20.6 GPa and 13.5 GPa were found for each of the 3%, 10%, 30% and 50% TiN containing composites respectively.

The fracture toughness values obtained for the materials were relatively similar when comparing the nanocomposites with the same amounts of the reinforcing components added. However, the Al_2O_3-3% TiC and the Al_2O_3-10% TiC nanocomposites that were sintered at 1800°C using a pressure of 30 MPa were the only samples that were found to have a fracture toughness higher than 3 $MPa.m^{0.5}$.

Thus it was clear that the oxygen contamination within these samples, along with the increased difficulties in the densification due to the percolation limit being exceeded and also reduction of the samples had major effects on the samples. It resulted in lower densifications, hardness and fracture toughness values being obtained, which resulted in properties that are not favourable for many of the samples sintered at higher temperatures.

From these results, it is suggested that work be continued with the Al_2O_3-TiC nanocomposites. Although the Al_2O_3-50%TiC did achieve the highest hardness, from the densification results it is suggested that only composites containing up to 30%TiC be investigated. Since the Al_2O_3-TiN experiments showed that lower heating rates will improve the densification, this would be an option for the sintering of the Al_2O_3-30%TiC composites. Composites containing between 10 and 30% TiC may have the best properties and may be worth investigating.

Further research has to be done in order to fully understand the sintering and materials behaviour. Also an understanding of the formation of the $(Al,Ti)_3O_5$oxide phases as well as the possibility to avoid these is required as this strongly reduces the hardness of the composites. A possible way to accommodate small amounts of the titanium oxide phase that cannot be avoided would be to add some zirconia to the composite. The strength and wear behaviour of these materials in comparison to conventional composites will have to be tested in order to evaluate the potential of these materials.

Also, other surfactants and solvents may be investigated in order to improve the processing and reduce possible costs. In the end, a comparison of the costs involved in working with the nanopowder materials in comparison to the improved behaviour has to be carried out to understand if these materials could be suitable for a given application.

10.Appendix

Lubrizol 2155 Burn-off

Table 35: Effectiveness of Burn-off Procedure for Removing Lubrizol 2155.

Sample	Lubrizol 2155 Present (g)	Weight Loss during Burn Off (g)	Percent Lubrizol Burnt Off (%)
Al_2O_3-3%TiC	2	1.893	94.7
Al_2O_3-10%TiC	2	1.934	96.7
Al_2O_3-30%TiC	2.6	2.542	97.8
Al_2O_3-50%TiC	2.8	2.751	98.3
Al_2O_3-3%TiN	2.4	2.284	95.2
Al_2O_3-10%TiN	2.5	2.418	96.7
Al_2O_3-30%TiN	2.9	2.968	102.3
Al_2O_3-50%TiN	3.2	3.395	106.1

11.References

1. S.F. Hulbert, J.J. Klawitter: History of ceramic orthopedic implants. Mat. Res. Bull. vol. 7, Pergamon Press Inc., 1972. pp. 1239-1246.

2. S.M. Best, A.E. Porter, E.S. Thian, J. Huang: Bioceramics: Past,present and for the future. Journal of the European Ceramic Society (2008) pp. 1319-1327.

3. J. Rieu, P. Goeuriot: Ceramic composites for biomedical applications. Clinical Materials 12 (2003) pp. 211-217.

4. X. Wang, N.P. Padture, H. Tanaka, A.L. Ortiz: Wear-resistant ultra-fine-grained ceramics. Acta Materiala 53 (2005) pp. 271-277.

5. J.S. Reed: Principles of ceramics processing, Second edition. John Wiley and Sons, Inc. 1995.

6. M.N. Rahaman: Ceramic processing and sintering, second edition. Marcel Dekker, Inc. 2003.

7. M. Nygren, Z. Shen: On the preparation of bio-, nano- and structural ceramics and composites by spark plasma sintering. Solid State Sciences 5 (2003) pp. 125-131.

8. X.Q. You, T.Z. Si, N. Liu, P.P. Ren, Y.D. Xu, J.P. Feng: Effect of grain size on thermal shock resistance of Al2O3-TiC ceramis. Ceramics International 31 (2005) pp. 33-38.

9. T. Kokubo: Bioceramics and their clinical applications. Woodhead Publishing Limited, 2008.

10. D.F. Williams: The Williams' Dictionary of Biomaterials. Liverpool University Press, UK, 1999.

11. L. L. Hench: Bioceramics: From concept to clinic. Journal of the American Ceramic Society 74 (1991) pp. 1487-1510.

12. T. Kokubo, M. Shigematsu, Y. Nagashima, M. Tashiro, T. Nakamura, T. Yamamuro and S. Higashi: Apatite- and Wollastonite-containing glass ceramics for prosthetic applications. Bulletin of the Institute for Chemical Research, 60. (1982) pp. 260-268.

13. W. Holand: Biocompatible and bioactive glass-ceramics - state of the art and new directions. Journal of Non-Crystalline Solids 219 (1997) pp. 192-197.

14. http://www.cuneyttas.com/biomim.htm, Accessed on 22 April 2010.

15. E. D. Eanes: Thermochemical studies on amorphous calcium phosphate. Calcif Tissue Res, 5(2), 1970 pp.133–145.

16. S. Somrani,C. Rey,M. Jemal: Thermal evolution of amorphous tricalcium phosphate. J Mater Chem, 13, (2003) pp. 888–892.

17. G. Willman: Biolox® forte heads and cup inserts for THR – what a surgeon should know, in Bioceramics in Orthopaedics – New Application, Enke, Stuttgart. (1997).

18. S. Pramanik, A. K. Agarwal and K. N. Rai:Development of High Strength Hydroxyapatite for Hard Tissue Replacement. Trends Biomater. Artif. Organs, Vol 19(1), pp 46-51 (2005).

19. J. E. Park, A. Öztürk, S. H. You, S. S. Park, W. T. Bae and D. W. Shin: Effect of microstructure on the tribological properties of apatite-wollastonite glass ceramic. Journal of Ceramic Processing Research. Vol. 9, No. 3, pp. 230-233 (2008).

20. http://www.azom.com/article.aspx?ArticleID=940. Accessed on 4-12-2011.

21. http://www.ceramtec.com/downloads/mt_biolox_delta_en.pdf. Accessed on 28 November 2011.

22.http://www.zimmer.com/content/pdf/enUS/Biolox_Option_Ceramic_Femoral_Head_Data_Sheet_Surgical_Technique_97877500200_rev3_08_2011.pdf. Accessed on 22 February 2012.

23. L. L. Hench, R. J. Splinter, W. C. Allen, T. K. Greenlee: Bonding mechanisms at the interface of ceramic prosthetic materials. J. Biomed. Mater. Res., 2, (1971) pp. 117–141.

24. J. Wilson, G. H. Pigott, F. J. Schoen, L. L. Hench: Toxicology and biocompatibility of Bioglasses. J. Biomed. Mater. Res., 15 (1981) pp. 805–817.

25. J. Wilson, D. Noletti: Bonding of Soft Tissues to Bioglass®. In T. Yamamuro, L.L. Hench, J. Wilson (Eds.) Handbook of Bioactive Ceramics. Boca Raton,Fl, CRC Press, 1990.

26. I. Denry, J. R. Kelly: State of the art of zirconia for dental applications. Dental materials 24 (2008) pp. 299–307.

27. B. Basu: Nanoceramics and Nanocomposites. Current Science, Vol 95, No. 5 (2008) pp. 570-571.

28. R. VaBen, D. Stover: Processing and properties of nanophase ceramics. Journal of Materials Processing Technology, 92-93 (1999) pp. 77-84.

29. W.M. Sigmund, N.S. Bell and L. Bergström , Novel powder processing methods for advanced ceramics. Journal of the American Ceramic Society 83 (2000) pp. 1557–1574.

30. J. A. Lewis: Colloidal Processing of Ceramics, Journal of the American Ceramics Society, Vol. 83 (2000) pp.2341–2359.

31. J. Shi: Steric Stabilization, Center for Industrial Sensors and Measurements, Department Materials Science & Engineering, The Ohio State University (2002) .

32. http://www.lubrizol.com/Coatings/HD-002-Hyperdispersants-Tech-Benefits.pdf. Accessed on 22 February 2012.

33. A.L. Penard, F. Rossignol, H.S. Nagaraja, C. Pagnoux, T. Chartier, Dispersion of alpha-alumina ultrafine powders using 2-phosphonobutane-1,2,4-tricarboxylic acid for implementation of DCC process, J. Eur. Ceramic Society, 25(2005) 1109-1110.

34. L. Bergstrom: Rheology of Concentrated Suspensions. Surfactant Science Series, vol. 51. Dekker, Marcel, Inc. (1993) pp. 193-244.

35. Private communication with Dr. M Herrmann, Fraunhofer Institute for Ceramic Technologies and Sintered Materials.

36. C. B. Carter, M. G. Norton: Ceramic Materials - Science and Engineering. Springer, 2007.

37. M. W. Barsoum: Fundamentals of ceramics. IOP Publishing Ltd.,Bristol and Philadelphia, 2003.

38. Bioceramics: From concept to clinic. Hench, L. L. 1991, Journal of the American Ceramic Society, Vol. 77, pp. pp. 1487-1510.

39. Q. Like, L. Xikun, P Yang, M. Weimin, Q. Guanming, S. Yanbin: Types, Performance and application of Al_2O_3 System Ceramic Cutting Tool. Journal of rare earths, vol. 25, Suppl. (2007) pp. 322-326.

40. Y. Zhang, L. Wang, W. Jiang, L. Chen, G. Bai: Microstructure and properties of Al_2O_3–TiC nanocomposites fabricated by spark plasma sintering from high-energy ball milled reactants. Journal of the European Ceramic Society 26 (2006) pp. 3393–3397.

41. Z. Shen, M. Johnsson, M. Nygren: TiN/Al_2O_3 composites and graded laminates thereof consolidated by spark plasma sintering. Journal of the European Ceramic Society 23 (2003) pp. 1061-1068.

42. J. Li, L. Gao, J. Guo: Mechanical properties and electrical conductivity of TiN-Al2O3 nanocomposites. Journal of the European Ceramic Society 23 (2003) pp. 69-74.

43. A. Krell, P. Blank: TiC-strengthened Al_2O_3 by powder tailoring and doping procedures. Materials Science and Engineering, A161 (1993) pp. 295-301.

44. R.S. Averback, H.J. Hofler, R. Tao: Processing of nano-grained materials. Materials Science and Engineering, A166 (1993) pp. 169-177.

45. C.A. Schuh, T.G. Nieh: Hardness and Abrasion Resistance of Nanocrystalline Nickel Alloys Near the Hall-Petch Breakdown Regime. Materials Research Society. Symp. Proc. 740. (2003).

46. Z. B. Qi, P. Sun, F. P. Zhu, D. L. Peng, C. H. Wu: The inverse Hall–Petch effect in nanocrystalline ZrN coatings, Surface and Coating Technology, Vol 205 (2011) pp.3692-3697.

47. B. V. M. Kumar, W. S. Kim, S. H. Hong, H. T. Bae, D. S. Lim: Effect of grain size on wear behavior in Y-TZP ceramics. Materials Science and Engineering A 527 (2010) 474–479.

48. D.H. Jeong, U. Erb, K.T. Aust, G. Palumbo: The relationship between hardness and abrasive wear resistance of electrodeposited nanocrystalline Ni-P coatings. Scripta Materiala 48 (2003) pp. 1067-1072.

49. Malvern: Mastersizer 2000 - Integrated Systems for Particle Sizing. Malvern Instruments Ltd., Brochure MRK501-02 (2005).

50. Malvern: Zetasizer nano series: User manual. Man 0317, Issue 5.0, Malvern Instruments Ltd. (2009).

51. Anto Paar: RheolabQC - Rotational Rheometer for Quality Control. Anton Paar Austria, Brochure C04IP01 (2005).

52. Fritsch: Planetary Mono Mill - Pulverisette 6. Fritsch, Germany, Brochure p6e-05-04-5/P.

53. American Society for Testing and Materials (ASTM C373-88 2006) as obtained from http://www.astm.org/Standards/C373.htm on 06-12-2011.

54. Struers: CitoPress - 10/ - 20. Struers, Denmark, Brochure 11.2008 / 62127374 (2008).

55. W. D. Callister: Fundamentals of Materials Science and Engineering, 5th edition. John Wiley and Sons, Inc. 2001.

56. G.R. Anstis, P. Chantikul, B.R. Lawn, D.B. Marshall: A critical evaluation of indentation techniques for measuring fracture toughness: I Direct crack measurements. Journal of the American Ceramic Society,Vol.64 (1981) pp. 533-538.

57. http://medical-dictionary.the freedictionary.com/succinimide. Accessed on 11 November 2012.

58. http://www.chemicalbook.com/ChemicalProductProperty_EN_CB4852973.htm. Accessed on 11 November 2012.

59. Y. J. Kim, U. Platt, M. B. Gu and H. Iwahashi: Atmospheric and Biological Environmental Monitoring. Springer Science and Business Media B.V. (2009) .

60. A. Tsetsekou, C. Agrafiotis, A. Milias: Optimization of the rheological properties of alumina slurries for ceramic processing applications, Part 1: Slip-casting. Journal of the European Ceramic Society, 21 (2001) pp 363-373.

61. H.Y. He: Comparison study of photocatalytic Properties of $SrTiO_3$ and TiO_2 Powders in Decomposition of Methyl Orange. Int Jour Environ Res. 3(1) pp.57-60 (2009).

62. T. Busami, R.A.B. Devine: Physical and Optical Properties of Room Temperature Microwave Plasma Anodically Grown TiO2. Jour Vac Sci Technology A27, 725 (2009).

63. N. Taylor, D. C. Dunand and A. Mortensen: Initial Stage Hot Pressing of Monosized Ti and 90% Ti-10% TiC Powders. Acta metall, mater. VoI. 41, No. 3, (1993) pp. 955-965.

64. W. Acchar, C. A. Cairo and A. M. Sagadaes: TEM Study of a Hot Pressed Al_2O_3-NbC Composite Material. Materials Research, Vol.8, No.1, (2005) pp. 109-110.

65. Y. W. Kim, J. G. Lee: Pressureless Sintering of Alumina- Titanium Carbide Composites. J. Am. Ceram. Soc. 72(8) (1989) pp. 1333-1337.

66. W. Acchar, A. E. Martinelli, F. A. Vieira, C. A. A. Cairo: Sintering behaviour of alumina–tungsten carbide composites. Materials Science and Engineering A284 (2000) pp. 84–87.

67. A. Krell: A new look at grain size and load effects in the hardness of ceramics. Materials Science and Engineering, A245 (1998) pp. 277-284.

68. H. O. Pierson: Handbook of refractory carbides and nitrides - Properties, Characteristics, Processing and Applications. Noyes Publications, New Jersey, United States of America, 2006.

69. A. Krell, S. Schadlich: Nanoindentation hardness of submicrometer alumina ceramics. Materials Science and Engineering, A307 (2001) pp. 172-181.

70. E. D. Whitney: Ceramic cutting tools: materials, development, and performance. Noyes Publications, United States of America. (1994).

71. K. W. Chae, D. Y. Kim and K. Niihara: Sintering of Al_2O_3-TiC composite in the presence of liquid phase. J. Am. Ceram. Soc. 78(1) (1995) pp. 257-259.